SIMPLE MODEL OF ELECTROCHEMICAL REACTOR FOR SIMULATION STUDIES

A Thesis
Submitted to the College of Engineering
of Nahrain University in Partial Fulfillment
of the Requirements for the Degree of
Master of Science
in
Chemical Engineering

by

Saif Talal Munji
B.Sc. 2003

Ramadhan **1427**
October **2006**

Certification

We certify that the preparation of this thesis entitled "**Simple Model of Electrochemical Reactor for Simulation Studies**" was made by **Saif Talal Munji** under our supervision at Nahrain University / College of Engineering in partial fulfillment of the requirements for the degree of Master of Science in Chemical Engineering.

Signature:
Name: **Prof. Dr. Qasim J. Slaiman**
Date: /

Signature: K.S. Abdul Masih
Name: **Dr. Kamal S. Abdul Masih**
Date: 6 / 12 / 2006

Signature:
Name: **Prof. Dr. Qasim J. Slaiman**
(Head of Department)
Date: /

Certificate

We certify, as an examining Committee, that we have read the thesis entitled **"Simple Model of Electrochemical Reactor for Simulation Studies"**, and examined the Student **Saif Talal Munji** in its content and found it meets the standard of thesis for the degree of Master of Science in Chemical Engineering.

Signature:
Name: **Prof. Dr. Qasim J. Slaiman**
(Supervisor)
Date: / /

Signature:
Name: **Dr. Kamal S. Abdul Masih**
(Supervisor)
Date: 6 / 12 / 2006

Signature:
Name: **Assist. Prof. Dr. Cecilia K. Haweel**
(Member)
Date: 15 / 11 / 2006

Signature:
Name: **Assist Prof. Dr. Shatha A. Sameh**
(Member)
Date: 27 / 11 / 2006

Signature:
Name: **Assist. Prof. Dr. Sami I. Al-Rubaiey**
(Chairman)
Date: 20 / 11 / 2006

Approval of the College of Engineering

Signature:
Name: **Prof. Dr. Muhsin J. Jweeg**
(Acting Dean)
Date: 17 / 12 / 2006

Abstract

In this work it has been attempted to create a computer program for the purpose of simulation studies of fixed bed electrochemical reactor, both kinetically and hydrodynamicaly. The simulated reactor conditions are steady state one - dimensional flow - through operation at mixed (activation and mass transfer) controlled current conditions. The electrolyte is passing in a reverse and parallel direction to the direction of the current, i.e. counter flow. The studied reaction simulation is the deposition of copper from electrolyte solution of copperic sulfate and sulfuric acid as a supporting electrolyte with no side reaction to occur. Mixed control polarization region is studied with applied current density of 80% of corresponding limiting current. Packing particles used are of a spherical geometry made of copper.

The influences of electrolyte flow rate, bed thickness, and molar concentration of copperic sulfate on the behavior of the electrochemical reactor are studied as follows: flow rates of 5, 10, and 50 mL / min, copperic sulfate concentrations of 0.001 and 0.01, bed depths of 2, 3, and 4 cm.

The first problem in this simulation is to find the main two variables (concentration and potential distributions), through which any other variable may be found. Concentration and potential distributions are found from the solution of the material balance equation together with the Butler-Volmer equation according to a method, suggested in this work, which combines between the finite difference for solution of second order differential equation of cathode potential and the analytical solution of second order differential equation of the mass balance equation by special technique.

The pressure drop in the packed bed, described by Forcheimer's equation, is evaluated as a function of distance along the bed.

The model obtained is subjected to two comparisons with literature; the first one is comparing the analytical equation derived for the total limiting current density applied to the reactor with experimental values obtained from the work of Bennion and Newman (1972), where an excellent agreement has been observed. The second comparison is with the model of Olive and Lacoste (1980) under limiting current conditions which also was successful.

The results obtained from this simulation are classified into two groups, main and minor groups. The main results consist of concentration, overpotential, and reaction rate distributions. The concentration distribution is deceasing with increasing flow rate and increases with increasing bed thickness and feed concentration respectively. The overpotential is affected by feed concentration and bed thickness in a similar manner to the concentration distribution and is increasing when flow rate increased. The reaction rate behavior is shown to be similar to the overpotential behavior. The minor results, i.e. current and pressure drop distributions, the current distribution is behaving just like the reaction rate while the pressure drop is increasing when flow rate and bed depth are increased respectively.

The present model has successfully described the effect of flow rate, bed length, and feed concentration on the concentration distribution as well as the effect of Re on the collection effectiveness at different bed lengths which have matched the expected behavior.

Variable Notation

Variable	Notation	Unit
a	Activity coefficient of species, specific surface area of bed	[-], [m^{-1}]
A	Cross sectional area of bed	[m2]
c	Coefficient of inertial forces	[-]
C_b	Bulk concentration of copper ions	[gmol / liter]
C_o	Feed concentration of copper	[gmol / liter]
C_s	Surface concentration of copper ions	[gmol / liter]
D	Diffusion coefficient of copper ion	[gmol / liter]
D_E	Bed diameter	[m]
d	Diameter of spherical packing pellet	[m]
d_p	Diameter (equivalent diameter) of the sphere having the same volume as the particle	[m]
E	Cathode potential in volts	[Volts]
E_{eq}	Equilibrium potential in volts	[Volts]
F	Faraday's constant, 96487	[C / eq]
G	molal free energy,	[J / gmol]
h	Height of cylindrical packing pellet Reaction rate	[m]
i	Reaction rate	[A / m^2]
i_a	Anodic reaction rate	[A / m^2]
i_c	cathodic reaction rate,	[A / m^2]
i_o	Exchange current density	[A / m^2]
I	Total current density applied to the reactor	[A / m^2]
i_L	Local limiting current density	[A / m^2]
I_L	Total applied limiting current density	[A / m^2]
L	Bed length	[m]
Pm	Permeability factor	[m]
s	stoichiometric coefficient of species i	[-]
R	Ideal gas constant =8.314	[kJ / kg. K]
t	Time	[s]
T	Temperature	[K]
u	Electrolyte velocity out of the effect of packed bed	[m / s]
	Valance	[-]
V	Voltage applied to the reactor	[Volts]
x	Instantaneous length	[m]

Greek letters

Variable	Notation	Unit
α	Transfer coefficient	[-]
ε	Porosity of bed	[-]
η	Overpotential	[Volts]
κ	Electrical conductivity of electrolyte	[ohm^{-1}.m^{-1}]
μ	Electrolyte viscosity	[kg / m. s]
ρ	Electrolyte density	[kg / m^3]
σ	Electrical conductivity of solid matrix	[ohm^{-1}.m^{-1}]

Subscripts

a = anode
b = bulk electrolyte
c = cathode
o = initial state

List of Contents

Chapter Three: Theory and Computer Simulation

List of Figures

List of Tables

Chapter One

Introduction

1.1 Introduction to Electrochemical Engineering

Electrochemical engineering has strong interrelations to chemical engineering, to electrochemistry and to physical chemistry as well as to heat and mass transfer phenomena. It covers both processes where electrical energy is applied in electrolysis to form products and to the electrochemical generation of electrical energy [1].

Electrochemical reactor is defined as any device in which chemical reactions occur directly due to the input of electrical energy. Some of the characteristics of electrochemical processes are reversible in chemical sense, reversible in thermodynamic sense, high material and energy efficiency, high selectivity and product purity, extreme reaction conditions achieved at ambient temperature and pressure, control of structure and surface morphology, low space–time yield, therefore large number of reactor units required, and environmentally benign, low waste [2].

1.2 Types of Electrochemical Reactors

There are several types of electrochemical reactors, which can be classified to [3]: -

1. Tank reactor, Fig.(1.1.a), which has been used for many years in the metallurgical and chloro-alkali industries.

2. Plate and frame reactor, **Fig.(1.1.b)**, this reactor can operate at super atmospheric pressure with electrode gap to about 2 mm .the accumulation of gases between electrodes is a problem in this type, whose severity increase with decreasing electrode gap.
3. Capillary gap reactor, **Fig.(1.1-c)**, this type was developed primarily for operation with single phase, non-aqueous electrolytes and is used in commercial production of organics. Pumping power is relatively high but small fraction of total power for the process.
4. Swiss roll reactor, **Fig.(1.1.d)**, this is a rolled sandwich of flexible sheets or mesh electrodes with thin cloth or net separators in electrode gaps around 1 mm
5. Fixed bed reactor, **Fig.(1.1.e)**, fixed beds or porous matrices can be used as electrodes and it is well suited to processing multiphase electrolyte and give good gas liquid, liquid-liquid and solid-liquid mass transport. Fixed beds can operate at relatively low superficial velocity to give high conversion per pass and relatively high space-time yield.
6. Fluidized bed reactor, **Fig.(1.1.f)**, in this type the matrix resistivity is increased by fluidizing the particles with flowing electrolytes. The fluid bed gives good mass transport and has been developed to pilot scale for electrowinning metals.
7. Slurry reactor, **Fig.(1.1.g)**, suspensions of conductive particles has been used as electrodes in various experimental electro-synthesis. Electrode materials used are fine powders such as catalyzed carbon black.
8. Gas diffusion. reactor **Fig.(1.1.h)**, the electrodes consist of micro-porous plates with graded porosity and/or wettability. Gaseous reactant diffuses from behind the electrode and reaction takes place along three phase boundaries inside the electrode matrix.

9. Stacked porous electrode (SPE) reactor, **Fig.(1.1.i)**, in this device micro-porous electrode layers are bounded to each side of an ion conducting membrane to give compact divided cell, three dimensional electrode reactor .SPE reactors originated as fuel cells but have since been applied to water electrolysis and chloro-alkali production.

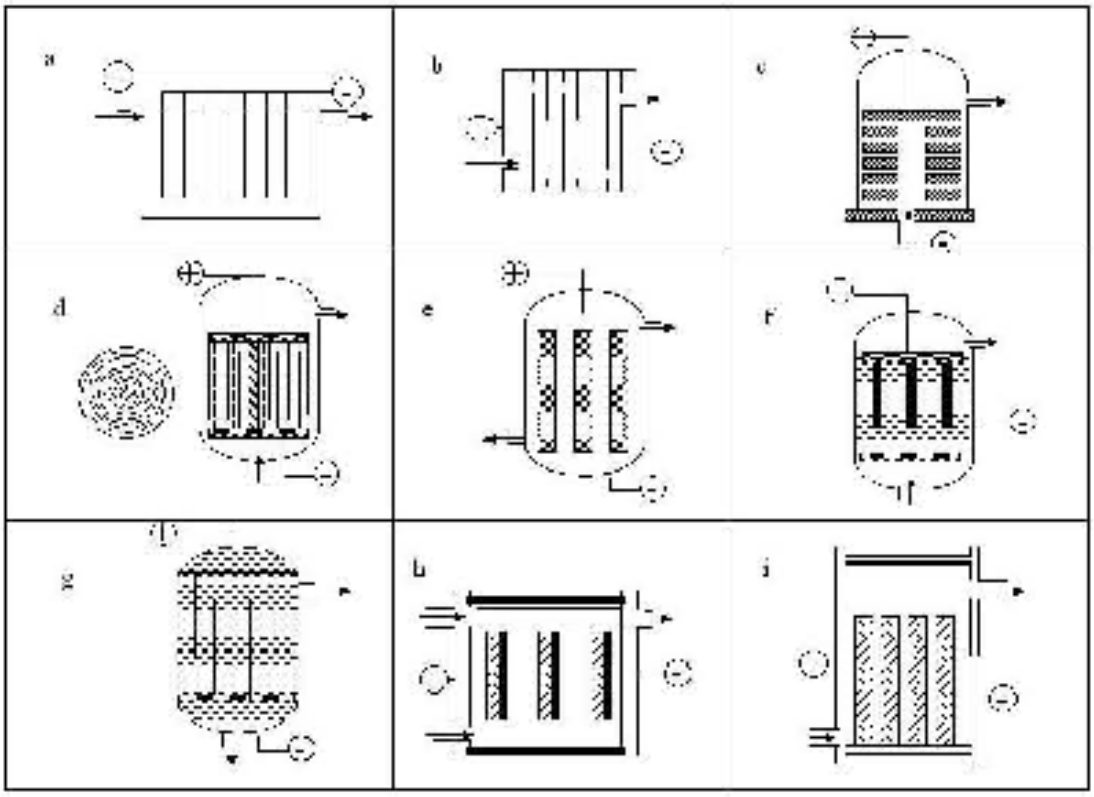

Figure 1.1 Types of electrochemical reactors [3]

1.3 Important Factors in Reactor Performance

There are many compromises during the process of reactor design/selection in order to accommodate the large number of factors acting as drivers [4], which are uniform current density distribution, uniform electrode potential distribution, high mass transport rates, ability to handle solid, liquid, or gaseous products, the form of the product and the ease of product extraction, simplicity of design, installation, and maintenance,

availability of electrode and membrane materials, capital and running costs, Integration with other process needs

1.4 Advantages of Modeling and Simulation

Mathematical model consists of set of equations containing informations, which are intended to simulate technological processes. In many cases it is more convenient to solve these equations of mathematical models instead of performing program of purely experimental measurements [5].

The advantages of computer simulation are as follows [6]

1. System performance can be observed under all conceivable conditions.
2. Decisions concerning future system presently in a conceptual stage can be examined.
3. Trails of systems under test can be accomplished in a much reduced period of time.
4. Simulation results can be obtained at lower cost than real experimentation.
5. Computer modeling and simulation is often the only feasible safe technique to analyze and evaluate a system.

Examples of industrial applications of flow-through porous electrodes are:

1. Electro-organic synthesis, which offer opportunities for performing many reactions at controlled rates and at great product selectivity, without added catalysts, than do conventional means [7]. Examples of the electro-organic synthesis are the synthesis of aniline,benzoquinone and p-aminophenol [3].
2. Removal of electrodepositive cations by electrodeposition, such as [8]:

Cu from 600 ppm to < 1

Pb from 1.45 ppm to 0.05 ppm from H_2SO_4 solution

Hg from 10 ppm to 0.01 ppm from NaCl solution

Ag processing of waste photographic emulsions

Au from waste plating solution

3. Oxidation of organic pollutants and CN^- (from 24 to 0.1 ppm). Also oxidation of organic surfactant and reducing of foaming in process for manufacturing of Na_2CO_3 [8].
4. Wastewater treatment: wastewater containing toxic metal ions, such as cadmium, chromium, copper, gold, lead, nickel, silver, tin and zinc, is generated in large quantities during electroplating, manufacturing of microelectronic parts, mining and processing of photographic films. These toxic metals should be removed from wastewater before discharge for environmental and economic reasons. Although many separation technologies, such as membrane processes and chemical precipitations, are used to remove toxic metal ions, the electrolytic process is attractive because of it's ability to remove the contaminants at low operating costs. In addition, the metals in wastewater are recovered for reuse. A variety of electrolytic cells have been designed using porous plate, packed-bed and fluidized bed electrodes. These have large surface area and high reaction rate per unit volume [9].

The development of design and operation of electrochemical process and devices has remained largely an art, well past the time when quantitative methods were introduced relevant to the design of ordinary chemical processes. The rather complex interaction between component phenomena in cells, and the hybrid backgrounds in science and engineering necessary for

understanding them, are probably responsible for the relative slowness of the development of the electrochemical engineering, Tobais (1981) [2].

1.5 Scope of Present Work

The limitations of this work are presented as follows:

The electrochemical reactor to be simulated in this work is a fixed one-dimensional porous electrode (cathode), one-dimensional means that the concentration, current, and potential are varying only axially so that the radial changes of these variables are negligible, flow-through electrode (electrolyte is passing in a direction parallel to the direction of the current and against it and flow is called counter flow), the electrochemical reaction studied is the deposition of copper from electrolyte solution of copperic sulfate and sulfuric acid and assuming no side reaction occurs, region of polarization curve studied is the mixed controlled region (activation & mass transfer), conduction within electrolyte and metal phases obey Ohm's law, neglecting migration effects, hydrodynamics of flow are assumed to be plug flow, the mass transfer coefficient is assumed constant along the bed , operating temperature is 25°C, and electrolysis is done under steady state.

The aim of this work is to study the following variables at various volumetric flow rates and bed lengths

1. The concentration variation with distance (inside porous cathode).
1. The current changing (current in solution phase) with distance.
2. The reaction rate with distance.
3. The overpotential variation with distance.
4. The pressure drop occurring in the packed bed.

Chapter Two

Literature Survey

2.1 Introduction

When a chemical reaction can proceed spontaneously via an ionic mechanism, it is possible in principle to convert part of the energy change directly into electric energy without the intermediaries of a heat engine and generator. Conversely, some chemical reactions can be made to occur, via an ionic mechanism, by the addition of electric energy to a suitable contrived reactor system. Devices for accomplishing either of these ends are called Electrochemical Cells [10].

2.2 Factors Affecting The Selection of an Electrochemical Reactor

It is important to design (or select) an electrochemical reactor for a specific process, so that adequate attention must be paid to the form of the electrode, its geometry and motion, together with the need for cell division or a thin electrolyte gap. The form of the reactants and products and the mode of operation (batch or continuous) are also important design factors.

The desirable factors in reactor design are:

1. Moderate costs (low-cost components, a low cell voltage, and a small pressure drop over the reactor)
2. Convenience and reliability in operation (designed for facile installation, maintenance, and monitoring)

3. Appropriate reaction engineering (uniform and appropriate values of current density, electrode potential, mass transport, and flow)
4. Simplicity and versatility, in an elegant design, which is attractive to the users [4].

2.3 Electrochemical Processes (Faradaic and Non-Faradaic Processes)

Two types of processes occur at electrodes, one kind comprises those at which charge (e.g. electrons) are transferred across the metal–solution interface. This electron transfer causes oxidation or reduction to occur. Since these reactions are governed by Faraday's law (i.e. the amount of chemical reaction caused by the flow of current is proportional to the amount of electricity passed), they are called faradaic processes. Electrodes at which faradaic processes occur are sometimes called charge transfer electrodes. Under some conditions a given electrode-solution interface will show a range of potentials where no charge transfer reactions occur because such reactions are thermodynamically or kinetically unfavorable. However, processes such as adsorption and desorption can occur, and the structure of the electrode-solution interface can change with changing potential or solution composition. These processes are called non-faradaic processes. Although charge does not cross the interface under these conditions, the external currents can flow (at these transiently) when the potential, electrode area, or solution composition changes. Both faradaic and non-faradaic processes occur when electrode reactions take place. Although the faradaic processes are usually of primary interest in the investigation of an electrode reaction (except in studies of the nature of the electrode-solution interface itself), even here the effects of the non-faradaic processes must be taken into

account in using the electrochemical data to obtain information about the charge transfer and associated reactions [11].

2.4 Basic Components of Electrochemical Reactors

A simple electrochemical reactor is shown schematically in **Fig. (2.1)**. When an electromotive force (emf) of a sufficient magnitude is applied electron transfer occurs between each electrode and the liquid, resulting in a flow of electricity in the external circuit and chemical reactions at each electrode. This phenomenon is referred to as electrolysis

The potential difference between the two electrodes cause a movement of the negatively charged ions, the anions, towards the positive electrode or anode. Simultaneously the positively charged ions known as cations move towards the negative electrode or cathode.

The electron flow is in the opposite direction to the conventional flow of positive electricity but nevertheless it is evident that in a chemical sense oxidation occurs where electrons pass into metallic conductor (at the anode), and reduction where they flow into the ionic media (at the cathode)[2].

The reactor is frequently divided into two compartments by means of an ion exchange membrane made of solid polymer or by a diaphragm which may made of porous plastic, porous ceramic or asbestos deposits on a gauze. Accordingly the term anolyte is used to denote the electrolyte solution in the anode compartment and catholyte describes the solution in the cathode compartment [12].

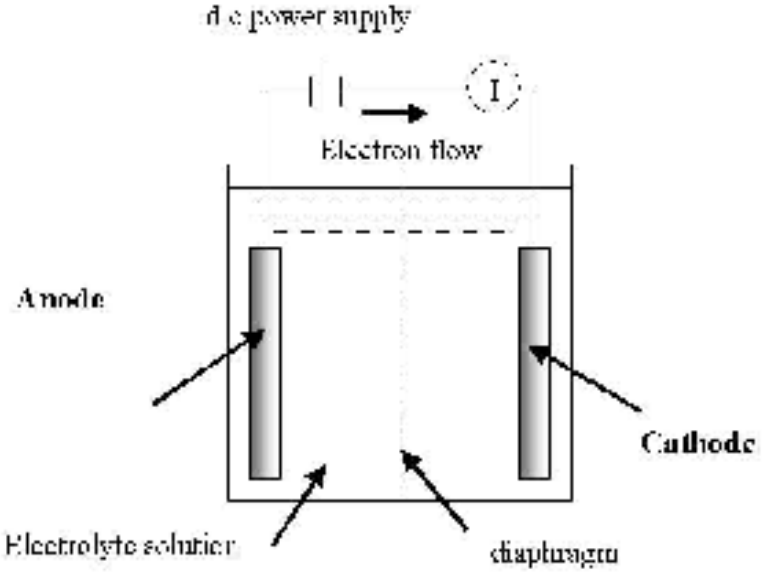

Figure 2.1 Schematic diagram of a simple electrochemical cell [12]

2.5 The Nernst Equation

Based on the thermodynamic reasoning, an equation can be derived to express the emf of a cell in terms of the concentrations of reactants and products. The general reaction for a galvanic cell can be assumed to be

$$s_A A + s_B B \longrightarrow s_C C + s_D D \qquad \ldots(2.1)$$

The corresponding change of Gibbs free energy of products and reactants, where G_C represents the molal free energy of substance C, etc.

$$\Delta G = (s_D G_D + s_C G_C) - (s_A G_A + s_B G_B) \qquad \ldots(2.2)$$

A similar expression is obtained for each substance in the standard state or arbitrary reference state, the symbol G° indicating standard molal free energy:

$$\Delta G^\circ = (s_D G_D^\circ + s_C G_C^\circ) - (s_A G_A^\circ + s_B G_B^\circ) \qquad \ldots(2.3)$$

If a_A is the corrected concentration or pressure of substance A, called its activity, the difference of free energy for A in any given state and in the standard state is related to a_A by the expression

$$s_A(G_A - G_A) = RT \ln a_A = RT \ln a_A^{\nu} \qquad \ldots(2.4)$$

where R is the gas constant (8.314 J / gmol.K) and T is the absolute temperature. Subtracting equation (2.3) from (2.2) and equating to corresponding activities, the following expression will obtained

$$\Delta G - \Delta G^{\circ} = RT \ln \frac{a_C^{\nu C} \cdot a_D^{\nu D}}{a_A^{\nu A} \cdot a_B^{\nu B}} \qquad \ldots(2.5)$$

When the reaction is at equilibrium, there is no tendency for it to go, $\Delta G = 0$, and

$$\frac{a_C^{\nu C} \cdot a_D^{\nu D}}{a_A^{\nu A} \cdot a_B^{\nu B}} = K$$

where K is the equilibrium constant for the reaction. Hence

$$\Delta G^{\circ} = RT \ln K \qquad \ldots(2.6)$$

On the other hand, when all the activities of reactants and products are equal to unity, the logarithm term becomes zero ($\ln 1 = 0$) and $\Delta G = \Delta G^{\circ}$.

Since $\Delta G = -E_{eq} \times F$, it follows that $\Delta G^{\circ} = -E^{\circ}_{eq} \times F$, where E°_{eq} is the emf when all reactants and products are in their standard state (activities equal to unity). Corresponding to equation (2.5)

$$E_{eq} = E^{\circ}_{eq} - \frac{RT}{zF} \ln \frac{a_C^{\nu C} \cdot a_D^{\nu D}}{a_A^{\nu A} \cdot a_B^{\nu B}} \qquad \ldots(2.7)$$

This is the Nernst equation, which expresses the exact emf of a cell in terms of activities of products and reactants in the cell. The activity a_A of a dissolved substance A is equal to its concentrations in moles per thousand grams of water (molality) multiplied by a correction factor γ, called the activity coefficient. The activity coefficient is a function of temperature and

concentration and, except for very dilute solutions, must be determined experimentally.

If reactant A is a gas, its activity is equal to its fugacity, approximated at ordinary pressures by the pressure in atmospheres. The activity of pure solid is arbitrarily set equal to unity, similarly for a substance like water whose concentration is essentially constant throughout the reaction, the activity is set equal to unity [14].

2.6 The Rate of an Electrochemical Reaction And Minimum Voltage Requirements for Electrolysis

Faraday discovered the two laws which express the relationship between amounts of product formed during electrolysis and the quantity of electricity passed. These can be combined in the following statement: the passage of 96487 coulombs through an electrochemical reactor produces in total one gram equivalent of products at an electrode.

$$N_i = \frac{I_i t}{x_i F} \qquad \ldots(2.8)$$

To estimate the electrolysis voltage requirements for a given process, it is useful to consider the process at equilibrium. For a simple electrochemical process in which only one reaction occurs at each electrode, it is represented by the stoichiometric equation of the reaction

Figure (2.2) illustrates a simple reactor in which the electrolysis takes place. The reaction represented by equation (2.1) in unnatural process at temperature and pressure of the reactor without applied voltage. This unnatural state is conveniently represented by the positive sign of the free energy change of the reaction, ΔG [12]

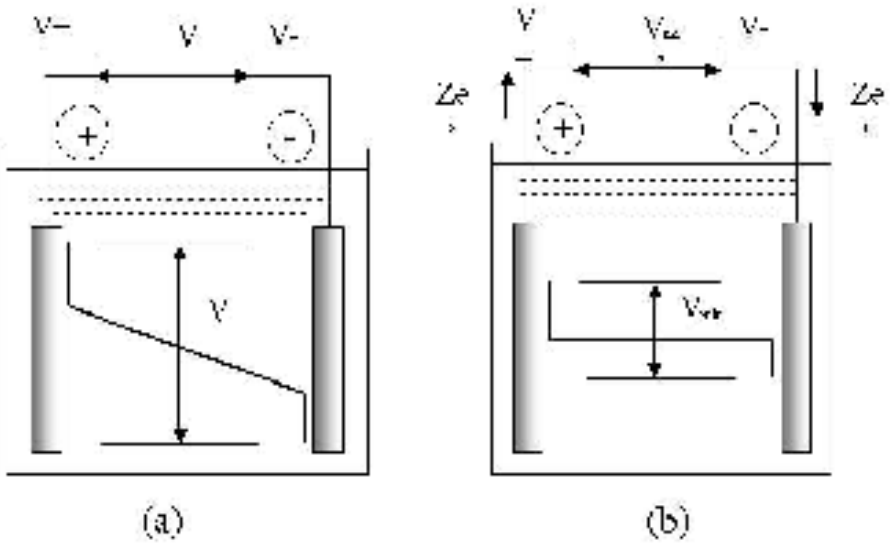

Figure 2.2 The voltage components in a single compartment electrochemical reactor [12]

(a) Finite current (b) Zero current

When the applied voltage (V) is decreased until the current illustrated in **Fig.(2.2)** is reduced to zero, the solution potential drop necessarily disappears but the two interfacial potential difference remains although they are decreased in magnitude. At this zero current condition the voltage applied keeps the system at an equilibrium state. This voltage is the minimum electrolyzing voltage. At equilibrium the free energy of the system is a minimum and under this condition

$$n\mu_{ee} - s_A\mu_A - s_B\mu_B - n\mu_{ea} + s_C\mu_C - s_D\mu_D \qquad \ldots(2.9)$$

Where μ_A, μ_B, μ_C and μ_D are the chemical potentials of species A, B, C and D respectively, μ_{ee} and μ_{ea} represent an electron consumed and produced at the cathode and anode respectively as indicated in **Fig. (2.1)**. Substitution of equation (2.2) into equation (2.9) and rearranging gives

$$\Delta G = z(\mu_{ea} - \mu_{ee}) \qquad \ldots(2.10)$$

At equilibrium the chemical potential of an electron in an electrode is equal to the chemical potential of an electron in the adjacent power supply terminals. Thus one can rewrite equation (2.10) as

$$\Delta G = zFV_{rev} \qquad \ldots(2.11)$$

Equation (2.11) enables the minimum electrolyzing voltage for a system to be calculated from free energy data [12].

2.7 Polarization

Polarization is the departure of the electrode potential (or cell potential) from the reversible (i.e. Nernstian or equilibrium) value upon passage of faradaic current. The larger this departure is the larger the extent of polarization is said to be. The ideal polarized electrode shows a very large change in potential upon the passage of an infinitesimal current: thus ideal polarizability is characterized by a horizontal region of an i-E curve. A substance that tends to cause the potential of an electrode to be nearer its equilibrium value by virtue of its being oxidized or reduced is called a depolarizer. An ideal nonpolarizable electrode (or ideal depolarized electrode) is thus an electrode whose potential does not change due to passage of current, that is, an electrode of fixed potential. Nonpolarizability is characterized by a vertical line on an i-E curve .The extent of polarization is measured by the overpotential, η, which is the deviation of the potential from the equilibrium value [11].

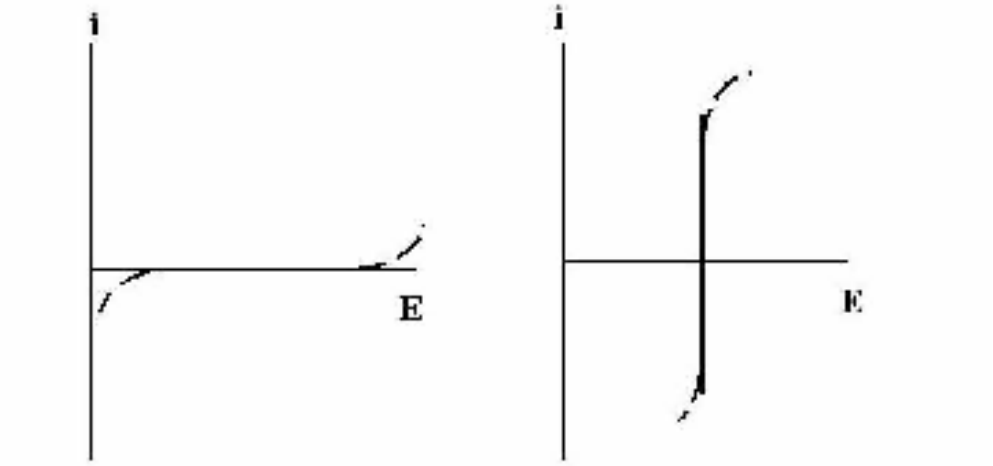

Figure 2.3 Polarization of electrodes: Ideal polarization electrode to the left and to the right ideal nonpolarization electrode [11]

The electrolyzing voltage for a typical electrochemical reactor is expressed as

$$V = V_{electr} + \eta_a + \eta_c + V_{ohmic} \qquad \ldots (2.11)$$

where η_a and η_c are the anodic and cathodic overpotentials , V_{ohmic} represents voltage contribution due to the solution resistance [11].

2.7.1 Activation polarization

The electrode kinetics will be commenced by considering the general electrode reaction. At equilibrium

$$O^{z} + ne \leftrightarrow R^{(z-n)}$$

The letters O and R represent molecules of an oxidized and reduced species respectively .The equilibrium of the reaction is disturbed by altering the electrode potential.

The current which flows when the electrode is polarized cathodically, represents the difference between the rates of the forward (cathodic) and reverse (anodic) reactions .The current density (current per unit area), i

(reaction rate), which will be considered a positive quantity is in this case given by

$$i = i_c - i_a \qquad \ldots(2.12)$$

where i_c is the partial current density for the cathodic reaction and i_a that for the anodic reaction. By analogy with chemical kinetics the rate of the forward reaction can be written as

$$\frac{i_c}{zF} \quad k_c C_{O_s} \qquad \ldots(2.13)$$

$$\frac{i_a}{zF} = k_a C_{R_s} \qquad \ldots(2.13.a)$$

where k_a and k_c are the electrochemical rate constants and C_{Rs} and C_{Os} are the concentration of R and O at that point close to the electrode surface respectively where R is discharged, after substitution

$$i = zFk_c C_{O_s} - zFk_a C_{R_s} \qquad \ldots(2.14)$$

By using Arrenhenius type of rate constant/activation energy relationship, the rate constants k_c and k_a can be expressed in terms of the electrode potential, which is a measure of the free energy requirements, by the formulas

$$k_c \quad k_c^o \exp\left[\frac{-\alpha zFE}{RT}\right. \qquad \ldots(2.15)$$

$$k_a = k_a^o \exp\left[\frac{(1-\alpha)zFE}{RT}\right. \qquad \ldots(2.16)$$

k^o_a and k^o_c are standard rate constants referenced to some particular electrode potential. Equations (2.15) and (2.16) imply that a fraction, αL, of the cathode potential is effective in promoting the cathodic process, the remainder suppressing the reverse (anodic) process. E is measured relative to the SHE and the quantity α is referred to as the transfer coefficient.

The forms of equations (2.15) and (2.16) are such that a positive increase in i_c and hence i is achieved by making E more negative.

Now elimination of rate constants

$$i = zFk_c^o \exp\left[\frac{-\alpha zFE}{RT}\right]C_{O_s} - zFk_a^o \exp\left[\frac{(1-\alpha)zFE}{RT}\right]C_{R_s} \qquad \ldots(2.17)$$

At equilibrium $E = E_{eq}$ the bulk concentrations of O and R denoted by C_{Ob} and C_{Rb} respectively are uniform throughout, and $i = 0$ so that

$$zFk_c^o \exp\left[\frac{-\alpha zFE_{eq}}{RT}\right]C_{O_b} = zFk_a^o \exp\left[\frac{(1-\alpha)zFE_{eq}}{RT}\right]C_{R_b} = i_o \qquad \ldots(2.18)$$

where i_o is called the exchange current density and represents the rates of the forward and reverse reactions at equilibrium.

Substitution of equation (2.17) into (2.18) and rearrange gives

$$i = i_o\left\{\frac{C_{O_s}}{C_{O_b}}\exp\left[\frac{-\alpha zF\eta}{RT}\right] - \frac{C_{R_s}}{C_{R_b}}\exp\left[\frac{(1-\alpha)zF\eta}{RT}\right]\right\} \qquad \ldots(2.19)$$

Equation (2.19) serves as a general expression for the rate of an electrode reaction in terms of electrode overpotential and known as Butler-Volmer equation [13]. **Fig.2.4** shows the general form of current density / overpotential relationship given by equation (2.19) for both cathodic and anodic overpotential. The lack of symmetry between the anodic and cathodic portions of the curve is quite intentional since a symmetrical plot can only occur if $\alpha = ½$ and $C_{Ob} = C_{Rb}$.

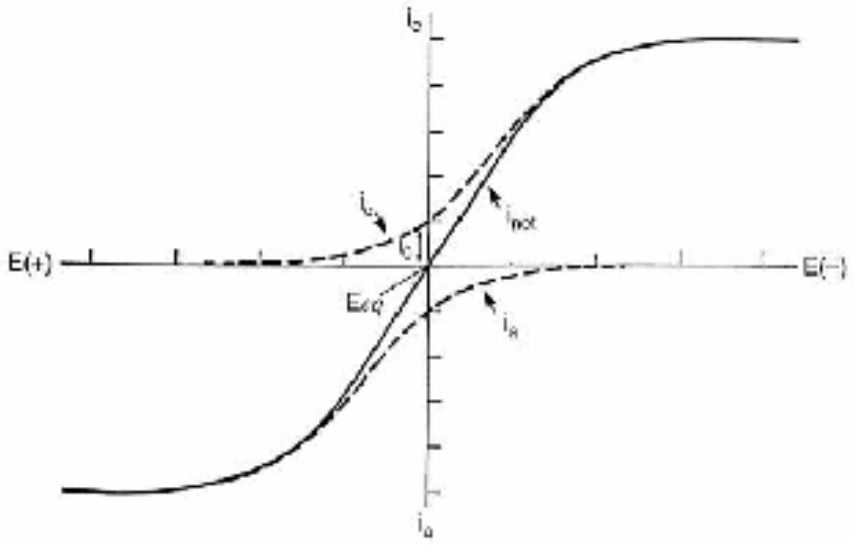

Figure 2.4 Current density / potential variations for cathodic and anodic polarization of an electrode [13]

2.7.2 Concentration polarization

Is caused by changes in the concentrations of species participating in an electrode reaction. When a current is passing, a depletion or accumulation of some species occurs in the electrolyte solution adjacent to an electrode .The electrode is thus surrounded by a solution of different composition to that in the bulk which would cause a shift in the electrode potential away from it's equilibrium value. The overpotential will evidently reduced if the concentrations of the participating species close to the electrode are maintained as near as possible to their values in the bulk of the solution. This is accomplished by insuring that high rates of mass transfer between the electrode and solution bulk take place by means of stirring or flow of the solution.

The larger the current, the smaller is the surface concentration of ions, or the smaller is the C_s; therefore the larger is the corresponding polarization. Infinite concentration polarization is approached when C_s approaches zero at

the electrode surface; the corresponding current density producing this limiting lower value of C_s is called the limiting current density, obviously, in practice, polarization can reach infinity; instead another electrode reaction establishes itself at a more active potential than corresponds to the first reaction [12]

2.8 Types of electrodes

Electrodes are classifies into two types according to operation type

2.8.1 Monopolar electrodes

In **Fig. (2.5)** alternative electrodes are connected to the opposite power supply terminals giving a number of individual reactor units electrically in parallel with one another. This configuration is referred to as monopolar connection and in this system each unit operate at the same voltage, the total current being the sum of the individual unit currents. In practice a number of mono-polar stacks will often be connected electrically in parallel so as to be compatible with the main electricity supply voltage.

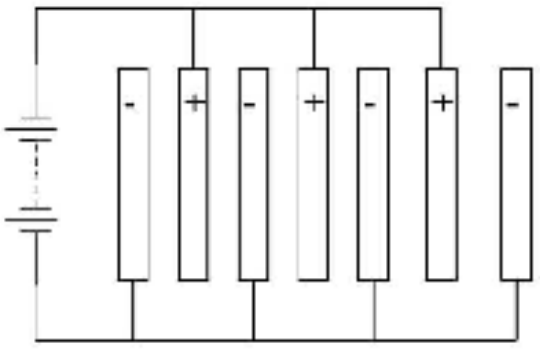

Figure 2.5 Monopolar connection of electrodes in electrochemical reactors [15]

2.8.2 Bipolar electrodes

Bipolar electrodes are electronically conducting particles that must be isolated from each other.

The alternative configuration of **Fig. (2.6)** is known as bipolar connection. Here only the end electrodes in the stack are connected to the power supply, electrical continuity being due to both intermediate electrolytic and electronic conduction. Each electrode except for those at each end thus functions as an anode on one face and as a cathode on the other. Thus every two adjacent electrodes and the intervening solution is a single unit as with monopolar connection. Each reactor unit is electrically in series with the others and the same current flows through every unit apart from leakage currents that occur sometimes between every other electrode. The total voltage drop across a bipolar stack is equal to the sum of the individual unit voltages and connection of stacks in parallel to the power supply is frequently adopted [12,15].

Both monopolar and bipolar methods of connection are extensively used. The bipolar system is preferred because fewer electrical connections are required and less power dissipation occurs in the external circuit. On the other hand it can be difficult to make [12].

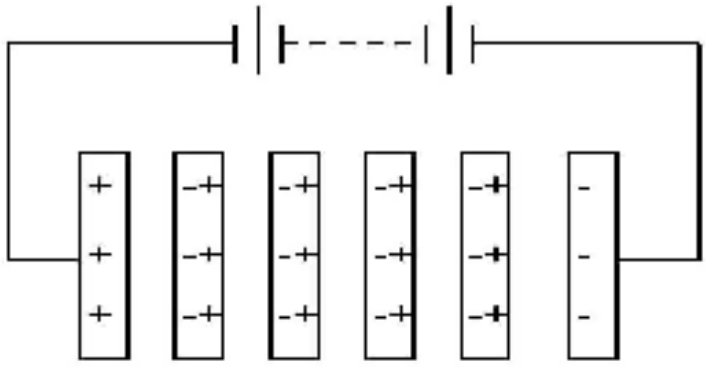

Figure 2.6 Bipolar connection of electrodes in electrochemical reactors [15]

2.9 The Three-Dimensional Porous Electrodes

The application of porous electrodes of high specific surface area and mass transfer coefficient is a promising approach to electrochemical process intensification. At present, porous electrodes are commonly used in chemical power supplies, fuel cells and metal extraction from industrial solutions and wastewater. **Fig.2.9-a** Flow-through electrolyte and current passed in cocurrently, **Fig.2.9-b** shows a flow-by two-compartment reactor, and **Fig.2.9 c** shows a flow-through single compartment reactor [15, 16 and 17].

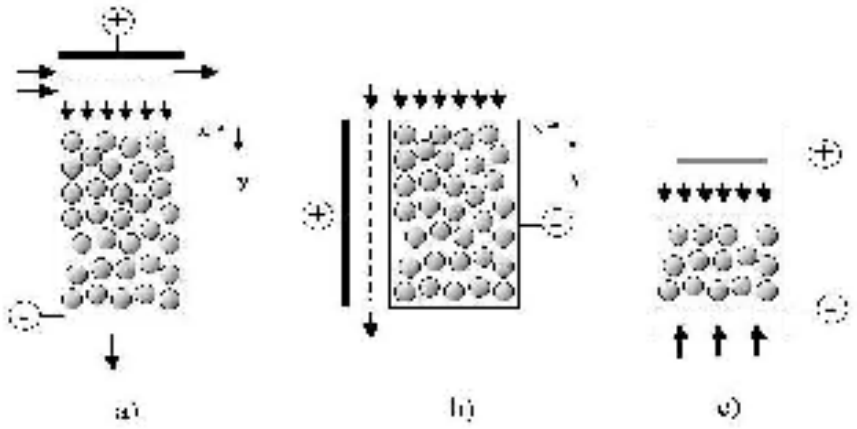

Figure 2.9 Porous electrode configurations [17, 18]

(a) Flow-through electrolyte and current passed in cocurrently

(b) Flow-by two compartment reactor

(c) Flow-through electrolyte and current passed in counterourrently

The main problem in porous electrode theory is the search for conditions providing the most efficient utilization of their extended surface for the performance of the specified main process. These conditions commonly involve attainment of the most uniform potential distribution over the porous electrode depth [16].

The important characteristics of the porous electrode are explained below

2.9.1 Porosity

The porosity or void fraction is one of important parameters of the packed bed, is defined as follows [19]

$$\varepsilon = \frac{volume\ of\ voids\ in\ bed}{total\ volume\ of\ bed\ (voids\ plus\ solids)} \qquad \ldots(2.20)$$

2.9.2 Specific Surface Area

The specific surface area of a particle a in m^{-1} is defined as:

$$a = \frac{S_p}{V_p} \qquad \ldots(2.21)$$

where S_p is the surface area of a particle in m^2 and V_p the volume of a particle in m^3. Therefore for spherical particle

$$a = \frac{6}{d} \qquad \ldots(2.22)$$

where d is the particle diameter in m. For a packed bed of non-spherical particles. The effective particle diameter d_p

2.9.3 Shape Factor

When particles in packed bed are of irregular shape, the equivalent diameter of a particle is defined as the diameter of a sphere having the same volume as this particle. The sphericity shape factor ϕ_s of a particle is the ratio of the surface area of this sphere having the same volume as the particle to the actual surface area of the particle. For a sphere, the surface area $S_p = \pi d_p^2$, and the volume is $V_p = \pi d_p^3/6$. Therefore for any particle $\phi_s = \pi d_p^2 / S_p$ [19].

$$a = \frac{S_p}{V_p} = \frac{\pi d_p^2 \cdot \phi_f}{\pi d_p^3 / 6} = \frac{6}{\phi_f d_p} \quad \ldots(2.23)$$

Table 2.1 Shape factors for different shapes [19]

Shape	Shape Factor
Spheres	1.0
Cubes	0.81
Cylinders $d_p = h$ (length)	0.87

where d_p is the diameter (equivalent diameter) of the sphere having the same volume as the particle

2.10 Advantages of Porous Electrode

Porous electrodes have numerous industrial applications primarily because they promote intimate contact of the electrode material with the solution. Specific factors are as follows [20, 21]

1. Porous electrode provide a very large electrode area in proportional to their size (e.g. 10^5 m^2/m^3 volume) and this is several times greater in magnitude than that for non-porous structure (typically not greater than 10^3 m^2/m^3 for a parallel plate system).
2. Double-layer adsorption constitutes the basis for novel separation processes involving cycling of the electrode potential. Just as in conventional fluid-solid adsorption, a high specific interfacial area is desirable.

3. Important reactants may be stored in the solution in close proximity to the electrode surface by means of porous electrodes. This permits sustained high rate discharging of the lead-acid battery.
4. A dilute contaminant can be removed effectively with a flow-through porous electrode. The proximity of the flowing stream to electrode surface is a gain important.
5. Similar arguments apply to non-conducting reactants of low solubility. Then another solid phase (as in batteries) or gas phase (as in fuel cells) may be incorporated into the system, or the reactants may be dissolved and forced through the porous electrode.
6. The compactness of the porous electrode can reduce the ohmic potential drop by reducing the distance through which the current must flow.

2.11 Previous Works

This section will be mainly concerned with the previous works for modeling and simulation of porous electrode electrochemical reactor working at both activation control process and mass transfer control process.

The first work on modeling of porous electrode reactor was done by Newman and Tobias (1962)[22], described the behavior of one-dimensional porous electrode from a macroscopic point of view and developed general equations for the prediction of current distribution and reaction rate in such electrode, regardless the geometry of the electrode.

Sioda (1971)[23] derived an equation for the potential distribution in the porous electrode working under limiting current for the condition of a flowing solution. Also he obtained an equation for the ohmic potential drop in the solution between the two ends of the porous electrode.

Alkire and Gracon (1975)[24] had investigated experimentally the region of operating conditions where mass transfer restrictions affect behavior and developed a general mathematical model for flow-through porous electrodes for two systems first is the deposition of copper and the second one is the reduction of ferricyanide under limiting current

Coeuret, Hutin and Gaunad (1976)[25] studied the fixed flow-through electrodes when they are working near equilibrium, i.e., at low local overpotentials in order to determine, from local overpotentials measurements, the conditions in which the electrode is working as a 2 or 3-dimensional electrode and to compare the results with theory.

Trainham and Newman (1977)[26] developed a mathematical model for flow-through porous electrodes operating above and below the limiting current for a specific application to metal-ion removal from dilute streams. The model assumes that there is one primary reactant species in an excess of supporting electrolyte and that a simultaneous side reaction may occur.

Gaunand, Hutin, and Coeuret (1977)[27] investigated experimentally the metal solution potential distribution within flow-through fixed electrode under limiting current conditions for a solution of about 0.001 M potassium ferricyanide in 0.75 N sodium hydroxide electrolyte. They examined bed heights of 1 and 2 cm, the bed particles they used was consists of graphite spherical particles plated with nikel and gold respectively. They compared their results with a theoretical model which was in agreement with the experimental results.

Risch and Newman (1984) [17] made a theoretical comparison between flow–through and flow-by configuration at limiting current using the maximum solution-phase potential difference as basis for comparison. They concluded that at low conversions, a flow-by electrode is favorable, providing it can be constructed with length-to-width ratio greater than one. At high

conversions, however a flow by electrode is favorable if the ratio of the electrode width and penetration depth is less than 2.218.

Lahurd (1985) [28] suggested the voltage balance (VOLBAL) model, which is based upon the overall local voltage balance across single cell and is a one-dimensional simulation easily modified for different types of electrochemical reactors (flat plate, porous electrodes). She compared her model with a rigorous two-dimensional model suggested by White.

Bertazzoli and workers (1997)[29] presented an electrolytic cell with a porous cathode of reticulated vitreous carbon (RVC) designed to remove metals from aqueous streams by flowing simulated effluent metal ion containing through porous cathodes.

Maslij and Poddubny (1997)[16, 30] presented a mathematical simulation of a flow-through porous electrode operation on the basis of a one-dimensional model with a uniform conducting matrix and a cathodic process involving the main and side reaction (i.e. hydrogen evolution); they first considered the case of constant metal electrical conductivity then variable metal electrical conductivity.

Hunsom and workers (2002)[31] described the effect of parameters (current intensity, pulse frequency, cathode type and flow rate of solution) on copper recovery in 3PE (see chapter three) reactor constructed of graphite bed particles and a counter electrode made of titanium coated with ruthenium oxide. They obtained the optimum current density applied and optimum pulse frequency and they used a synthetic solution.

Chapter Three

Theory and Computer Simulation

3.1 Introduction

This chapter is dealing with two categories, the first one is theory of the packed bed electrochemical reactor and its use in waste treatment and the second category is dealing with the simulation of the packed electrochemical reactor.

3.2 Heavy Metals Recovery and its Importance

Metals contamination in processed water is a serious problem for several industrial sectors such as surface treatment, electroplating and the electronic industry. The outlet wastewater from these industrial processes normally contains a metal concentration higher than the acceptable limit set by law. Therefore, the treatment of contaminated water before it is directly discharged is required in order to reduce the amount of metal to an acceptable level [9]. In its daily operation, the electroplating industry generates a significant amount of discharge water containing heavy metals. Heavy metals are toxic to living organisms and tend to accumulate in the environment over a period of time [32]. The toxicity of heavy metals has been known for many years, and the clinical symptoms of prolonged exposure to a heavy metal-contaminated environment are well defined. Heavy metals enter waterways via effluent discharging from electroplating, metal finishing, explosive pigments and paint producing, and metal/mechanics manufacturing industries

in general. As a result of high toxicity, the concentration of highly toxic metallic ions in drinking water is restricted to ppb. Besides that the prospect of recovery has attracted interest among industries for environmental and economic reasons. For example, valuable heavy metals are recycled and reused while the outlet water is permitted to discharge to the environment [29].

3.3 Theory and Application of Packed Bed Electrochemical Reactors in Electrodeposition Processes

Different types of porous electrochemical reactors are used in the electrodeposition processes and that is because of their high efficiency, high conversion. They are classified according to the packing type and operation mode (fixed bed or fluidized bed).

3.3.1 3PE Reactor (Pulsed Porous Percolated Reactor)

The 3PE reactor can be considered as a compromise between fixed and fluidized bed reactors. It is composed of four components [31]:

1. A solid matrix composed of particles that act as voluminal cathode in contact with the current feeder.
2. A counter electrode or anode having a small geometrical surface area.
3. A circulation pump is used to circulate the electrolyte in the system through the granular bed.
4. A pulsating system creates movement of the granular bed in the reactor forcing the movement of metal-coated particles to the bottom of the bed and avoiding the problem of clogging.

3.3.2 The Porous Cathode of Reticulated Vitreous Carbon (RVC)

The RVC reactor is used for materials having the following properties

1. Chemically and electrochemically inert over a wide range of potentials and on a wide range of chemicals
2. Has a high surface area within the porous structure that is accessible to electrochemically active species
3. Has a high fluid permeability
4. Is easily shaped as required by cell design considerations and has good mechanical resistance [29].

3.3.3 Fixed Bed Electrochemical Reactor

This type of packed bed reactors consists of a column containing the cathode (packed bed or working electrode) and anode (counter electrode) placed above the cathode. The anode may be of different types (perforated plate, or another packed bed). In present work the anodic reactions were discarded because the anode is not affecting the kinetics of the cathode but it is just a current source. The electrolyte solution is flowing upwards from the upstream (current feeder) through the lower hole of the column passing through the cathode where the reaction is occurring, then the electrolyte solution leaves the cathode and penetrates the anode to leave the reactor at the downstream. The circulation of the electrolyte solution is done by a QVF pump. **Fig. 3.1** demonstrates the fixed bed electrochemical reactor features.

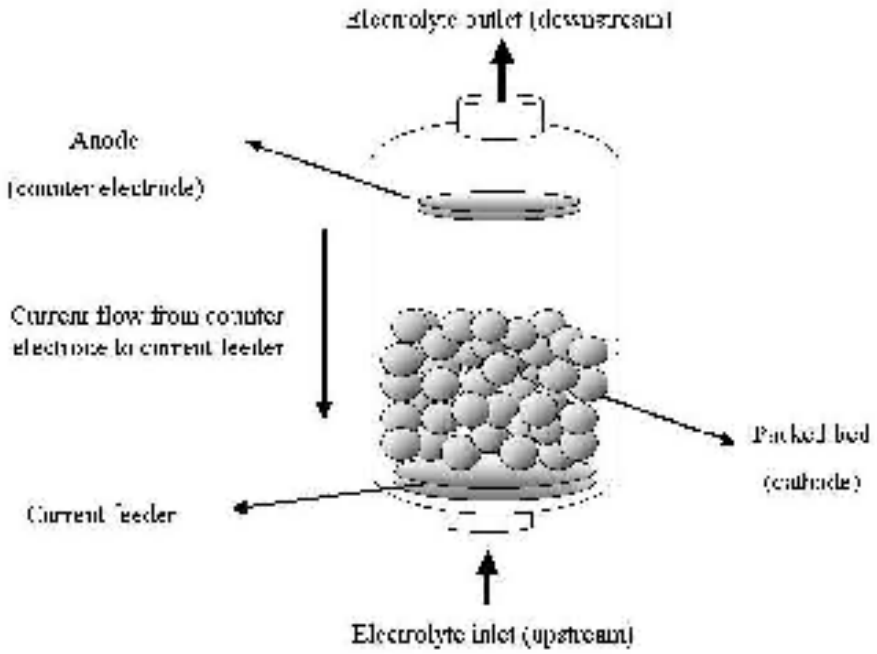

Figure 3.1 Schematic diagram of the porous electrode reactor to be simulated in present work

3.3.3.1 Hydrodynamic Parameters of Fixed Packed Bed Electrochemical Reactor

The main hydrodynamic parameters that are related to the fixed bed electrochemical reactor are velocity change, porosity and its change, the pressure drop associated with the decrease in porosity.

Pressure Drop

The general expression for pressure drop through porous medium (in this work packed bed) was stated by Bear (1972) [33] and is expressed as widely accepted in the following formula

$$\frac{dp}{dx} = -\frac{\mu u}{Pm} \qquad \ldots(3.1)$$

It is seen that the pressure drop is directly proportional to the fluid viscosity μ and inversely proportional to the permeability of the porous medium, Pm.

Effect of Pore Clogging on Pressure Drop

The effect of pore clogging on the hydrodynamics of the system was evaluated based on permeability (Pm) and factor c (the coefficient for the inertial forces), using the quadratic Forchheimer equation, which can be applied to high rates of flow through a porous medium [34].

$$\frac{\Delta P}{L} = \frac{\mu}{Pm(\varepsilon)}u + \frac{c(\varepsilon)\rho}{\sqrt{Pm}}u^2 \qquad \ldots(3.2)$$

where ΔP is the pressure drop (Pa), L is bed thickness (m), μ is electrolyte viscosity ($kg.m^{-1}.s^{-1}$), ρ is electrolyte density ($kg.m^{-3}$), ε is electrode porosity (non-dimensional), Pm(ε) is permeability at given ε (m^2), c(ε) is Forchheimer's factor c at given ε and u is the superficial velocity of the electrolyte ($m.s^{-1}$).

Permeability and factor c are porosity-dependent and for spherical shape this dependence is shown below [35]

$$Pm = \frac{\varepsilon^3 d^2}{150(1-\varepsilon)} \qquad \ldots(3.3)$$

$$c(\varepsilon) = \frac{1.75}{\sqrt{150\varepsilon^3}} \qquad \ldots(3.4)$$

3.3.3.2 Kinetic Parameters

The most important kinetic parameter needed to represent in this work is the mass transport of copper ions through the electrolyte to the packing particles of the cathode. Reconsidering the simple general electrochemical reaction:

$$O + ze \leftrightarrow R$$

The mechanism of mass transfer is occurring as in the following steps.

1. Mass transfer (e.g., of O from the bulk solution to the electrode surface).
2. Electron transfer at the electrode surface.
3. Chemical reactions proceeding or following the electron transfer. These might be homogeneous processes, such as protonization, or dimerization, or heterogeneous, such as catalytic decomposion on the electrode surface.
4. Other surface reactions, such as adsorption, desorption, or crystallization (electrodeposition). **Fig. 3.2** illustrates the above steps schematically

The simplest reactions involve only mass transfer of a reactant to the electrode, heterogeneous electron transfer involving non-adsorbed species and mass transfer of the product to the bulk solution. More complex reaction sequences involving a series of electron transfers and protonations, branching mechanisms, parallel paths, or modifications of the electrode surface are quite common. When a steady-sate current is obtained, the rates of the all reaction steps are the same. The magnitude of this current is often limited by the inherent sluggishness of one or more reactions called *rate-determining steps*.

The more facile reactions are then held back from maximum rates by the slowness with which such a step disposed of their products or creates their participants [11].

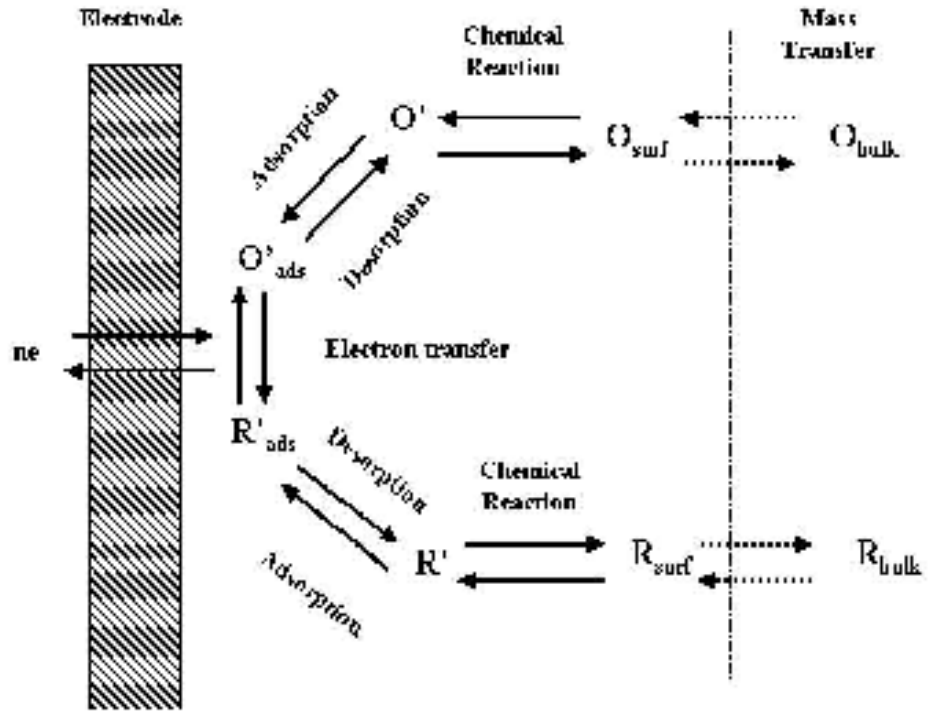

Figure 3.2 Mechanism of mass transport of ions [11]

Many workers have attempted to model convective mass transfer in packed beds by considering an isolated particle and the flow field around it.

Although theoretical predictions have a common analytical form the most useful information is that obtained experimentally. Particularly relevant are the data Jolls and Hanratty [36] obtained electrochemically from a single sphere in a randomly packed bed. They found that

$$\frac{k_m d}{D} = 1.44\left(\frac{u d \rho}{\mu}\right)^{0.58}\left(\frac{\mu}{D\rho}\right)^{1/3} \qquad \ldots(3.5)$$

Where d is the particle diameter and u is the superficial velocity based on the empty cross-section of the bed. Equation (3.5) applies for Reynolds numbers

between 35 and 142. Above Re = 142 they recommended alteration of the constant to 1.59 and the Reynolds number power to 0.56. Equation (3.5) corresponds to non-electrochemical packed bed data.

The most reliable estimate of the rate of mass transfer in a packed bed appears to be that obtained by Yip [37] for Re < 0.1 with 5/32 inch diameter spherical particles

$$\frac{k_m d}{D} = \frac{1.09}{\varepsilon}\left(\frac{u d \rho}{\mu}\right)^{1/3}\left(\frac{\mu}{D\rho}\right)^{1/3} \qquad \ldots(3.6)$$

where ε is the porosity and the one-third power on Re in equation (3.7) is indicative of Stokes flow. For higher flows a Reynolds number power of one-half would be anticipated. Correlations for packed beds in the range 0.1 < Re < 23 are not evident in the literature.

Hunsom [31] and workers obtained an empirical correlation for the mass transfer coefficient to be

$$\frac{k_m d}{D} = \frac{1.09}{\varepsilon}\left(\frac{u d \rho}{\mu}\right)^{1/3}\left(\frac{\mu}{D\rho}\right)^{1/3} \qquad \ldots(3.7)$$

for Re between 6 and 16 and Sc = 1568.

For packed bed electrochemical reactor that is operated for recovery of heavy metals the most preferred correlations in many similar works are the Wilson and Geankoplis [38] correlations [24, 26] because of the fact that in electrodeposition process the porosity of the bed (cathode) decreasing and since these correlations account the porosity as a variable so they are preferred to use as shown in Table 3.1

Table 3.1 Wilson and Geankoplis Mass transfer correlations [38]

Mass transfer equation	Geometry of packing particles	Validity range	Equation number
$Sh = \frac{k}{u} = \frac{0.4548}{\varepsilon} Re^{0.4069} Sc^{2/3}$	Bed of spherical particles	$10 < Re < 1500$	(3.8)
$Sh = \frac{k}{u} = \frac{1.09}{\varepsilon} Re^{-2/3} Sc^{-2/3}$	Bed of spherical particles	$0.0016 < Re < 55$ $165 < Sc < 70600$	(3.9)
$Sh = \frac{k}{u} = \frac{0.25}{\varepsilon} Re^{0.31} Sc^{1/3}$	Bed of spherical particles	$55 < Re < 1500$ $165 < Sc < 10690$	(3.10)

3.4 Simulation of Electrochemical processes

Electrochemical processes are complex because they involve many different simultaneous phenomena during the passage of an electrical current. Conduct of electrolysis brings about, for example, charge transfer within the double layer region, structural variation of electrode surface, ohmic resistance effects, and mass transport limitations of reactants and products to name a few. The relative importance of such processes depends upon the geometry and current density. Because the reaction rate along the surface is generally not uniform, the relative importance of such processes can therefore vary strongly within a cell [39].

In order to perform a theoretical analysis of such a complex problem, it is necessary to establish a model that accounts for essential features of an actual electrode without going into exact geometric details. Furthermore, the model should be described by parameters, which can be obtained by suitably simple physical measurements. For example, a porous material of arbitrary random structure can be characterized by its porosity, average surface area per unit volume, volume average resistivity, etc. [20].

Equations describing the electrochemical reactor behavior are always differential equations particularly second order non-linear differential equations. So in order to predict the behavior of an electrochemical reactor we need to solve these equations which require the use of numerical methods because there is no analytical method which can solve them unless certain assumptions are made. The numerical method which will be used in this work is the finite difference method. There are many computer programs utilized for engineering calculations like MATLAB. In the present work the programming language used is Visual Basic 6 to solve the differential equations according to predefined numerical methods. This chapter is dealing with the numerical methods for the solution of the differential equations governing the packed bed electrochemical reactor behavior and the programming language that will be used to solve them.

In this simulation three main categories will be simulated, first is the physical parameters (porosity changes, pressure drop), physical properties, and the third category is the kinetic parameters which are concentration distribution, current distribution, potential and reaction rate.

3.4.1 Simulation of Porosity Change Inside The Packed Bed

The type of particle geometry which will be studied here is the spherical geometry as the porosity of particles depends on the particle size (diameter). For the pressure drop it was shown in chapter three that the pressure drop in a packed bed depends on two parameters: permeability and the coefficient of inertial forces which are both function of the porosity, hence the pressure drop is a function of the porosity

For spherical particles the equation that describe the change of porosity with particle and reactor diameters is given by Furnas (1993) [40].

$$\varepsilon = 0.375 - 0.34\frac{d}{D_R} \qquad \ldots(3.11)$$

where

d : is the particle diameter

D_R: is the bed diameter

The variation of porosity with distance may be deduced from the global mass balance on a porous medium [34] as follows:

$$\varepsilon = \varepsilon_o - \frac{m_{Co}}{\rho_M . V_L}\left[1 - \frac{C_{b\,x\,=\,x}}{C_{b\,x\,=\,0}}\right] \qquad \ldots(3.12)$$

where ε_o is the initial porosity of the fixed bed (non-dimensional), m_{Co} is the initial mass of copper in the electrolyte (kg), ρ_M is the density of the porous matrix, V_L is the total fixed bed volume. $C_{b\,x=x}$ is the copper concentration in the electrolyte measured instantaneously (kmol/m^3) and $C_{b\,x=0}$ is its value at the inlet to the reactor.

3.4.2 Physical Properties

Physical properties used are obtained from literature; since there are no explicit correlations for these properties therefore curve fitting is needed. The temperature is kept constant at 25°C (isothermal operation), therefore the following properties are function of molar concentration for both cupric sulfate and sulfuric acid.

3.4.2.1 Electrolyte Density

The density of electrolyte solution is obtained at several concentrations of copperic sulfate and sulfuric acid. This was realized using the ChemCAD software, the method is explained in Appendix B. the resulting equation was

$$\rho = 1103.262 + 61.46M_{H_2SO_4} - 13M_{CuSO_4} + 77.63\left(M_{H_2SO_4} \cdot M_{CuSO_4}\right)^{0.0556} - 180M_{CuSO_4}^{0.00868M_{H_2SO_4}} \quad \ldots(3.13)$$

3.4.2.2 Electrolyte Viscosity

The viscosity of electrolyte solution as a function of molar concentration of cupric sulfate and sulfuric acid was obtained in a similar manner by ChemCAD software. See Appendix B.

$$\mu = -3\times10^{-3} + 2.23\times10^{-4}M_{H_2SO_4} - 8.3\times10^{-7}M_{CuSO_4} - 8.3\times10^{-7}\left(M_{H_2SO_4} \cdot M_{CuSO_4}\right)^{0.14} - 0.00106M_{CuSO_4}^{2.287\times10^{-3}M_{H_2SO_4}} \quad \ldots(3.14)$$

μ: viscosity of electrolyte in kg / m .s

$M_{H_2SO_4}$: Molar concentration of sulfuric acid in gmol / liter

M_{CuSO_4}: Molar concentration of copperic sulfate in gmol / liter

3.4.2.3 Diffusion Coefficient

Using the modified form of Stokes-Einstein equation given in [41]:

$$\frac{D\mu^{0.74}}{T} = Constant \qquad \ldots(3.15)$$

Since the operation is isothermal (constant temperature) the above equation is rewritten as $D\,\mu^{0.74} = constant$. The constant value must be evaluated. Hunsom et al (2002) [31] evaluated the diffusion coefficient (D) and viscosity at 25C° for electrolyte consists of sulfuric acid and copperic sulfate to be as follows:

$D = 5.89*10^{-10}$ m^2/s and $\mu = 9.29 * 10^{-4}$kg/m s.

The constant value will be $3.36 * 10^{-12}$, therefore the relation will be

$$D = \frac{3.36 \times 10^{-12}}{\mu^{0.74}} \qquad \ldots(3.16)$$

3.4.2.4 Electrical Conductivity of Electrolyte

Electrolytic conductivity is the measurement of the ability of a solution to conduct an electric current and is sometimes referred to as "specific conductance." Electrolytic conductivity is defined as the inverse or reciprocal of electrical resistance (ohms). Resistivity as the inverse of conductivity is defined as the measure of the ability of a solution to resist an electric current flow [42]. The experimental values of the electrical conductivity of the electrolyte are given by [12], and [21] as follows:

$$\kappa_e = 74.92 - 6.1459M_{CuSO_4} - 25.7M_{H_2SO_4} + 3.92M_{CuSO_4}M^{2.0}_{H_2SO_4} - 5.1444M^{0.1394M_{H_2SO_4}}_{CuSO_4} \qquad \ldots(3.17)$$

where κ_0 is the electrical conductivity in the bulk of the electrolyte. The true value of the electrical conductivity (κ) for the electrolyte inside the packed bed must be adjusted using the equation proposed by Neale (1975)[43].

$$\frac{\kappa}{\kappa_0} = \frac{2\varepsilon}{(3-\varepsilon)} \qquad \ldots(3.18)$$

3.4.2.5 Exchange Current Density

The experimental values of the exchange current density for the copper deposition reaction are given by [25], see Appendix B

$$i_o = 1.861266 + 39.71 M_{CuSO_4} - 31.80 M^2_{CuSO_4} \qquad \ldots(3.19)$$

3.4.3 Kinetic Parameters

The kinetic parameters in this simulation are for a specified region in the polarization curve that is mixed controlled process (Activation and Mass Transfer).

3.4.3.1 Mass Balance Equation

Using the general mass balance equation is made as follows [12]:

$$D\frac{d^2 C_b}{dx^2} - u\frac{dC_b}{dx} = ak_m(C_b - C_s) \qquad \ldots(3.20)$$

The term of surface concentration in the mass balance equation must be included because of the fact that in mixed control process the transfer of copper ions due to mass transfer will appear significantly and therefore C_b will not be equal to C_s

The relation between bulk concentration and surface concentration is as follows [12]

$$\frac{C_b}{C_s} = \frac{i_L}{i_L - i} \qquad \ldots(3.21)$$

where i is the reaction rate in A / m^2, and i_L is the limiting current obtained from equation below

$$i_L = zF k C_b \qquad \ldots(3.21\text{-a})$$

where

k: is mass transfer coefficient in m/s obtained using equations of Wilson and Geankoplis [38]

C_b: is the bulk concentration in kmol/ m^3; D: is the diffusion coefficient

Rearranging equation (3.20) gives

$$D\frac{d^2C_b}{dx^2} - u\frac{dC_b}{dx} = akC_b\left(1 - \frac{C_s}{C_b}\right) \qquad \ldots(3.22)$$

Transformation of equation (3.21) gives

$$\frac{C_s}{C_b} = \frac{i_L - i}{i_L} = 1 - \frac{i}{i_L} \qquad \ldots(3.23)$$

Substitution of equation (3.23) into equation (3.22) and rearranging gives

$$D\frac{d^2C_b}{dx^2} - u\frac{dC_b}{dx} - akC_b\frac{i}{i_L} = 0 \qquad \ldots(3.24)$$

Equation (3.24) cannot be solved by analytical methods because of variable ratio of reaction rate & limiting current according to every x value throughout the bed, therefore other equations are needed to obtain values of reaction rate & limiting current

3.4.3.2 Potential distribution

By applying Ohm's law to the electrolyte solution and solid phase matrix [22]:

$$i_s = -\kappa \frac{d\phi_s}{dx} \quad \ldots(3.25)$$

$$i_m = -\sigma \frac{d\phi_m}{dx} \quad \ldots(3.26)$$

Rewriting equations (3.25) & (3.26) gives the following forms

$$\frac{d\phi_s}{dx} = -\frac{i_s}{\kappa} \quad \ldots(3.27)$$

$$\frac{d\phi_m}{dx} = -\frac{i_m}{\sigma} \quad \ldots(3.28)$$

Subtracting equation (3.27) from (3.28)

$$\frac{d\phi_m}{dx} - \frac{d\phi_s}{dx} = \frac{d}{dx}(\phi_m - \phi_s) = -\frac{i_m}{\sigma} + \frac{i_s}{\kappa} \quad \ldots(3.29)$$

The potential of the cathode (E) is defined as the difference between the metal and solution potentials $(\phi_m - \phi_s)$

The overpotential $(\eta) = E - E_{eq}$

Using the current conservation equation, total applied current density is equal to the sum of currents in solution phase and that in metal phase

$$i_m + i_s = I \quad \ldots(3.30)$$

where

i_m : current in metal phase (solid bed) in A / m^2

i_s : current in electrolyte solution phase in A / m^2

I : is the total current passing through the cell in A / m^2

ϕ_m : is the potential in metal phase in volts

ϕ_s : is the potential in electrolyte solution phase in volts

κ : is the electrical conductivity of solution

σ: is the electrical conductivity of the solid metal

The area in the current densities above is the cross sectional area of the reactor [25]

From equation (3.30)

$$i_{sc} \quad I \quad i_s$$

Equation (3.28) is written as

$$\frac{d}{dx}(\phi_m - \phi_s) = -\frac{(I - i_s)}{\sigma} - \frac{i_s}{\kappa} = i_s\left(\frac{1}{\kappa} + \frac{1}{\sigma}\right) - \frac{I}{\sigma} \qquad \ldots(3.31)$$

therefore

$$\frac{dE}{dx} - i_s\left(\frac{1}{\kappa} \; \frac{1}{\sigma}\right) \quad \frac{I}{\sigma} \qquad \ldots(3.32)$$

differentiation of equation (3.32) gives

$$\frac{d^2E}{dx^2} - \left(\frac{1}{\kappa} + \frac{1}{\sigma}\right)\frac{di_s}{dx} \qquad \ldots(3.33)$$

the reaction rate is as follows [44]:

$$\frac{di_s}{dx} = ai \qquad \ldots(3.34)$$

the reaction rate for deposition of copper process is given by Buller-Volmer equation

$$i \quad i_o\left[\frac{C_s}{C_b}\exp\left(\frac{\alpha z F}{RT}\left(E \quad E_{eq}\right)\right) \quad \exp\left(\frac{(1 \quad \alpha) z F}{RT}\left(E \quad E_{eq}\right)\right)\right] \qquad \ldots(3.35)$$

substitution of equation (3.23) into equation (3.35) gives after some transformations

$$i = i_o \left[\begin{array}{c} \exp\left(\frac{\alpha z F}{RT}\left(E \quad E_{eq}\right)\right) \quad \exp\left(\frac{(1 \quad \alpha) z F}{RT}\left(E \quad E_{eq}\right)\right) \\ 1 - \frac{i_o}{i_l}\exp\left(-\frac{\alpha z F}{RT}\left(E - E_{eq}\right)\right) \end{array}\right] \qquad \ldots(3.36)$$

Now combining equations (3.33) with (3.34)

$$\frac{d^2E}{dx^2} = a\left(\frac{1}{\kappa} + \frac{1}{\sigma}\right)i \qquad \ldots(3.37)$$

The cathodic potential variation is found from the combination of equations (3.36), and (3.37)

$$\frac{d^2E}{dx^2} = ai_0\left(\frac{1}{\kappa} + \frac{1}{\sigma}\right)\left\{\frac{\exp\left(-\frac{\alpha zF}{RT}\left(E - E_{eq}\right)\right) - \exp\left(\frac{(1-\alpha)zF}{RT}\left(E - E_{eq}\right)\right)}{1 + \frac{i_2}{i_1}\exp\left(-\frac{\alpha zF}{RT}\left(E - E_{eq}\right)\right)}\right\} \qquad \ldots(3.38)$$

In order to solve equation (3.38) we need numerical values for the equilibrium potential, using Nernst equation as follows:

$$E_{eq} = E^{\circ} + \frac{RT}{zF}\ln(C_B) \qquad \ldots(3.39)$$

For copper deposition process E° value at 25 °C is 0.34 V as stated by [12], therefore equation (3.39) will be

$$E_{eq} = 0.34 + 0.012845 \times \ln(C_B) \qquad \ldots(3.40)$$

the concentration profile, and the potential profile are found from the solution of equations (3.24) and (3.38) simultaneously with the following boundary conditions concluded from equation (3.29)[26, 30].

$$\text{At } x = 0;\ \frac{dE}{dx} = 0 \qquad \ldots(3.41)$$

Because at $x = 0$ the solution current density equal to zero and the electrical conductivity of the copper particles (metal phase) is very large

$$\text{At } x = L;\ \frac{dE}{dx} = -\frac{i_s}{\kappa} = -\frac{I}{A\kappa} \qquad \ldots(3.42)$$

The negative sign in equation (3.42) is because of that the potential variation in the metal phase is so small, i.e. constant metal potential, so that the cathode potential will be equated to the solution potential.

3.5 Method of Solution

The governing equations (3.24) and (3.38) are needed to be solved simultaneously with the aid of boundary conditions given above (3.11) and (3.42).

Writing equation (3.38) in finite difference form using the general expression for the second derivative,

$$\frac{d^2y}{dx^2} = \frac{y_{e+1} - 2y_e + y_{e-1}}{\Delta x} \qquad \ldots(3.43)$$

so that equation (3.38) will be for interior nodes as

$$E_n = \frac{E_{e+1} - E_{e-1}}{2} - \frac{di_o}{2\kappa}\left\{\frac{\left[\exp\left(-\frac{\alpha zF}{RT}\left(E_e - E_{eq}\right)\right) - \exp\left(\frac{(1-\alpha)zF}{RT}\left(E_e - E_{eq}\right)\right)\right]}{1 - \frac{i_o}{i_{L_m}}\exp\left(-\frac{\alpha zF}{RT}\left(E_n - E_{eq}\right)\right)}\right\} \qquad \ldots(3.44)$$

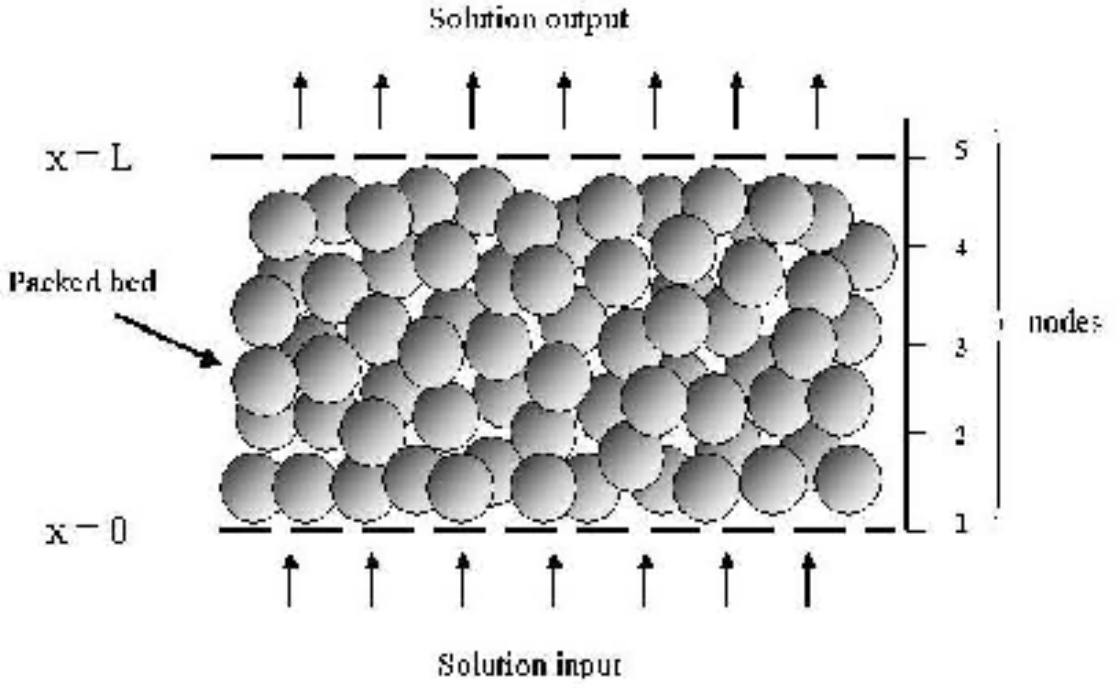

Fig. 3.3 Schematic diagram of the working electrode

Equation (3.44) is now should be written for all nodes starting from 1 and up to node n (see **Fig.3.3** above), noticing that for the outer nodes, boundary conditions for potential must be included, and this is done by introducing them in finite difference using the expression for the first derivative

$$\frac{dy}{dx} = \frac{y_{(i)} - y_{(i)}}{\Delta x} \qquad \ldots(3.45)$$

therefore the first boundary condition of the potential for the node at upstream will be

$$E_0 = E_1 \qquad \ldots(3.46)$$

Similarly the second boundary condition of the potential at the downstream will be as follows:

$$\frac{E_{n+1} - E_n}{\Delta x} = \frac{1}{\Delta \kappa}$$

from which the potential at the node after to the downstream node will be:

$$E_{n-1} = E_n - \Delta x \frac{1}{\Delta \kappa} \qquad \ldots(3.47)$$

The mass balance equation (3.24) is a second order linear differential equation can be solved analytically by the method of inverse operator if the term i / i_L is assumed as an instantaneous constant

$$D\frac{d^2 C_b}{dx^2} - u\frac{dC_b}{dx} - akC_b\frac{i}{i_L} = 0 \qquad \ldots(3.24)$$

equation (3.24) is written as

$$Dm^2 - um - ak\frac{i}{i_L} = 0 \qquad \ldots(3.48)$$

where m is given by

$$m = \frac{u - \sqrt{u^2 - 4D\left(ak\frac{i}{i_L}\right)}}{2D} \qquad \ldots(3.49)$$

where m should be evaluated for every node. Noticing that only one value is taken (see equation (3.49)) the other value will lead to unstable results.

Therefore the solution of equation (3.24) with m as an instantaneous constant is given by

$$C_b = C_1 e^{m_1 x} + C_2 e^{m_2 x} \qquad \ldots (3.50)$$

Since one value of m is taken equation (3.50) is reduced to

$$C_b = C_1 e^{m x} \qquad \ldots (3.51)$$

knowing the feed concentration at $x = 0$ the constant C_1 can be evaluated as follows:

$$C_b = C_f e^{m x} \qquad \ldots (3.52)$$

where C_f is feed concentration of Cu^{2+} ion

After equations were derived and arranged, the solution method is done by assuming an initial concentration and potential distribution as a start of calculations, then calculating the reaction rate using the assumed concentration and potential followed by calculating new potential and concentration values. The total solution current density is evaluated by integrating equation (3.34) numerically for the whole bed thickness using trapezoidal rule and check the initial assumed total current with that evaluated from numerical integration, i.e.

$$\frac{di_s}{dx} = ai \qquad \ldots (3.34)$$

Chapter Four

Results and Interpretation

The purpose behind this work is to create software that enables the electrochemical engineer to study the behavior of fixed bed electrochemical reactor (kinetic and hydrodynamic behaviors) at different operating parameters like feed concentrations, feed flow rate, bed thickness, and operating under mixed control process.

In this chapter the parameters mentioned above and their ranges are outlined, simulation input variables classified as groups are also outlined with results of simulation runs.

4.1 The Studied Parameters in This Work

- Concentration of the feed electrolyte was 0.5 M H_2SO_4 and 0.001 and 0.01 M $CuSO_4$
- Range of polarization curve studied is the mixed control region
- Electrolyte volumetric flow rates are 5, 10, and 50 ml./min
- Packing particles of spherical shape of diameter 3.5 mm
- Bed of a 4 cm diameter and of thickness 2, 3, and 4 cm
- Total current applied to the reactor is 80% of the limiting current corresponding to each of above conditions

4.2 Set of Simulation Runs

The simulation was carried out according to the following input parameters presented as runs, these are as follows:

Table 4.1 Input variables as runs of computer program

Run No.	Bed thickness (cm)	Flow rate (mL / min)	Cu^{2-} concentration (M)
1	2	5	0.001
2	2	10	0.001
3	2	50	0.001
4	3	5	0.001
5	3	10	0.001
6	3	50	0.001
7	4	5	0.001
8	4	10	0.001
9	4	50	0.001
10	2	5	0.01
11	2	10	0.01
12	2	50	0.01
13	3	5	0.01
14	3	10	0.01
15	3	50	0.01
16	4	5	0.01
17	4	10	0.01
18	4	50	0.01

4.3 Simulation Results

In this simulation the results are classified into two categories, major and minor results. The major results include concentration, overpotential, and

reaction rate distribution. The purpose behind using this convention is that the above-mentioned parameters are obtained directly from the solution of the model equations. The minor parameters that are solution current density and pressure drop are found from the major parameters.

4.3.1 Polarization Curves

Before presenting the results the polarization data are presented in Tables 4.2 and 4.3 below

Table 4.2 Current-potential values for 0.001 M Cu^{2+} ion, bed length of 2 cm at flow rates 5, 10, and 50 mL / min

5 mL / min flow rate		10 mL / min flow rate		50 mL / min flow rate	
I (A / m^2)	E (V)	I (A / m^2)	E (V)	I (A / m^2)	E (V)
0	0.25127	0	0.25127	0	0.25127
2.1477253	0.23127	2.41299	0.23127	2.7882	0.23127
4.0357949	0.21127	4.86599	0.21127	6.27172	0.21127
5.6040188	0.19127	7.26402	0.19127	10.7258	0.19127
6.688035	0.17127	9.17059	0.17127	15.3985	0.17127
7.3187219	0.15127	10.3926	0.15127	19.1614	0.15127
7.6461651	0.13127	11.0639	0.13127	21.5682	0.13127
7.8057968	0.11127	11.4009	0.11127	22.8855	0.11127
7.8811938	0.09127	11.5624	0.09127	23.5452	0.09127
7.9162687	0.07127	11.638	0.07127	23.8609	0.07127
7.93247	0.05127	11.673	0.05127	24.0087	0.05127
7.9399289	0.03127	11.6892	0.03127	24.0771	0.03127
7.9433576	0.01127	11.6966	0.01127	24.1087	0.01127

Table 4.3 Current-potential values for 0.01 M Cu^{2-} ion, bed length of 2 cm at flow rates 5, 10, and 50 mL / min

5 mL / min flow rate		10 mL / min flow rate		50 mL / min flow rate	
I (A / m^2)	E (V)	I (A / m^2)	E (V)	I (A / m^2)	E (V)
0	0.28085	0	0.28085	0	0.28085
3.65857	0.26085	3.72863	0.26085	3.80754	0.26085
9.02829	0.24085	9.38778	0.24085	9.81063	0.24085
17.8823	0.22085	19.2939	0.22085	21.0965	0.22085
30.9574	0.20085	35.409	0.20085	41.9366	0.20085
46.2628	0.18085	56.9449	0.18085	75.9197	0.18085
59.7838	0.16085	78.9048	0.16085	120.687	0.16085
69.0377	0.14085	95.8619	0.14085	165.443	0.14085
74.3172	0.12085	106.352	0.12085	199.381	0.12085
77.0209	0.10085	111.977	0.10085	220.11	0.10085
78.3291	0.08085	114.764	0.08085	231.142	0.08085
78.9447	0.06085	116.09	0.06085	236.585	0.06085
79.2305	0.04085	116.709	0.04085	239.171	0.04085
79.3625	0.02085	116.996	0.02085	240.378	0.02085
79.4232	0.00085	117.128	0.00085	240.936	0.00085

Tables 4.2 and 4.3 show the polarization behavior for the bed length of 2 cm at various flow rates and Cu^{2-} ion feed concentrations, where the current density (I) attained at a given cathode potential value will be greater when flow rate is increased. The limiting current in the polarization curve was calculated according to the following method.

The concentration distribution at pure limiting current controlled process may be calculated analytically from reducing equation (3.23) as follows:

$$D\frac{d^2C_b}{dx^2} - u\frac{dC_b}{dx} = ak\left(C_b - C_s\right) \qquad \ldots(3.23)$$

at limiting current C_s (surface concentration) = 0 and neglecting the second derivative term equation (3.23) (small D) will be reduced to the following form:

$$\frac{dC_b}{dx} = -\frac{akC_b}{u} \qquad \ldots(4.1)$$

equation (4.1) is integrated using the boundary condition: at x = 0, $C_b = C_f$ where C_f is copperic sulfate feed concentration, to get

$$C_b = C_f e^{\left[-\frac{ak}{u}x\right]} \qquad \ldots(4.2)$$

Also the total current when the reactor is operating at limiting current is:

$$I_L = \int_0^L a \cdot i_L(x)\,dx \qquad \ldots(4.3)$$

where $i_L(x)$ is the instantaneous limiting current found from

$$i_L = zFkC_b$$

The concentration C_b is given as a function of distance in equation (4.2).

After introducing C_b into the expression of i_L and substitution of the resultant expression into equation (4.3) and carrying out integration we will get the total current density if all bed is working under limiting current density [32]

$$I_L = uzFC_f\left[1 - e^{\left(-\frac{ak}{u}L\right)}\right] \qquad \ldots(4.4)$$

where I_L is total current density if the whole bed is operating at limiting current conditions and can be calculated if the mass transfer coefficient, velocity of electrolyte, feed concentration of Cu^{2+}, surface area of bed, and bed length are known. The equilibrium potentials can be calculated from Nernst equation and from Butler-Volmer equation, equation (3.35), with the obtained I_L value the polarization curve can be drawn by setting the initial potential to be that of equilibrium value and using a potential step of −0.01 V

until limiting current is reached. Noticing that the exchange current density is calculated from the equation (3.18).

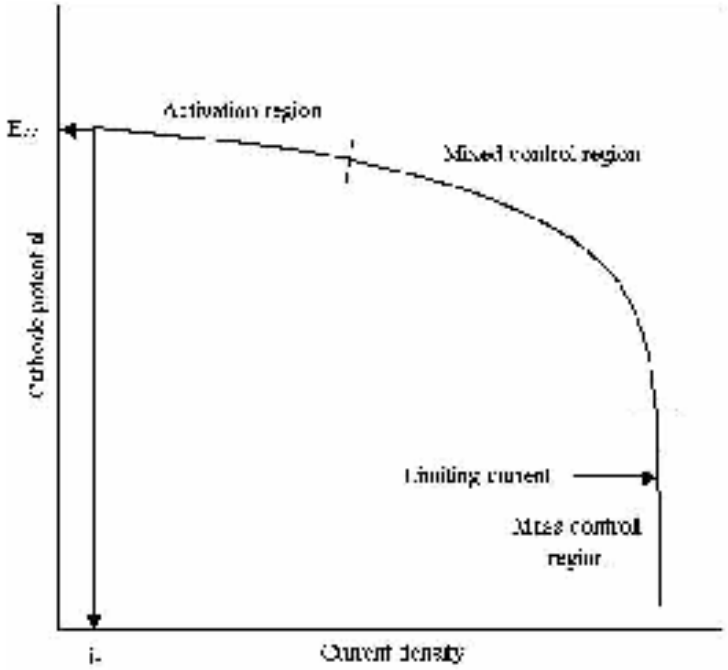

Figure 4.1 Typical polarization curve

Figure 4.1 above shows the polarization curve regions activation, mixed control, and mass control

4.3.2 Major Parameters Results

The results given below are of the major parameters Tables 4.5 through 4.10, each table for one flow rate value, are presented in this section. The results of the first two sets are outlined in this chapter while the rest of the Tables are included in Appendix A.

The total applied current to the reactor in all runs performed in this work was set to be of 80% of the corresponding limiting current calculated by equation (4.4), the reason is explained in chapter five, after the total current density is set the method of solution can now be applied. In each run the total

current applied to the reactor can be found from the numerical integration of equation (3.33) for the whole bed. The criterion of reaching the right values of potential and concentration is the match between the set total current and the one calculated from equation (3.33) for the lowest percent error as possible.

Here is below the values of the set total current density (I) and the closest calculated total current after numerous iterations are made.

Table 4.4 Values of set total current, corresponding limiting current, calculated total current, and % error of the calculated current density

Run No.	Total current set initially (mA)	Total limiting current (mA)	Total current calculated (mA)	% Error
1	7.98816	9.98558	8.01723	0.36009
2	11.76509	14.70636	11.74679	0.15553
3	24.26368	30.32960	24.24307	0.08496
4	9.86263	12.32829	9.87115	0.08640
5	15.44184	19.30229	15.45932	0.11325
6	34.62128	43.27660	36.36456	5.03529
7	11.01650	13.77062	10.97488	0.37780
8	18.15054	22.68818	18.16797	0.09601
9	43.95115	54.93894	44.80151	1.93478
10	79.89679	99.87099	79.89998	0.00399
11	117.67286	147.09108	118.08638	0.35141
12	242.69297	303.36621	247.63829	2.03769
13	98.63753	123.29691	98.29241	0.34988
14	154.44263	193.05329	158.77382	2.80440
15	346.28868	432.86085	376.22757	8.64561
16	110.17422	137.71778	112.92380	2.49566
17	181.52927	226.91158	185.64952	2.26975
18	439.60266	549.50333	467.43566	6.33140

where the % error is defined as follows:

$$\% \text{ error} = \left| \frac{\text{total current set} - \text{total current calculated}}{\text{total current set}} \right| \times 100\% \qquad \ldots(4.5)$$

Table 4.5 Major results of run 1 (0.001 M Cu^{2+} ion concentration, 5 mL / min flow rate, and 2 cm bed length)

Distance (m)	Overpotential (V)	Reaction Rate (A/m^2)	Concentration (gmol / L)
0	-0.01959	0.4141	0.001
0.002	-0.019636	0.3912	0.00094
0.004	-0.019733	0.3694	0.00087
0.006	-0.019883	0.3486	0.00082
0.008	-0.020091	0.3287	0.00076
0.01	-0.02036	0.3096	0.0007
0.012	-0.020692	0.2911	0.00065
0.014	-0.021092	0.2733	0.0006
0.016	-0.021563	0.2561	0.00056
0.018	-0.022107	0.2394	0.00051
0.02	-0.022727	0.2232	0.00047

Table 4.6 Major results of run 2 (0.001 M Cu^{2+} ion concentration, 10 mL / min flow rate, and 2 cm bed length)

Distance (m)	Overpotential (V)	Reaction Rate (A/m^2)	Concentration (gmol / L)
0	-0.02254	0.5428554	0.001
0.002	-0.02262	0.523864	0.000957
0.004	-0.02278	0.5059224	0.000916
0.006	-0.02303	0.488843	0.000875
0.008	-0.02337	0.4721398	0.000835
0.01	-0.0238	0.4565342	0.000796
0.012	-0.02432	0.4409623	0.000757
0.014	-0.02494	0.4255802	0.000719
0.016	-0.02565	0.4102699	0.000681
0.018	-0.02647	0.3949435	0.000645
0.02	-0.0274	0.3795455	0.000609

Table 4.7 Major results of run 3 (0.001 M Cu^{2+} ion concentration, 50 mL / min flow rate, and 2 cm bed length)

Distance (m)	**Overpotential (V)**	**Reaction Rate (A/m^2)**	**Concentration (gmol / L)**
0	-0.029537	0.967733	0.001
0.002	-0.029729	0.958377	0.0009846
0.004	-0.030114	0.951559	0.0009692
0.006	-0.030692	0.946887	0.0009536
0.008	-0.031465	0.943919	0.0009378
0.01	-0.032431	0.942179	0.0009218
0.012	-0.033591	0.941181	0.0009054
0.014	-0.034944	0.940455	0.0008886
0.016	-0.036489	0.939561	0.0008716
0.018	-0.038228	0.938127	0.0008542
0.02	-0.040016	0.935829	0.0008367

Table 4.8 Major results of run 4 (0.001 M Cu^{2+} ion concentration, 5 mL / min flow rate, and 3 cm bed length)

Distance (m)	**Overpotential (V)**	**Reaction Rate (A/m^2)**	**Concentration (gmol / L)**
0	-0.016342	0.37441	0.001
0.003	-0.016419	0.34741	0.00091
0.006	-0.016584	0.32207	0.00083
0.009	-0.016844	0.2981	0.00075
0.012	-0.017207	0.27524	0.00068
0.015	-0.017681	0.25323	0.00061
0.018	-0.018272	0.23193	0.00054
0.021	-0.018989	0.21124	0.00048
0.024	-0.019837	0.19116	0.00042
0.027	-0.020826	0.17176	0.00037
0.03	-0.021963	0.15319	0.00032

Table 4.9 Major results of run 5 (0.001 M Cu^{2+} ion concentration, 10 mL / min flow rate, and 3 cm bed length)

Distance (m)	Overpotential (V)	Reaction Rate (A/m^2)	Concentration (gmol / L)
0	-0.0196799	0.5059599	0.001
0.003	-0.0198335	0.4826252	0.000941
0.006	-0.020148	0.461159	0.000883
0.009	-0.0206294	0.4409531	0.000826
0.012	-0.0212827	0.421428	0.000770
0.015	-0.0221127	0.4020786	0.000715
0.018	-0.0231245	0.3825147	0.000661
0.021	-0.0243235	0.3624904	0.000608
0.024	-0.0257163	0.3419168	0.000557
0.027	-0.0273103	0.3208555	0.000507
0.03	-0.0291145	0.2994925	0.000461

Table 4.10 Major results of run 6 (0.001 M Cu^{2+} ion concentration, 50 mL / min flow rate, and 3 cm bed length)

Distance (m)	Overpotential (V)	Reaction Rate (A/m^2)	Concentration (gmol / L)
0	-0.03022568	0.9780065	0.001
0.003	-0.03065272	0.9653506	0.0009766
0.006	-0.03150076	0.9575359	0.0009531
0.009	-0.03278761	0.9531005	0.0009291
0.012	-0.03418778	0.9501722	0.0009044
0.015	-0.03660217	0.9481381	0.0008791
0.018	-0.0391251	0.9447987	0.0008532
0.021	-0.04205242	0.9394764	0.0008269
0.024	-0.0453824	0.9315628	0.0008005
0.027	-0.04911642	0.9208066	0.0007743
0.03	-0.05325948	0.9072571	0.0007485

4.3.2.1 Concentration Distribution

In general the concentration is decreasing as the electrolyte is traveling in the bed (from upstream to downstream), in the concentration distribution for runs 1, 2, and 3 (see Tables 4.5, 4.6, and 4.7) the effect of increasing flow rate will lead to cause the concentration at downstream (top of bed) to increase, i.e. that is conversion is decreasing. e.g. at flow rate of 5 mL / min the outlet concentration achieved is 0.00047 M, at flow rate of 10 mL / min the concentration at the top of bed is 0.000609 M while at 50 mL / min the concentration is 0.0008367 M.

When the bed length is increased to 3 cm the concentration distribution for runs 4, 5, and 6 (see Tables 4.8, 4.9, and 4.10) for the three studied flow rate values was found to have a concentration drop manner similar to that of runs 1, 2, and 3 except that the downstream concentration obtained is lower than that obtained in runs 1, 2, and 3 (higher conversion achieved) such that at flow rate of 5 mL / min the outlet concentration achieved is 0.00032 M, at flow rate of 10 mL / min the concentration at the top of bed is 0.000467 M while at 50 mL / min the concentration is 0.0007486 M. For runs 7, 8, and 9 (see Tables A.1-A.3 Appendix A) a flow rate of 5 mL / min gives an outlet concentration of 0.00021 M, flow rate of 10 mL / min the concentration at the top of bed is 0.000311 M while at 50 mL / min the concentration is 0.0006712 M. The 0.01 M concentration (see Appendix A Tables A.4 - A.12) for the 2 cm bed thickness at a flow rate of 5 mL / min the concentration of downstream will be 0.004077 M, flow rate of 10 mL / min gives 0.00559 M top concentration, and 50 mL / min flow rate gives 0.008129 M at the top. Increasing the flow rate will cause the downstream concentration to increase, i.e. conversion will decrease. Examination the results of the bed lengths 3 and 4 cm leads to the same interpretation that was concluded when the same bed

lengths were used for the 0.001 M Cu^{2-} feed concentration at which increasing bed length will increase the conversion or decrease the downstream concentration.

4.3.2.2 Overpotential Distribution

The overpotential results as well as reaction rate results were given together with the concentration distribution. The overpotential is starting from a relatively small value (cathode potential is close to the equilibrium potential) at the upstream (x = 0) and increases along the bed until it reaches its maximum value at the downstream (x = L). The effect of flow rate on overpotential is to increase the overpotential. The effect of increasing bed length is causing the overpotential to reach higher values. As the copperic sulfate concentration is increased the overpotential obtained will be higher than that obtained at low concentration. For the 0.01 M concentration the overpotential obtained is higher than that for the 0.001 M concentration

4.3.2.3 Reaction Rate Distribution

The reaction rate or copper deposition is starting from some value at the bed upstream and increases or decreases according to certain situations discussed briefly in chapter five, along the bed until it reaches its final value at the bed downstream. The effect of flow rate on reaction rate will be increasing the reaction rate so that the higher the flow velocity the higher the reaction rate value obtained at the bed downstream. The effect of increasing bed length is causing the reaction rate to be of low values at the bed downstream. As the copperic sulfate concentration is increased the reaction rate obtained will be higher than that obtained at low concentration. For the

0.01 M concentration the reaction rate obtained is higher than that for the 0.001 M concentration.

4.3.3 Minor Parameters Results

The results given below are of the minor parameters (solution current density distribution, pressure drop distribution and collection effectiveness). The results are presented individually.

4.3.3.1 Solution Current Density Distribution

The solution current density in A / m^2 or current in electrolyte solution results here in this chapter are of the first nine runs, the remaining runs are included in Appendix A.

Table 4.11 Solution current density distribution for 0.001 M Cu^{2-} ion concentration, 5, 10, and 50 mL / min flow rate, and 2 cm bed length

Distance (m)	5 mL / min	10 mL / min	50 mL / min
0	0	0	0
0.002	0.821783	1.0885	1.9655
0.004	1.597986	2.1393	3.9144
0.006	2.330733	3.1544	5.8516
0.008	3.021933	4.1353	7.7811
0.010	3.673284	5.0833	9.7057
0.012	4.286293	5.9991	11.628
0.014	4.862302	6.8834	13.548
0.016	5.402524	7.7363	15.466
0.018	5.908079	8.558	17.382
0.020	6.379907	9.3478	19.292

Table 4.12 Solution current density distribution for 0.001 M Cu^{2+} ion concentration, 5, 10, and 50 mL / min flow rate, and 3 cm bed length

Distance (m)	5 mL / min	10 mL / min	50 mL / min
0	0	0	0
0.003	1.101846	1.5132	2.9746
0.006	2.129575	2.9578	5.9178
0.009	3.078837	4.3386	8.8423
0.012	3.956414	5.6586	11.756
0.015	4.76531	6.9191	14.662
0.018	5.507915	8.12	17.56
0.021	6.18624	9.2603	20.444
0.024	6.802159	10.339	23.308
0.027	7.357662	11.353	26.143
0.030	7.855212	12.302	28.938

Table 4.13 Solution current density distribution for 0.001 M Cu^{2+} ion concentration, 5, 10, and 50 mL / min flow rate, and 4 cm bed length

Distance (m)	5 mL / min	10 mL / min	50 mL / min
0	0	0	0
0.004	1.3164	1.86361	3.4667
0.008	2.523447	3.631799	6.9151
0.012	3.628011	5.312292	10.169
0.016	4.631525	6.907369	14.05
0.020	5.545529	8.414761	17.681
0.024	6.3625	9.829302	21.34
0.028	7.086811	11.14487	24.997
0.032	7.72062	12.35622	28.619
0.036	8.267516	13.46038	32.179
0.040	8.733532	14.45761	35.652

In general the solution current density is starting from zero at the bed upstream (x = 0) and increasing as the electrolyte is penetrating the bed until the downstream where the solution current density reaches its maximum value (total current density applied to the reactor).

Table 4.11 shows that the solution current density for 0.001 M Cu^{2+} ion concentration at the upstream (x = 0) is zero always and the downstream solution current density is increasing with increasing flow rate. Table 4.12 gives the solution current density results for bed length of 3 cm. It is seen that the solution current density at the downstream reaches higher values from those obtained with the 2 cm bed thickness. And finally examination of the feed concentration effect on the downstream solution current density shows an increase in the downstream current density of the electrolyte as the feed concentration is increased.

4.3.3.2 Pressure Drop Distribution

The pressure drop was found from equation (3.2) with the aid of equations (3.3) and (3.4) to give the permeability and coefficient of inertial forces

$$\frac{\Delta P}{L} = \frac{\mu}{Pm(\varepsilon)}.u + \frac{c(\varepsilon)\rho}{\sqrt{Pm}}u^2 \qquad \ldots(3.2)$$

$$Pm = \frac{\varepsilon^3 d}{150(1-\varepsilon)} \qquad \ldots(3.3)$$

$$c(\varepsilon) = \frac{1.75}{\sqrt{150\varepsilon^3}} \qquad \ldots(3.4)$$

and using equations (3.11) and (3.12) to calculate initial and instantaneous porosity

$$\varepsilon = 0.375 + 0.34\frac{d}{D_H} \qquad \ldots(3.11)$$

$$\varepsilon = \varepsilon_o - \frac{m_o}{\rho_m V_L}\left[1 - \frac{C_b}{C_b}_{x=x} \right] \qquad \ldots(3.12)$$

The pressure drop is now calculated with respect to the entrance pressure (at x = 0), such that $\Delta P = P_{x=0} - P_{x=x}$ where $P_{x=0}$ is the pressure at the bed upstream and $P_{x=x}$ is the pressure at any increment up to the downstream. So that equation (3.2) will be rewritten as follows:

$$\frac{\Delta P}{\Delta x} = \frac{\mu}{Pm(\varepsilon)^{n+1}} + \frac{c(\varepsilon)\rho}{\sqrt{Pm}}^{n} \qquad \ldots(4.6)$$

Table 4.14 Pressure drop as a function of x for 0.001 M Cu^{2+} ion concentration, 5, 10, and 50 mL / min flow rate, and 2 cm bed length

x	5 mL / min flow rate	10 mL / min flow rate	50 mL / min flow rate
0	0	0	0
0.002	5.5828E-05	0.000117859	0.000837436
0.004	0.000111656	0.000235719	0.001674872
0.006	0.000167484	0.000353578	0.002512309
0.008	0.000223312	0.000471438	0.003349747
0.01	0.000279141	0.000589298	0.004187185
0.012	0.000334968	0.000707157	0.005024624
0.014	0.000390796	0.000825017	0.005862063
0.016	0.000446624	0.000942877	0.006699503
0.018	0.000502452	0.001060736	0.007536943
0.02	0.000558828	0.001178596	0.008374384

Table 4.15 Pressure drop as a function of x for 0.001 M Cu^{2+} ion concentration, 5, 10, and 50 mL / min flow rate, and 3 cm bed length

x	5 mL / min flow rate	10 mL / min flow rate	50 mL / min flow rate
0	0	0	0
0.003	8.3742L-05	0.000176789	0.001256154
0.006	0.000167484	0.000353578	0.002512309
0.009	0.000251226	0.000530368	0.003768464
0.012	0.000334968	0.000707157	0.00502462
0.015	0.00041871	0.000883946	0.006280778
0.018	0.000502452	0.001060736	0.007536936
0.021	0.000586194	0.001237525	0.008793095
0.021	0.000669936	0.001414315	0.010049254
0.027	0.000753678	0.001591104	0.011305415
0.03	0.000837420	0.001767894	0.012561577

Table 4.16 Pressure drop as a function of x for 0.001 M Cr^{3+} ion concentration, 5, 10, and 50 mL / min flow rate, and 4 cm bed length

x	5 mL / min flow rate	10 mL / min flow rate	50 mL / min flow rate
0	0	0	0
0.004	0.000111656	0.000235719	0.001674872
0.008	0.000223312	0.000471438	0.003349745
0.012	0.000334968	0.000707157	0.005024618
0.016	0.000446624	0.000942876	0.006699491
0.02	0.000558280	0.001178595	0.008374369
0.024	0.000669936	0.001414314	0.010049246
0.028	0.000781592	0.001650033	0.011724125
0.032	0.000893248	0.001885753	0.013399004
0.036	0.001004904	0.002121472	0.015073885
0.04	0.001116560	0.002357192	0.016748766

The pressure drop values given in Tables 4.14 - 4.16 and A.16-A.18 are calculated using equation (4.6). it is clear that pressure drop is directly proportional with electrolyte velocity such that increasing flow rate will lead to increase the pressure drop obtained. The effect of increasing copper ion concentration is seen to decrease the pressure drop except at flow rate 50 mL / min where the opposition is occurred. The pressure drop is increasing as bed depth is increased.

Chapter Five

Discussion

In this chapter the figures, and their discussions, that describe the behavior of the major and minor simulation parameters are presented. These simulation results are classified into sections where feed concentration, volumetric flow rate, and bed length changes are studied to understand the reactor response to them.

- First, Section 5.1 is devoted for discussing the concentration distribution, the reaction rate (copper deposition) distribution, and overpotential distribution in the bed (cathode) under various flow rates, and feed concentrations as a function of bed thickness.
- Section 5.2 is devoted for discussing the minor results, i.e. current distribution and pressure drop.

First before presenting simulation results some of the assumptions made are explained. The first assumption is that of the one-dimensional model because of negligible dispersion effects in flow-through electrode so that the assumption of one-dimensional flow will save unnecessary time and effort wasted in solving the governing equations of two-dimensional models encountered in flow-by electrodes. Also the reason behind modeling with a flow direction from upstream to the downstream is that the electrolyte is allowed to penetrate into the deep portions of the bed and more contact will take place rather than flow from top of reactor where gravity as well as the flow itself will accelerate the electrolyte inside the bed. This advantage is well apparent in experimental works. The assumption of constant mass transfer

coefficient along the bed will lead to a noticeable error when comparisons with experimental works will be made. This assumption is widely used in such works as well as non-plug flow effects can cause the predicted values by simulation to deviate from experimental results [24, 26]. Finally the total current applied was chosen to be 80% of the corresponding total limiting required because the fraction 0.8 ensures that the reaction is taking place at the mixed controlled region of the polarization curve, and another reason is that the limiting current increases significantly as the Cu^{2+} concentration and flow rate are increased, so that if a certain value of total current was set for a low flow rate and concentration for mixed controlled the same current value for a higher concentration and flow rate might give operation under activation control.

5.1 Major Results

The major results (polarization curves, concentration distribution, overpotential distribution, and reaction rate distribution) are presented in chapter four and Appendix A. The discussion of these parameters variation is presented as sub-sections as will be shown below.

5.1.1 Polarization Curves

The following elected polarization curves for some of the performed runs in this simulation are chosen because they do represent the whole possible behavior of current-potential (polarization) diagrams under variable flow rates and different concentration of copperic sulfate. Current density is

taken with respect to cross sectional area of the electrochemical packed bed as described in the literature [25].

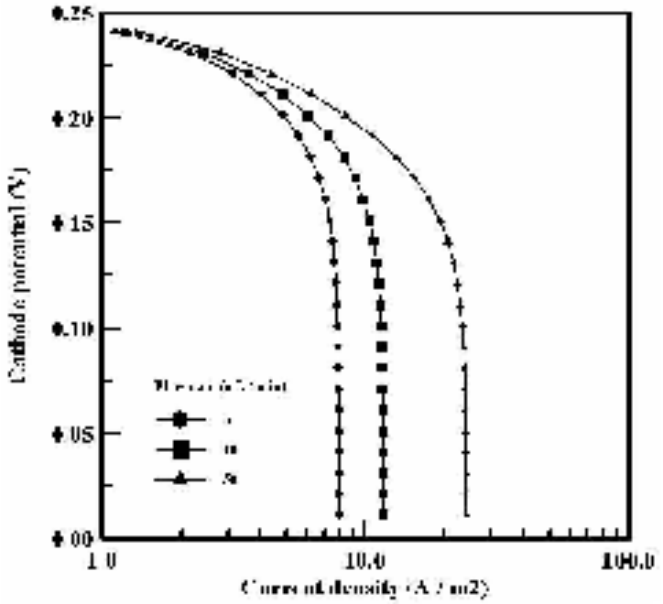

Figure 5.1 Polarization curve for 0.001 M Cu^{2+} ion solution and bed length of 2 cm at flow rates of 5, 10, and 50 mL /min

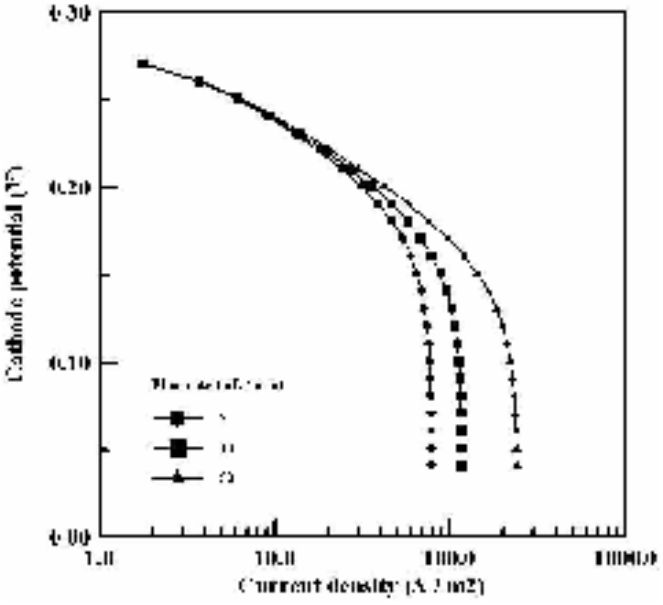

Figure 5.2 Polarization curve for 0.01 M Cu^{2+} ion solution and bed length of 2 cm at flow rates of 5, 10, and 50 mL /min

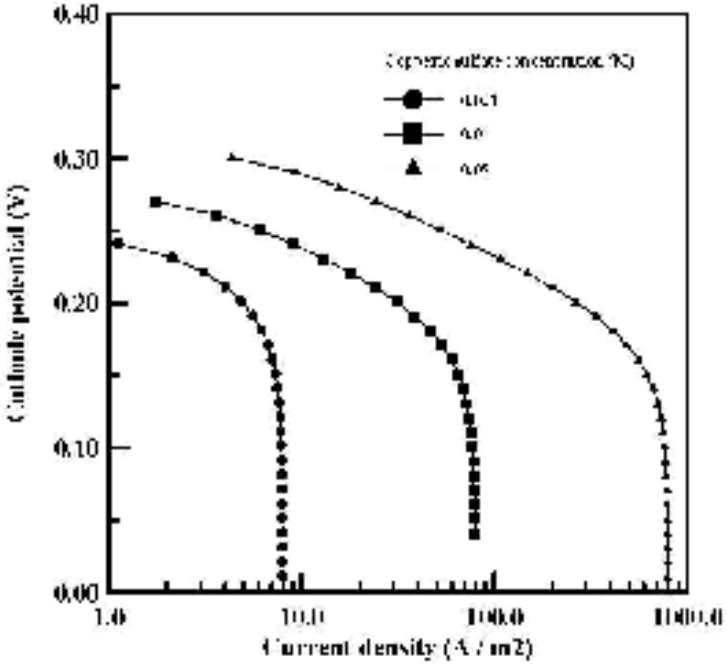

Figure 5.3 Polarization curve at flow rate of 5 mL /min for bed length of 2 cm in 0.001, 0.01, 0.05 M Cu^{2} ion solution

Figures 5.1 and **5.2** show that when flow rate is increased the polarization curve will be shifted to the right regardless the other effects (feed concentration and bed length) but the first point in the curve remains constant because the equilibrium potential is concentration dependent only (obtained from Nernst equation). The reason behind the shifting of the curves at flow rates of 10 and 50 mL / min to the right of 5 mL / min flow rate is that increasing the limiting current obtained due to increase in mass transfer coefficient. **Fig. 5.3** shows the effect of copperic sulfate concentration on the current density-potential diagram. an exceptional run for concentration of 0.05 M Cu^{2} ion is performed in order to clarify the concentration effect. The increasing of Cu^{2+} ion in the feed will not just shift the curve only but it will lead to change the first point in the curve because of the change in equilibrium potential which was stated to be concentration dependent only, the shift is also due to increase in limiting current when concentration is increased. The

effect of bed length on the polarization curve is quite the same as the effect of flow rate as follows.

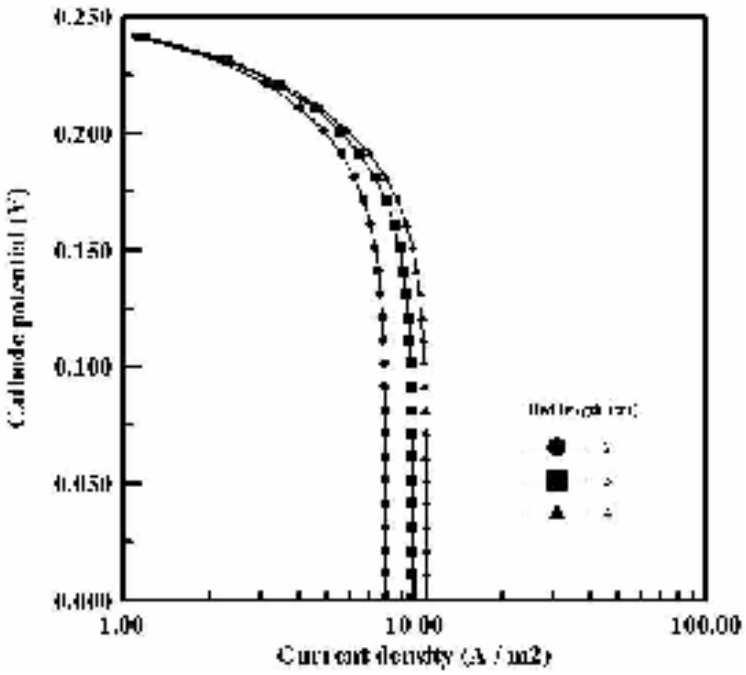

Figure 5.4 Polarization curve at flow rate of 5 mL /min, 0.01 M Cu^{2} ion solution and bed lengths of 2, 3, and 4 cm

Equation (4.4) is now subjected to a comparison with the experimental work of Bennion and Newman [45] to show the extent of its accuracy in predicting the limiting current density. The parameters of Ref. [45] are copperic sulfate concentration of 0.01 M, bed diameter and length are 10.1 and 6 cm respectively, specific surface area is 2500 m^{-1}, flow rates of electrolyte 8, 12, and 16 mL / min, and the mass transfer coefficient values presented in Table 5.1 below.

Table 5.1 Experimental and predicted limiting current density by equation (4.4) for the conditions of Ref. [45]

Flow rate (ml /min)	Mass transfer coefficient Ref. [45] (m /s)	I_L Ref. [45] (mA) Experimental	I_L predicted by equation (4.4) (mA)	% error
8	$1.315*10^{-6}$	260	257.265	1.0515
12	$1.62*10^{-6}$	395.78	385.876	2.5023
16	$1.922*10^{-6}$	541.66	514.444	5.024

It can be seen that the error introduced by using equation (4.4) for the prediction of the limiting current is insignificant and it may be due to the difference in reading the values from the polarization curve of Ref. [45]. Hence equation (4.4) is reliable for use for simulation purposes. An important notion should be revealed that equation (4.4) calculates the limiting current density (A / m^2) while Ref. [45] gave limiting current in mA, therefore to convert current density in (A / m^2) to current in A the current density should be multiplied by the cross sectional area of the bed as mentioned before.

5.1.2 Concentration Distribution

The concentration of copper ion in the electrolyte is decreasing as it passes through the cathode because of the deposition reaction that is occurring in the bed, which would cause the concentration in the electrolyte to drop.

5.1.2.1 Effect of Flow Rate on Concentration Distribution

The effect of flow rate on the concentration distribution is shown below in **Figs. 5.5-5.10**

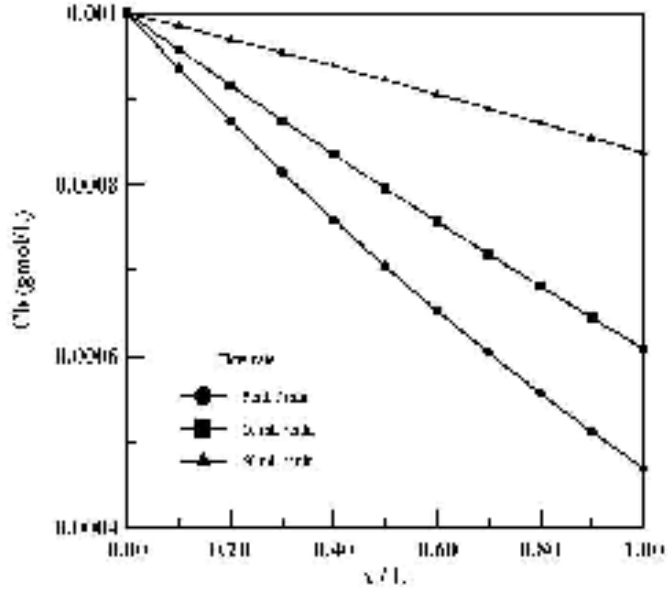

Figure 5.5 Concentration distribution in 0.001M Cu^{2+} ion solution and 2cm bed thickness

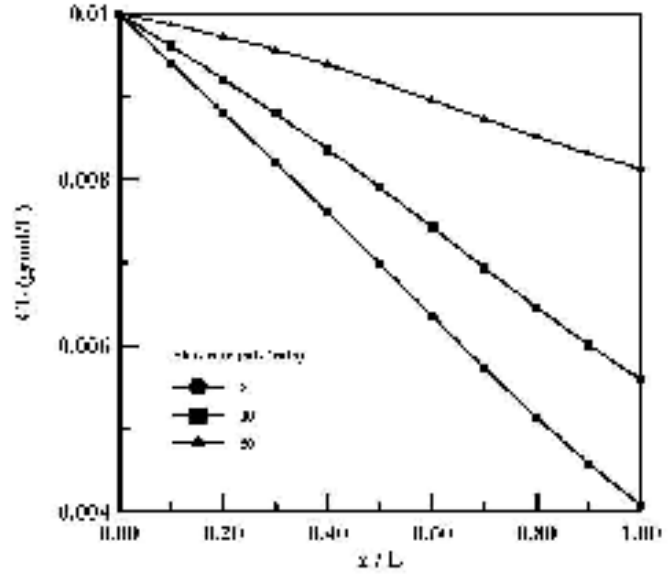

Figure 5.6 Concentration distribution in 0.01M Cu^{2+} ion solution and 2cm bed thickness

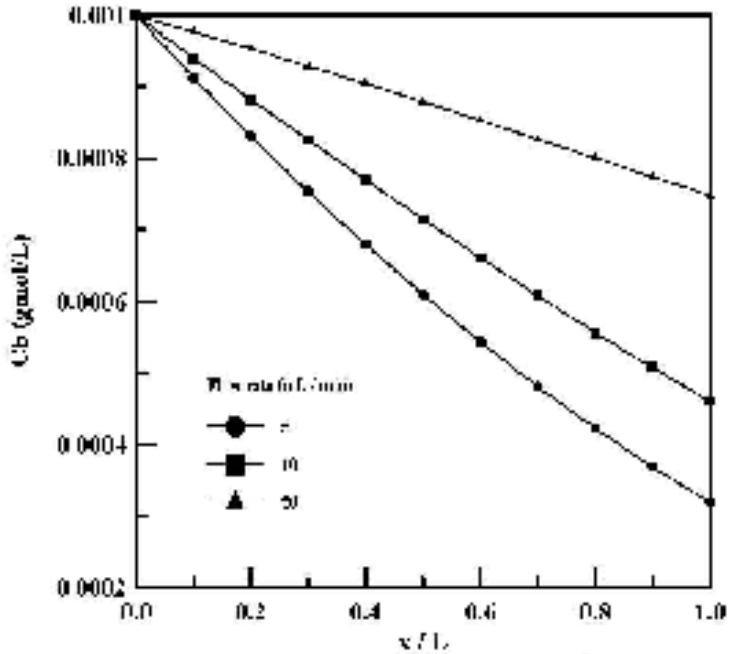

Figure 5.7 Concentration distribution in 0.001M Cu^{2+} ion solution and 3cm bed thickness

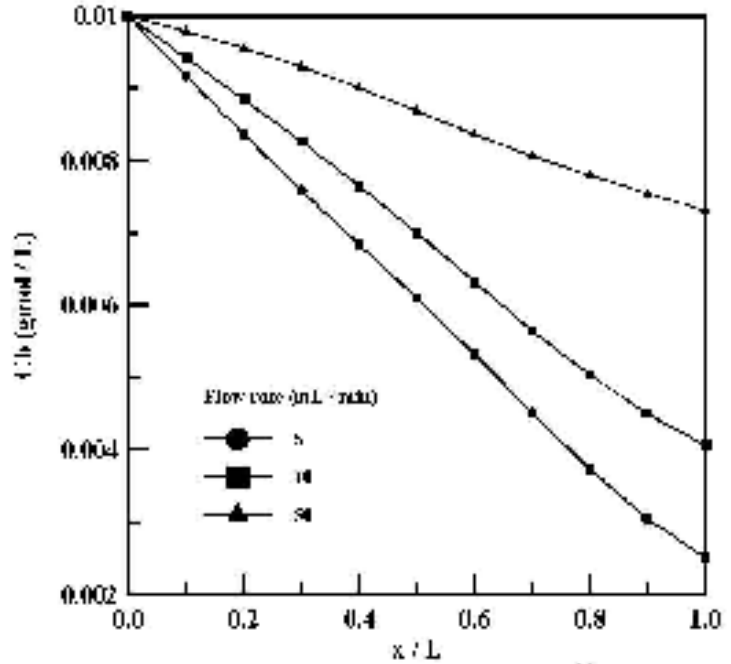

Figure 5.8 Concentration distribution in 0.01 M Cu^{2+} ion solution and 3cm bed thickness

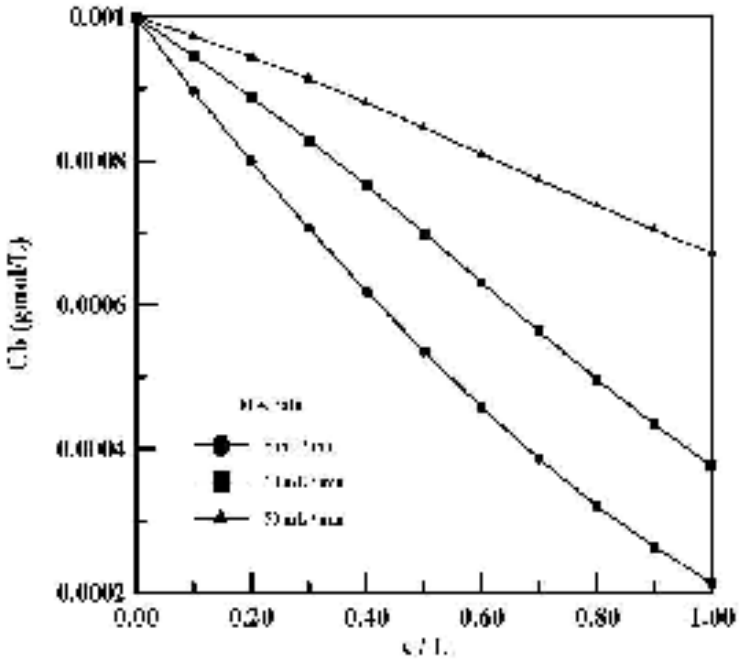

Figure 5.9 Concentration distribution for 0.001M Cu^{2+} ion solution and 4cm bed thickness

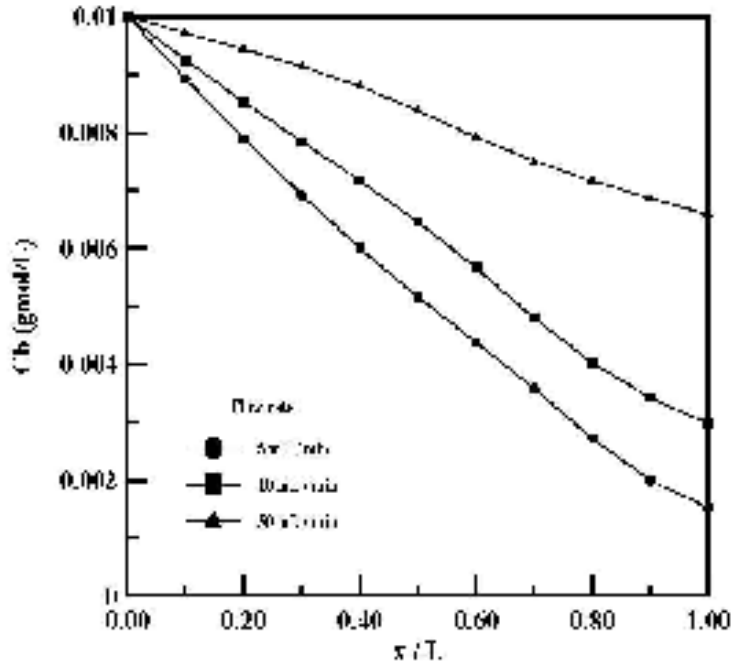

Figure 5.10 Concentration distribution in 0.01M Cu^{2+} ion solution and 4cm bed thickness

Examining **Figs. 5.5-5.10** show a common behavior which is a higher concentration drop to occur when flow rate is decreasing and vice versa. The reason behind this behavior is that at high flow rates the concentration drop within the packed bed is small under conditions of rapid diffusion, high flow rates, and large mass transfer coefficients as this was proved by the experimental work of Alkire and Gracon (1975), because the reaction rate becomes non-uniform within the porous electrode as well as the potential distribution, and consequently the current distribution is non-uniform. The non-uniformity in reaction rate distribution will be shown in the reaction rate section later.

While for low flow rates the residence time of the copper ions will be greater than that of high flow rates therefore further conversion would be achieved.

5.1.2.2 Effect of Bed Length on Concentration Distribution

The effect of increasing bed length will cause the downstream concentration to decrease much more because more reaction is allowed to take place especially when knowing that the maximum reaction is occurring in the last section of the bed (downstream) therefore concentration is reduced much greater. **Fig.5.11** and **Fig.5.12** show the concentration distribution for a copperic sulfate feed concentration of 0.001 M and flow rates of 5 and 50 ml. / min plotted separately versus dimensionless length (x / L) for the three bed lengths 2, 3, and 4 cm.

While **Fig. 5.13** and **Fig.5.14** show the concentration distribution for a copperic sulfate feed concentration of 0.01 M and same flow rates and bed lengths.

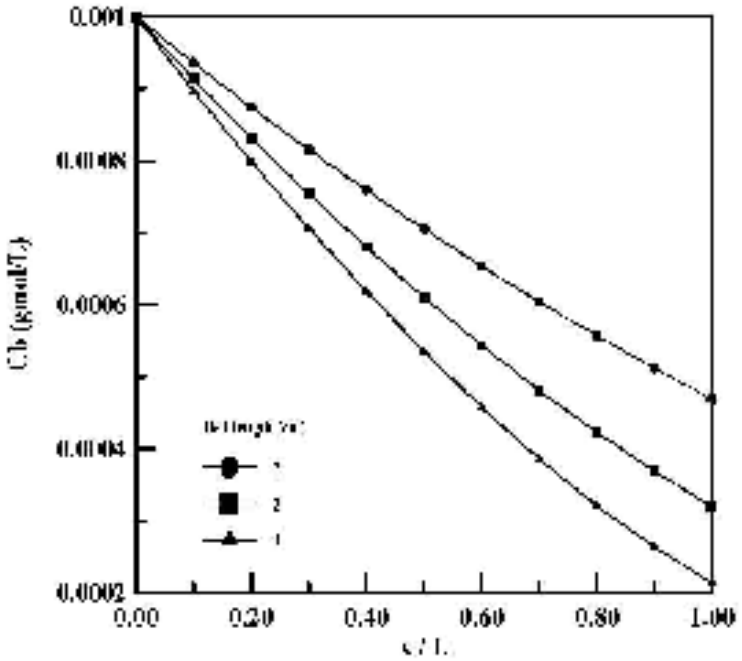

Figure 5.11 Concentration distribution in 0.001M Cu^{2+} ion solution and flow rate of 5 mL / min for bed thickness of 2, 3, and 4 cm

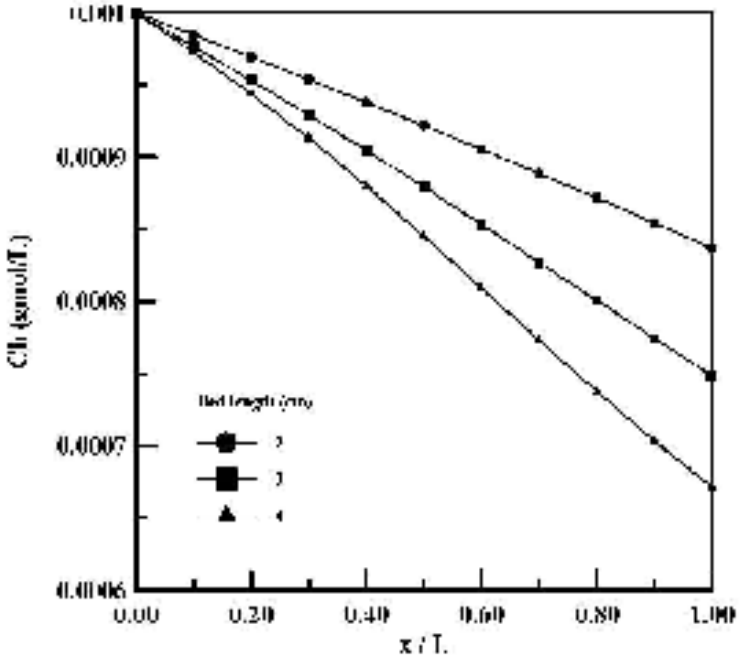

Figure 5.12 Concentration distribution in 0.001M Cu^{2+} ion solution and flow rate of 50 mL / min for bed thickness of 2, 3, and 4 cm

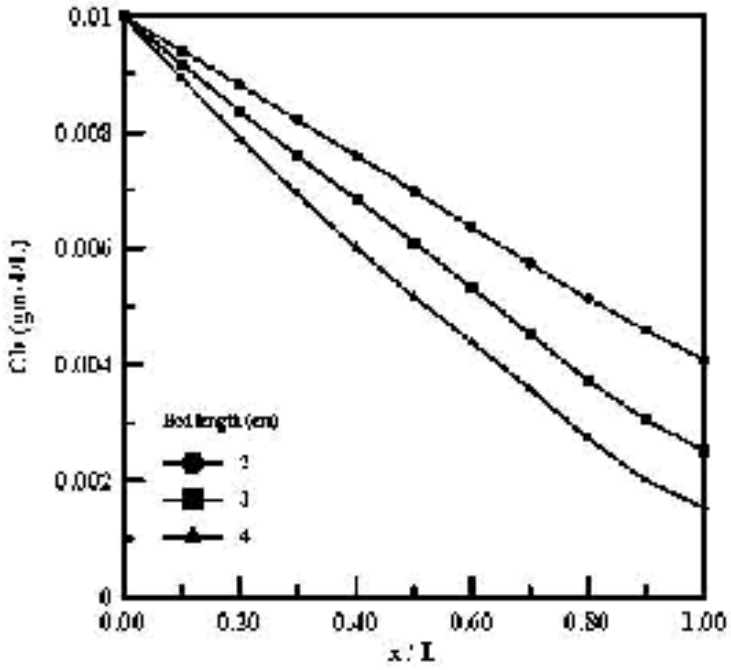

Figure 5.13 Concentration distribution in 0.01M Cu^{2+} ion solution and flow rate of 5 mL / min for bed thickness of 2, 3, and 4 cm

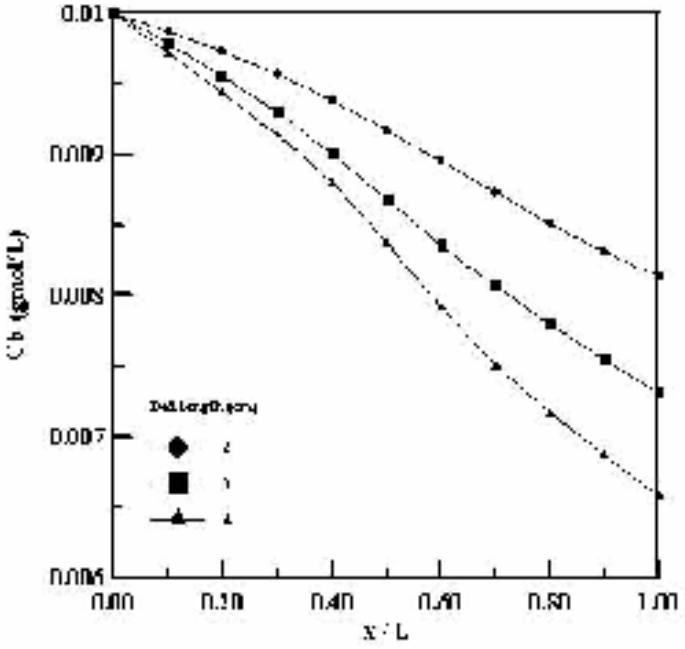

Figure 5.14 Concentration distribution in 0.01M Cu^{2+} ion solution and flow rate of 50 mL / min for bed thickness of 2, 3, and 4 cm

In most of the experimental works, e.g. [24] and [34], they stated that increasing the length of bed leads to make the lower portions of the bed

ineffective as well as leads to form the anodic pockets which are zones inside the working electrode where anodic reaction takes place. Unfortunately the phenomena of anodic pockets cannot be simulated by any means besides that there is no agreement or clear explanation in the literature about how do these pockets are formed, therefore it is recommended in literature to use bed lengths up to 1 cm. This might to be in contrast with the observed results from this work, see **Figs. 5.11-5.14**, actually for beds of lengths more than 2 cm the lower portions of the bed will be at lower overpotentials relative to bed thickness of 2 cm as will be shown later in the overpotential section. This does not permit obtaining higher overpotentials at the bed downstream because the local reaction rate (i) approaches the local limiting current density (i_L) at the bed downstream which will cause more deposition to takes place. The dependence of concentration distribution on the bed thickness for a given flow rate was presented by [24] as collection effectiveness (CE) or conversion, defined by equation (5.1) below, plotted against Reynolds number at different bed lengths

$$CE = \frac{C_{b,x=0} - C_{b,x=L}}{C_{b,x=0}} \qquad \ldots(5.1)$$

The plot shows a high collection effectiveness obtained at long beds and this CE is decreasing as the bed gets shorter. Increasing Reynolds number causes the CE, i.e. conversion, to decrease that would support and satisfy the results obtained in present work (**Fig. 5.15**).

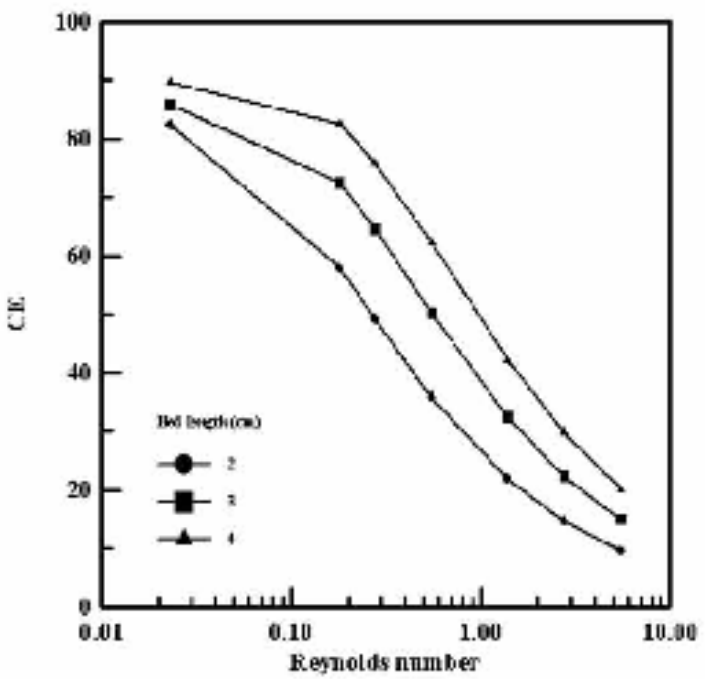

Figure 5.15 Collection effectiveness in 0.001M Cu^{+1} ion solution versus Reynolds number at bed lengths of 2, 3, and 4 cm

5.1.2.3 Effect of Feed Molar Concentration on Concentration Distribution

The changing of feed concentration can illustrated if the concentration is normalized with respect to the feed value as shown in **Figs. 5.16**, **5.17**, **5.18**, and **5.19** below where the bed of 4 cm thickness is considered with flow rates of 5 and 50 mL / min.

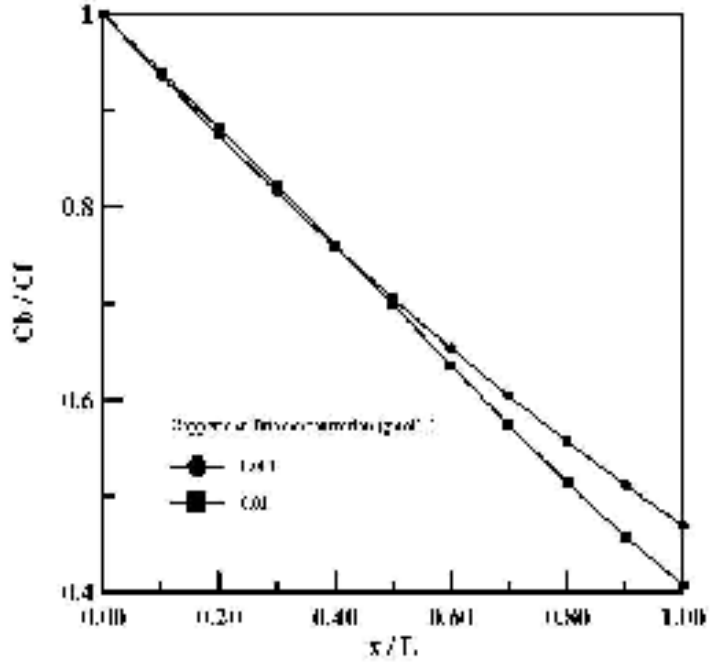

Figure 5.16 Normalized concentration distribution at flow rate of 5 mL / min and bed thickness of 2 cm in 0.001 and 0.01M Cu^{2+} ion solutions

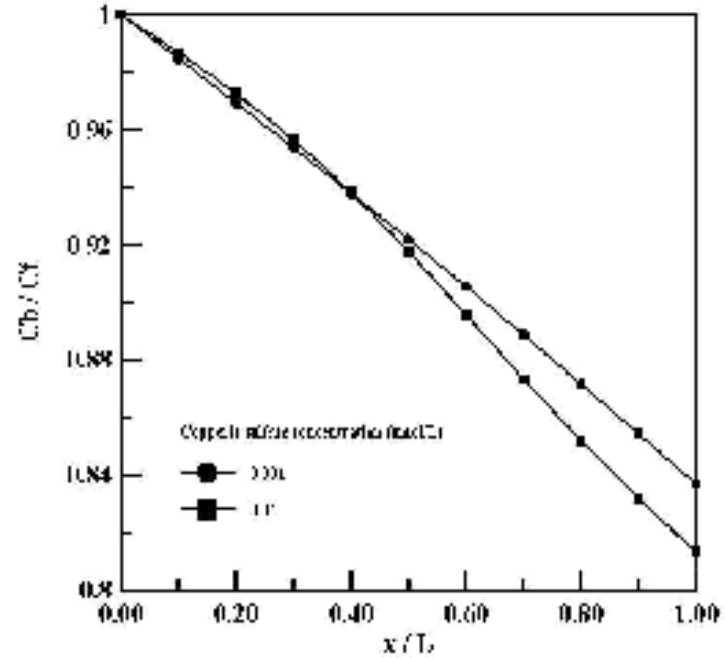

Figure 5.17 Normalized concentration distribution at flow rate of 50 mL / min and bed thickness of 2 cm in 0.001 and 0.01M Cu^{2+} ion solutions

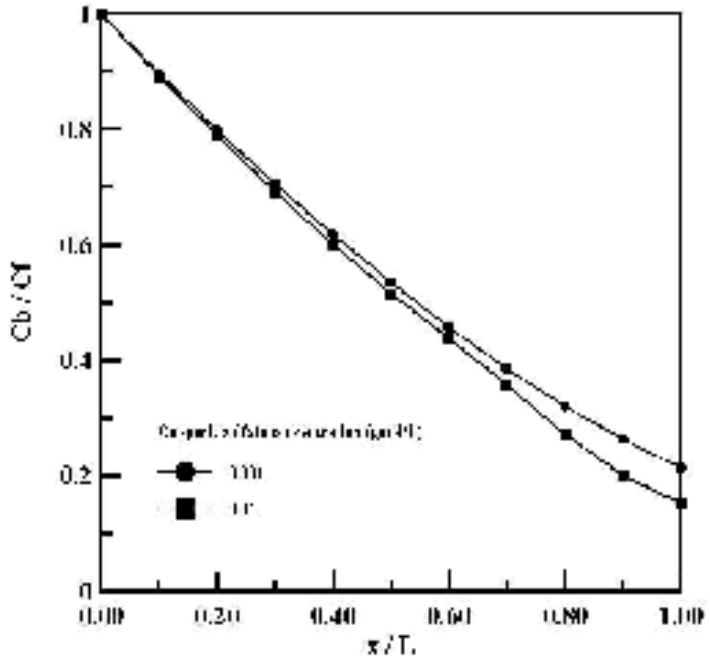

Figure 5.18 Normalized concentration distribution at flow rate of 5 mL / min and bed thickness of 4 cm in 0.001 and 0.01M Cu^{2+} ion solutions

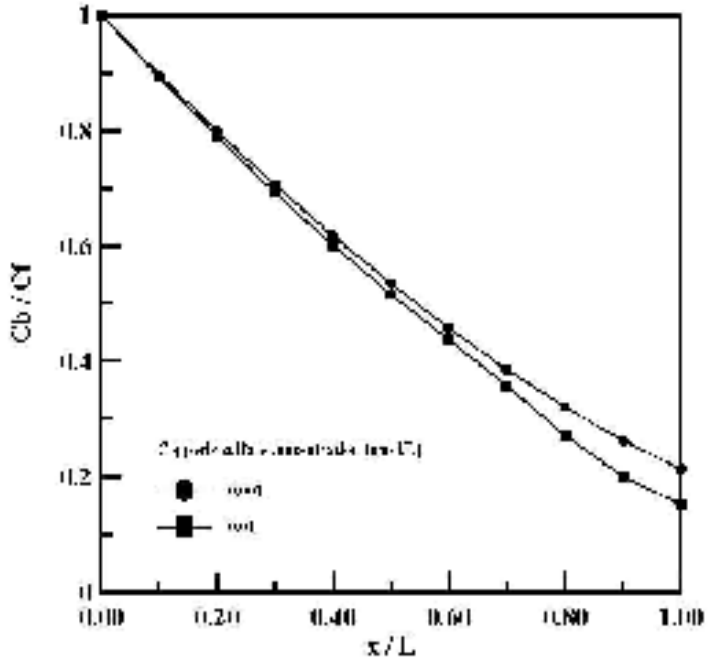

Figure 5.19 Normalized concentration distribution at flow rate of 50 mL / min and bed thickness of 4 cm in 0.001 and 0.01M Cu^{2+} ion solutions

The concentration of copperic sulfate has no effect on the mass transfer coefficient because of the fact that the mass transfer coefficient is a function of temperature and hydrodynamics (electrolyte velocity) but examining **Figs. 5.16** through **5.19** show that for the 0.01 M concentration the deposition will proceed to higher extents and that is because the mass transfer rate (the product of mass transfer coefficient and concentration) is increased which leads to further deposition. In literature, e.g. [34], at given applied total current, flow rate, and bed thickness the lower the feed concentration gave the higher consumption of copper ions, i.e. faster deposition, because local limiting current is achieved faster and therefore higher consumption of copper ions is obtained. Again a contrast between this simulation results and literature seems to appear at first glance but it should be remembered that the total current applied in all runs was 80% of the corresponding limiting current for each case. This will actually reflect the expected behavior of the concentration drop at different copper feed concentrations because generally all runs are close to the limiting current, therefore the factor that will govern the higher reaction rate is that mass transfer rate as mentioned before.

To show that this simulation is adequate to the literature results an exceptional runs were performed for the conditions of bed length of 4 cm, flow rate of 5mL / min, total current applied 0.125714 A (125 mA) at copper ion feed concentrations of 0.01, 0.011, and 0.012 M respectively, taken too close to ensure smaller deviation between limiting currents and hence ensuring that they are operating in the mixed region. **Fig. 5.20** and Table 5.2 below show the concentration drop for the above conditions.

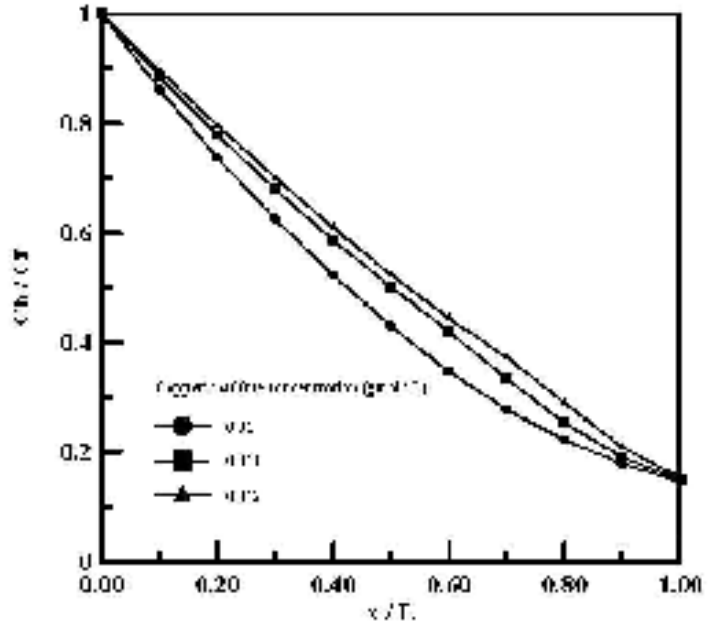

Figure 5.20 Normalized concentration distribution for bed length of 4 cm, flow rate of 5ml. / min, total current applied 125 mA at copper ion feed concentrations of 0.01, 0.011, and 0.012 M

Table 5.2 Normalized concentration distribution corresponding to **Fig. 5.20**

(x / L)	0.01 M	0.011 M	0.012 M
0	1	1	1
0.1	0.8620213	0.886496	0.896578333
0.2	0.7373466	0.779318	0.796955325
0.3	0.6249615	0.67929	0.700971167
0.4	0.5227733	0.586672	0.609831417
0.5	0.4296131	0.501774	0.523872083
0.6	0.3467365	0.419447	0.444096333
0.7	0.2768781	0.3337	0.372261333
0.8	0.2212574	0.252168	0.289629417
0.9	0.1782943	0.190252	0.207452583
1	0.1450306	0.148676	0.153224167

Therefore it can be concluded that if the total current is fixed the concentration drop of different feed concentrations will be higher for dilute concentrations.

5.1.3 Reaction Rate Distribution

Generally the reaction rate as the electrolyte is passed through the bed from the upstream is starting with a relatively low value because the lower portions of the bed near the upstream are less polarized and increasing as the electrolyte is reaching the downstream where the maximum reaction rate is attained because the upper portions of the bed are more polarized. In this work where the mixed controlled process is studied (activation and mass transfer) precisely 80% of total limiting current was applied the reaction rate at upstream will approach the local limiting current density ($i_{l,}$). The overall operation of reactor at sub-limiting current do not permit making a portion of the bed to reach the limiting current (local limiting current) [16].

5.1.3.1 Effect of Flow Rate on Reaction Rate Distribution

The effect of flow rate on reaction rate or copper deposition rate is illustrated in **Fig. 5.21- Fig. 5.26** below where the reaction rate was normalized by the local limiting current given by the following expression

$$i_l(x) \quad zF k C_b(x)$$

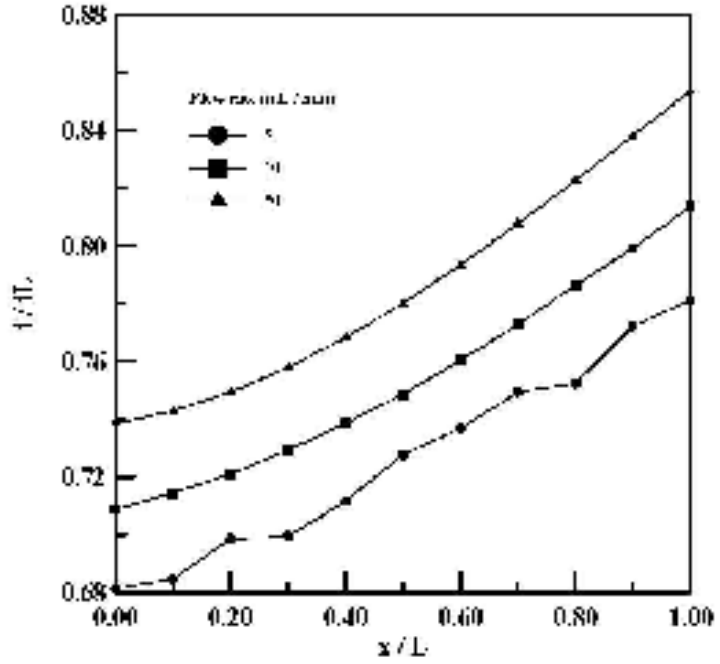

Figure 5.21 Normalized reaction rate distribution in 0.001M Cu^{2+} ion solution and 2cm bed thickness

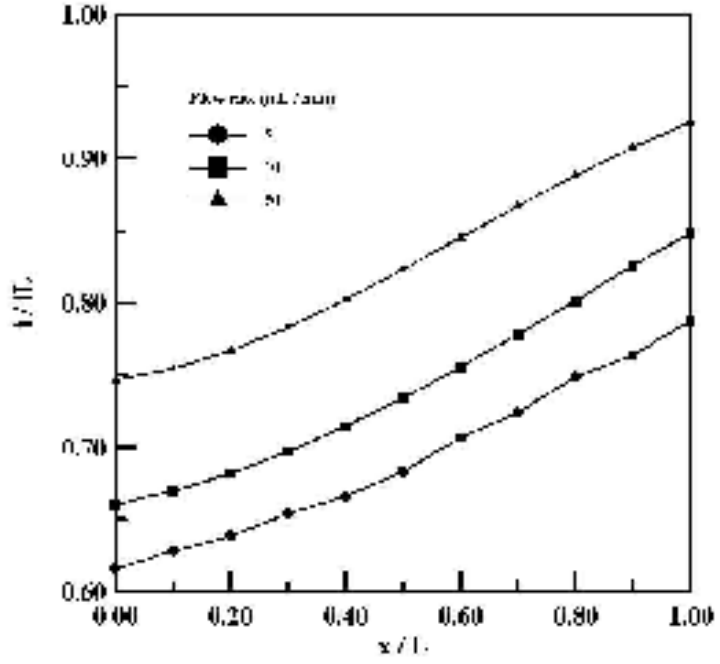

Figure 5.22 Normalized reaction rate distribution in 0.01M Cu^{2+} ion solution and 2cm bed thickness

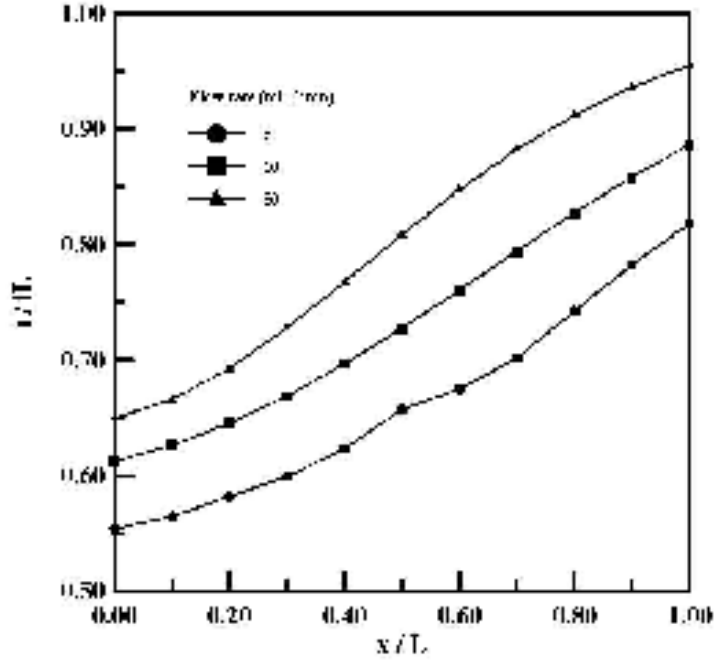

Figure 5.23 Normalized reaction rate distribution in 0.001M Cu^{2+} ion solution and 3cm bed thickness

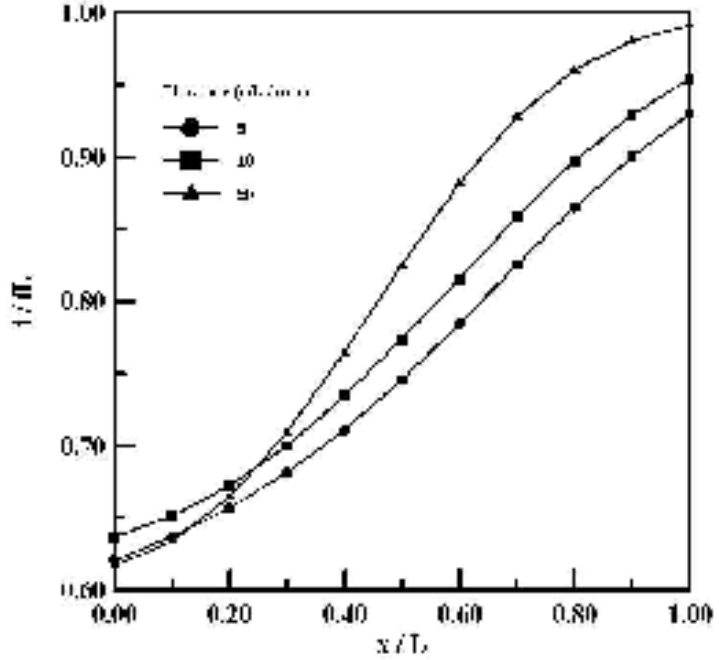

Figure 5.24 Normalized reaction rate distribution in 0.01M Cu^{2+} ion solution and 3cm bed thickness

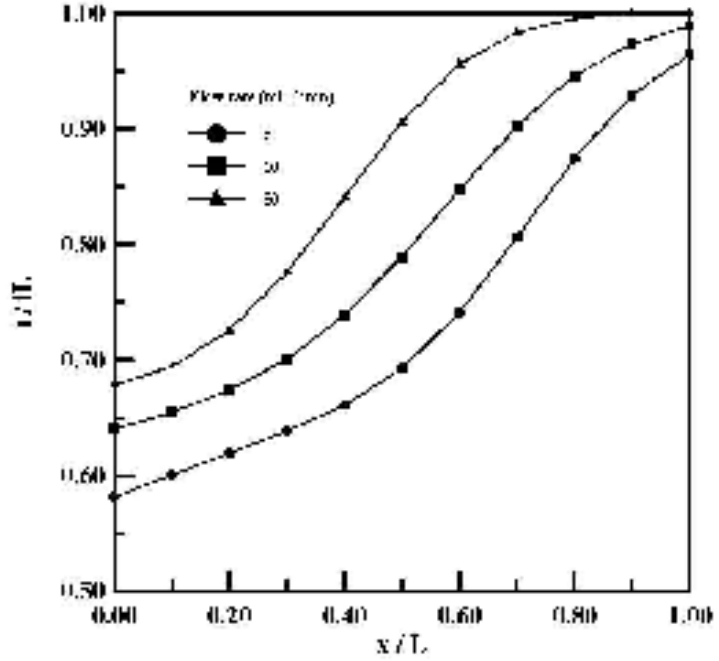

Figure 5.25 Normalized reaction rate distribution in 0.001M Cu^{2-} ion solution and 4cm bed thickness

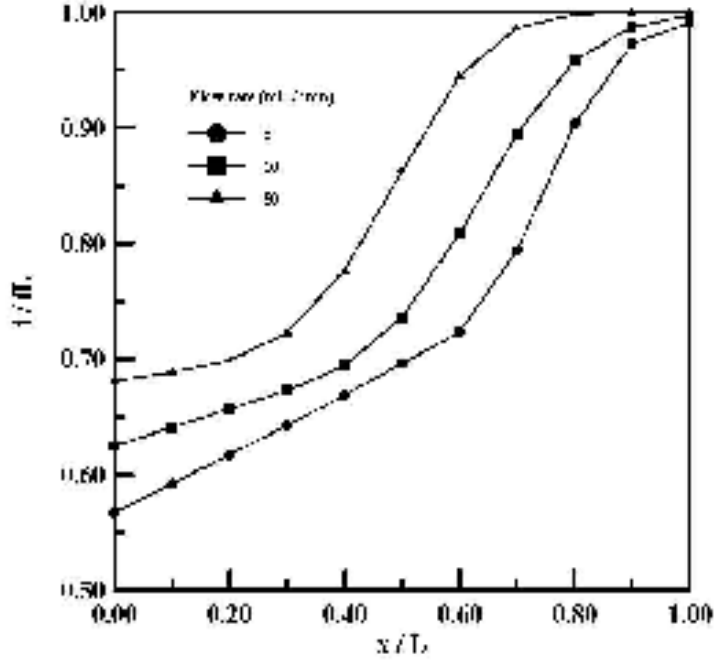

Figure 5.26 Normalized reaction rate distribution in 0.01M Cu^{2} ion solution and 4cm bed thickness

Figures 5.21-5.26 show that higher normalized reaction rates are obtained at high flow rates this is due to the faster approach of reaction rate to its local limiting current component (i_L) due to the high mass transfer rates of copper ions and since copper ions are deposited faster at low flow rates the reaction rate will be consequently low too. It is well observed that the reaction rate (i) is decreasing with distance and contrasting the previous explained behavior at the beginning of section 5.1.3 so that the decrease in the reaction rate is in its magnitude not in its quality (i/i_L). It is indicating that the last portion of the cathode is working at limiting current conditions since i/i_L approach unity in **Figs. 5.25** and **5.26** and the initial i/i_L increases as distance is increased.

5.1.3.2 Effect of Bed Length on Reaction Rate Distribution

The effect of increasing bed depth can be seen when examining **Figs. 5.21-5.26** above. It is noticed that the reaction rate (i) is decreasing in value and if **Figs. 5.10-5.13** are reviewed, it will be concluded that the high consumption of copper ion lead to make the reaction rate at the downstream relatively low as well as at the upstream because the upstream will be less polarized.

5.1.3.3 Effect of Feed Molar Concentration on Reaction Rate Distribution

Increasing feed concentration will increase the reaction rate because more copper ions are supplied at constant flow rate, so a higher reaction will

occur. This is shown below in **Figs. 5.27** and **5.28** by plotting normalized reaction rate (i/i_L) versus dimensionless bed length at copper ion concentrations 0.001 and 0.01 M

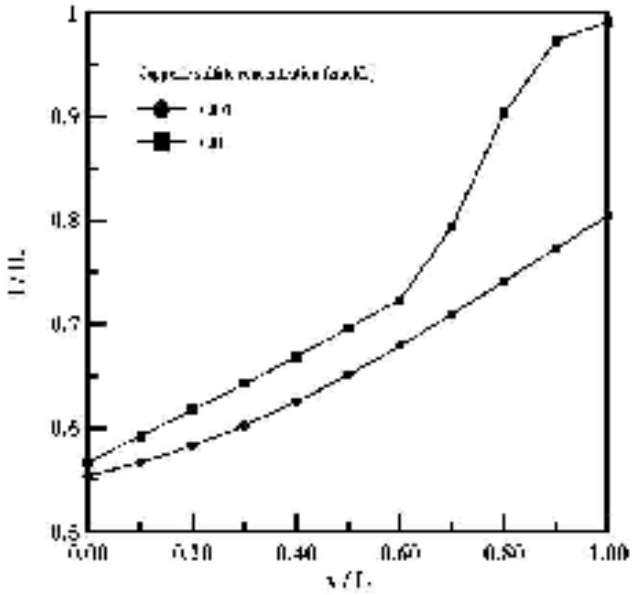

Figure 5.27 Dimensionless reaction rate at flow rate of 5 mL / min, bed thickness of 4 cm and Cu^{2+} ion feed concentration of 0.001 and 0.01M

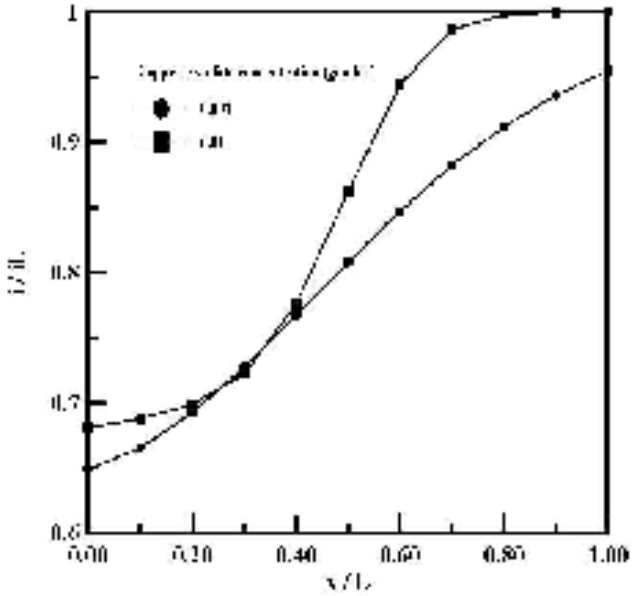

Figure 5.28 Dimensionless reaction rate at flow rate of 50 mL / min, bed thickness of 4 cm and Cu^{2+} ion feed concentration of 0.001 and 0.01M

It is seen that the reaction rate for 0.01 M concentration is higher than the 0.001 M and closest to its local limiting current which is consistent with the results of feed concentration effect on the concentration distribution as has been reasoned before.

5.1.4 Overpotential Distribution

The overpotential variation along the bed is such that it has a relatively low value at the bed upstream, where the electrolyte is introduced, because at this point the local cathode potential (E) is close to the equilibrium therefore the overpotential will be small at the upstream while after the entrance the cathode potential will drop and hence overpotential increases until downstream is reached.

5.1.4.1 Effect of Flow rate on Overpotential Distribution

The effect of flow rate on overpotential is presented below

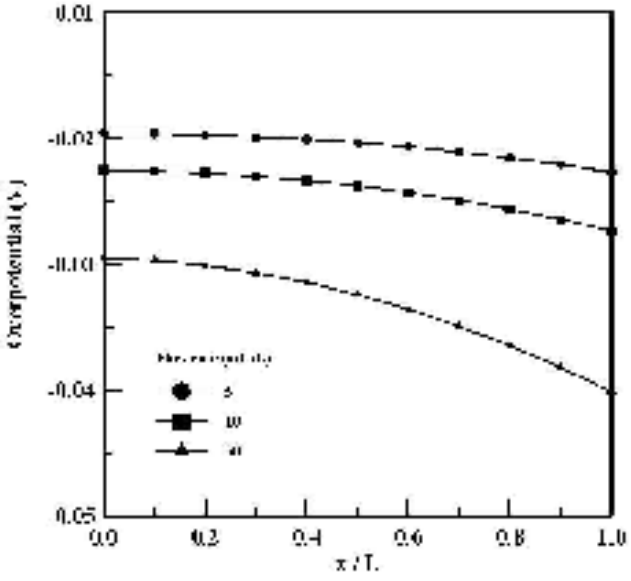

Figure 5.29 Overpotential distribution for 0.001M solution and 2cm bed thickness

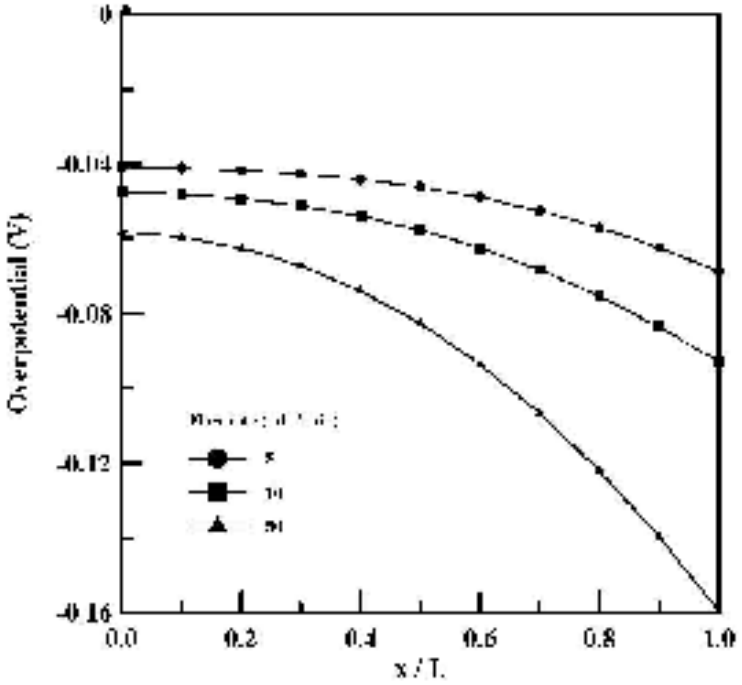

Figure 5.30 Overpotential distribution for 0.01M solution and 2cm bed thickness

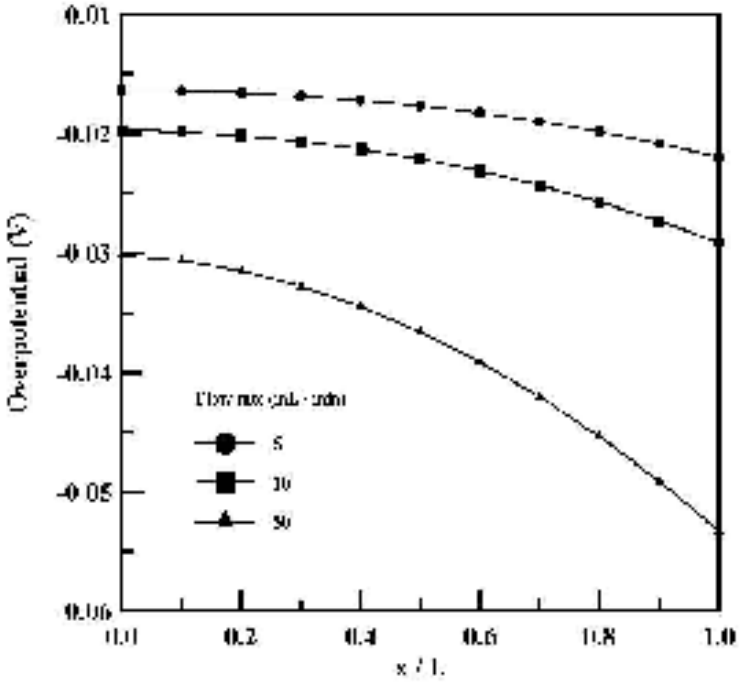

Figure 5.31 Overpotentia distribution for 0.001 M solution and 3cm bed thickness

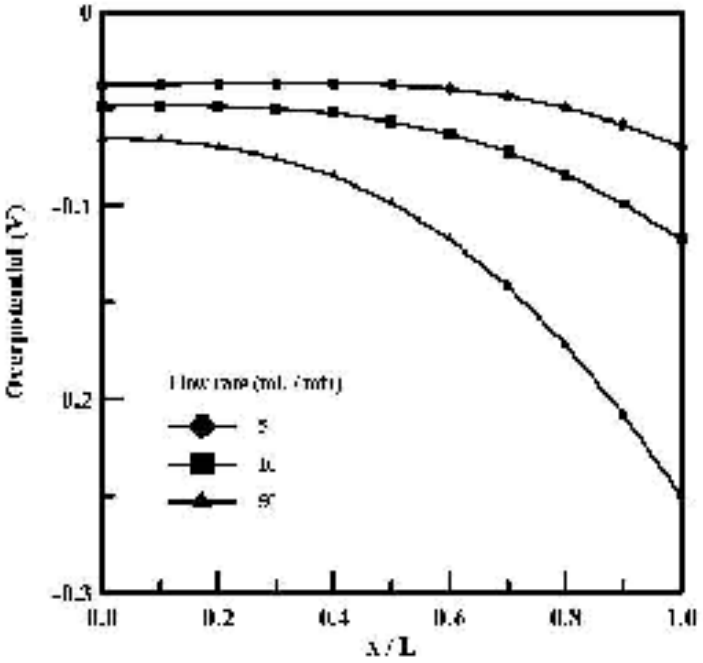

Figure 5.32 Overpotential distribution for 0.01M solution and 3cm bed thickness

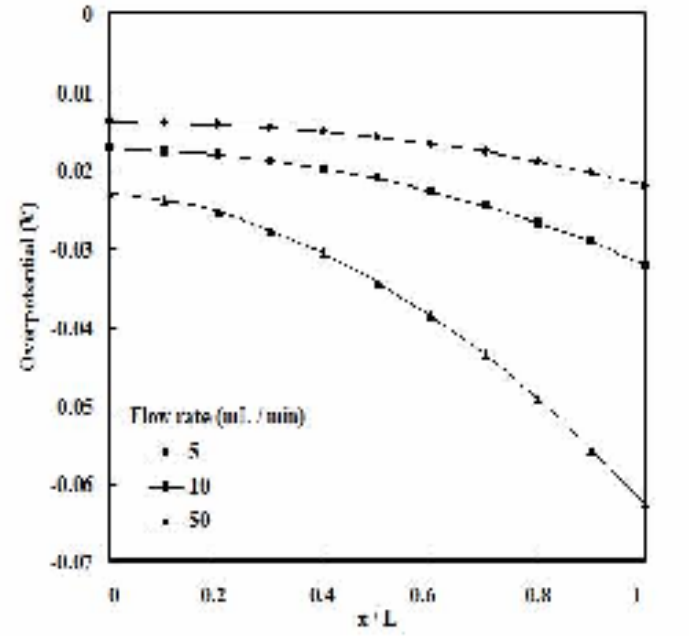

Figure 5.33 Overpotential distribution for 0.001M solution and 4cm bed thickness

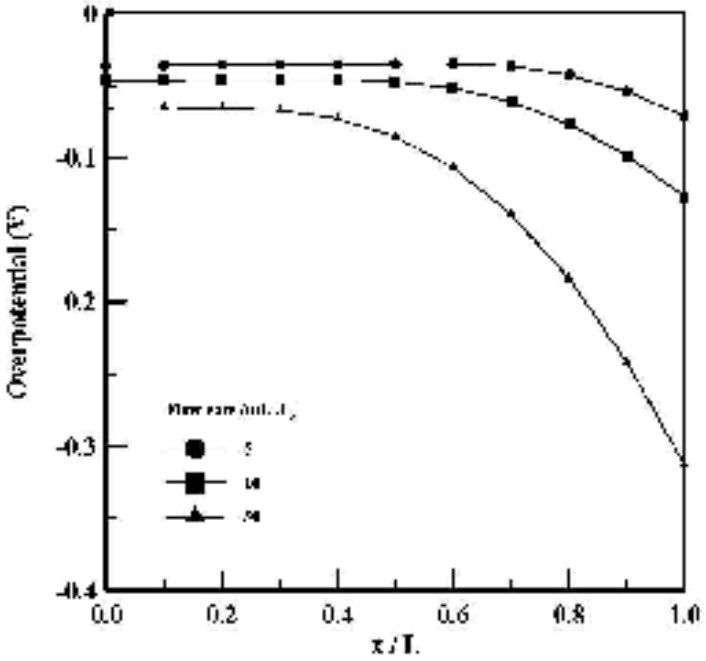

Figure 5.34 Overpotential distribution for 0.01M solution and 4cm bed thickness

The overpotential is increasing with increasing flow rate, which satisfies the behavior observed in the work of Olive and Lacoste (1980) [18]. The flow rate 50 mL / min exhibits a severe drop in overpotential relative to the other two flow rates and this might be due to the faster approach of the 50 mL / min flow rate reaction rate to its local limiting current density.

A comparison between this model and that of Olive and Lacoste [18] is as follows:

for the same boundary conditions used in present work the potential distribution for limiting current conditions is given by

$$\phi(x) = \phi(L) + \frac{zFC_0 u^{\alpha}}{\alpha k K}\left[\frac{\alpha k}{u}(L - x) + e^{-\frac{\alpha k}{u}L} - e^{-\frac{\alpha k}{u}x}\right] \qquad \ldots(5.2)$$

where E(L) is the potential at the downstream.

Equation (5.2) represents an analytical expression for the potential distribution at limiting current showing an appreciable agreement with the experimental work of [46], this model will be compared with the present model

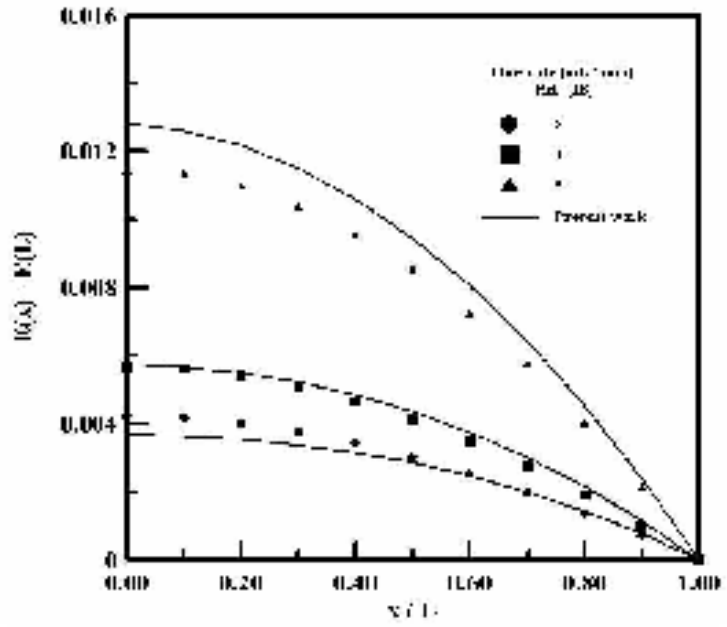

Figure 5.35 Comparison of overpotential distribution between present model and that of Ref. [18], for 0.001M and 2cm bed thickness

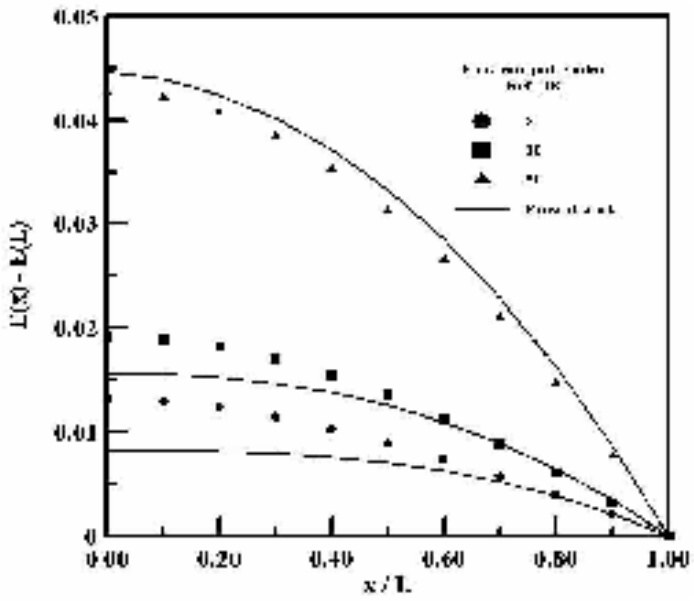

Figure 5.36 Comparison of overpotential distribution between present model and that of Ref. [18], for 0.001M and 4cm bed thickness

The comparison between current model and that of Ref. [18] has showed acceptable agreement as shown in **Fig. 5.35** & **Fig. 5.36**.

5.1.4.2 Effect of Bed Length on Overpotential

This effect is illustrated by examining **Figs. 5.29-34** which shows that when bed length is increased the overpotential becomes less negative.

5.1.4.3 Effect of Feed Concentration on Overpotential Distribution

This effect will be seen from examining chapter four and Appendix A for overpotential results to see that increasing the concentration leads to make the overpotential higher throughout the bed and actually this is the reason behind obtaining higher reaction rates with increasing flow rates because the overpotential represents the driving force for the reaction.

5.2 Minor Results

5.2.1 Solution Current Density

The current applied to the reactor is divided into two components. first is the solution current density and second the metal current density according to conservation of electrical current and from knowing one of these components it will be possible to predict the other, see equation (3.30) in chapter three. The solution current density may be obtained from evaluating the reaction rate according to equation (3.33) presented in chapter three. The solution current density increases from zero at bed upstream until it reaches the total current applied at the downstream.

5.2.1.1 Effect of Flow Rate on Solution Current Density

The effect of flow rate on solution current density is shown in the following figures (5.35-5.38) where 2 and 4 cm bed lengths are considered.

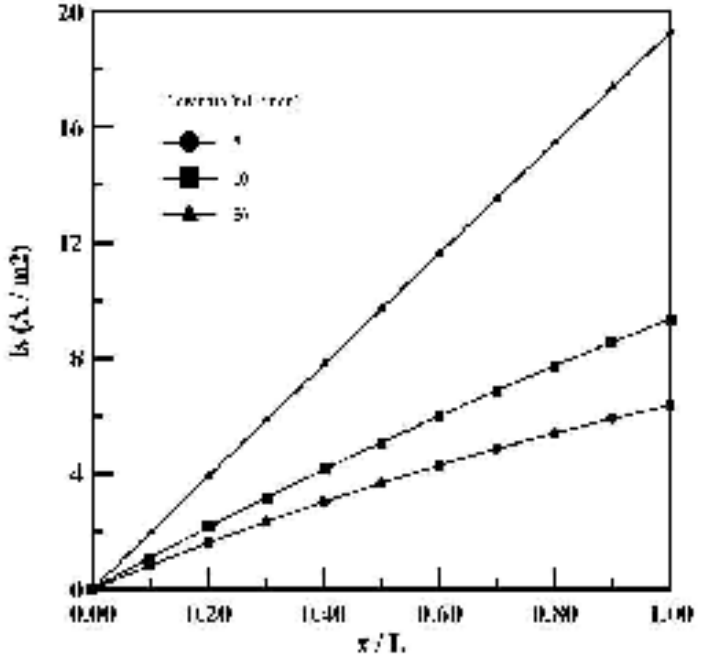

Figure 5.35 Solution current density distribution for 0.001 M solution and 2 cm bed length

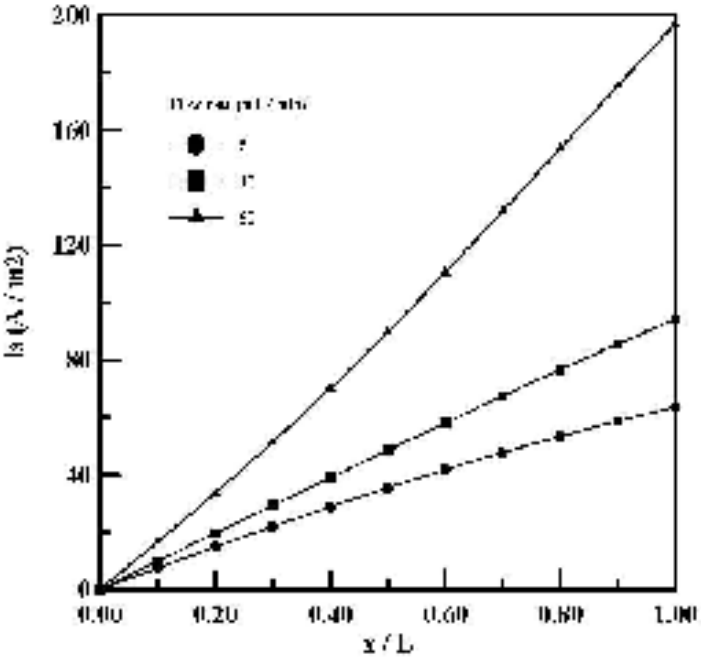

Figure 5.36 Solution current density distribution for 0.01 M solution and 2 cm bed length

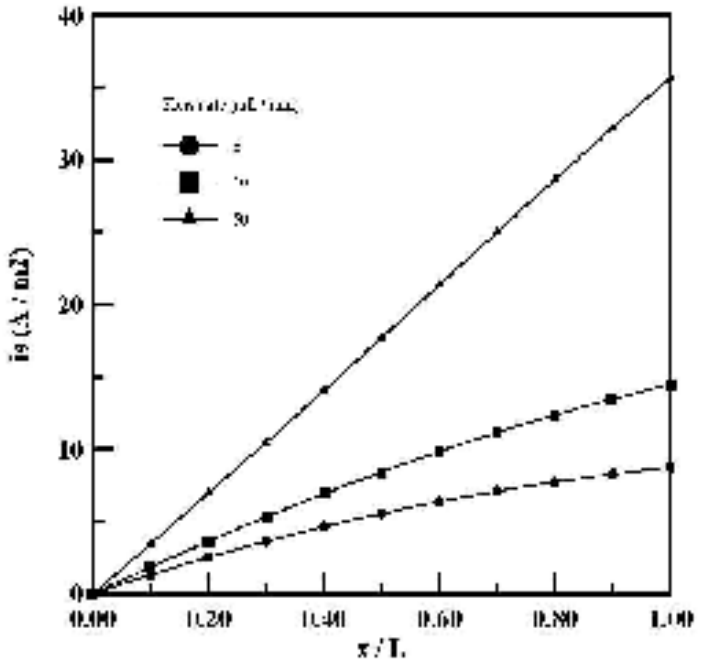

Figure 5.37 Solution current density distribution for 0.001 M solution and 4 cm bed length

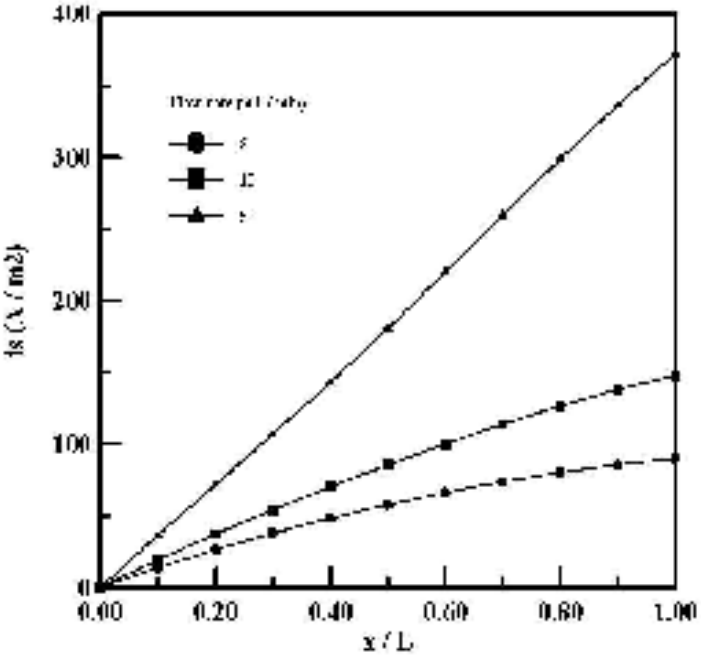

Figure 5.38 Solution current density distribution for 0.01 M solution and 4 cm bed length

Since the solution current density is strongly related to the reaction rate (see equation (3.33)

$$\frac{di_s}{dv} = ai \qquad \ldots(3.33)$$

but unlike the reaction rate it doesn't decrease but it still increases along the bed because when the electrolyte is introduced to the bed the total current is in the metal phase (packing material) and with moving inside the bed the electrolyte will gain the whole at the end of the bed where the electrolyte leaves the bed to go toward the anode. Increasing flow rate will increase the reaction rate and consequently the current density because of the increase in the total limiting current.

5.2.1.2 Effect of Feed Concentration on Solution Current Density

The increasing of concentration will increase the current density due to the increase in reaction rate leading to high current densities applied.

5.2.2 Pressure Drop Results

5.2.2.1 Effect of Flow Rate on Pressure Drop

The effect of flow rate on pressure drop is easily expected to increase the pressure drop since the electrolyte velocity is introduced directly into the Forchheimer equation.

$$\frac{\Delta P}{L} = \frac{\mu}{Pm(\varepsilon)}.u + \frac{c(\varepsilon)\rho}{\sqrt{Pm}}u^2 \qquad \ldots(3.2)$$

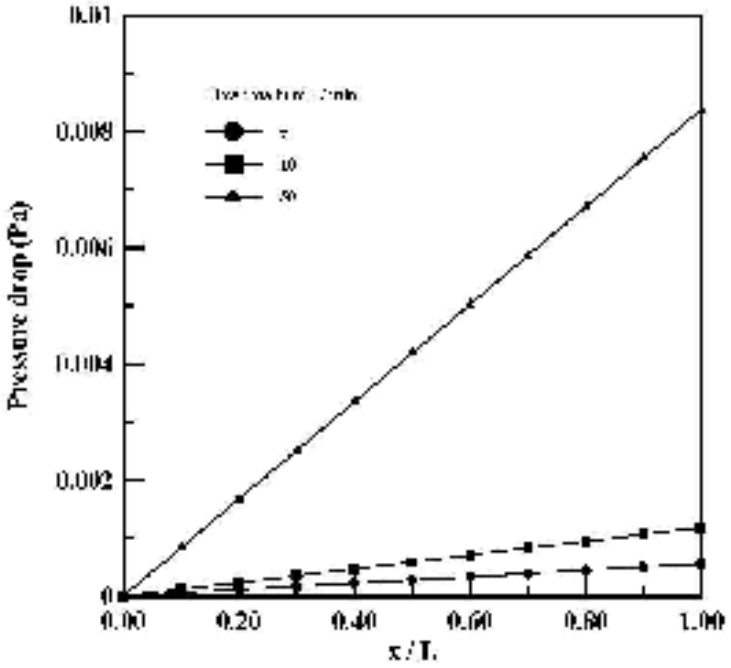

Fig. 5.39 Pressure drop inside cathode for flow rates 5, 10, and 50 mL / min and feed concentration of Cu^{2+} of 0.001 M and bed depth of 2 cm

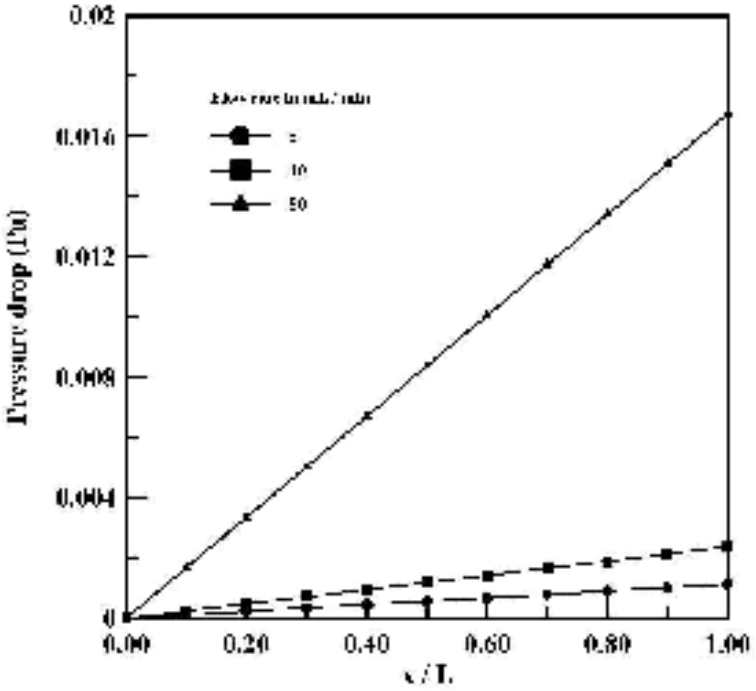

Fig. 5.40 Pressure drop inside cathode for flow rates 5, 10, and 50 mL / min and feed concentration of Cu^{2+} of 0.001 M and bed depth of 4 cm

When examining Figs 5.39 and 5.40 it is clear that pressure drop is increasing appreciably with increasing flow rate because of the increasing velocity which is an important factor in the pressure drop calculations, therefore the more the velocity is increased the higher the pressure drop obtained.

5.2.2.2 Effect of Bed length on Pressure Drop

The effect of bed length can be seen from tables presented in chapter four and appendix A to see that the pressure drop is increasing with increasing bed depth.

5.2.2.3 Effect of Feed Concentration on Pressure Drop

The pressure drop is decreased slightly when feed concentration is increased from 0.001 to 0.01 M for the flow rates 5 and 10 mL / min. which is unexpected behavior because at all flow rates the pressure drop is expected to increase at a given bed thickness. This might be due to the variation of density and viscosity while for the third flow rate 50 mL / min the pressure drop attaining slightly higher values when feed concentration is increased which is probably due to the close concentration drop profiles for different feed concentrations, see **Figs. 5.18** and **5.19**.

Chapter Six

Conclusions and Recommendations for Future Work

6.1 Conclusions

From examining this simulation results one can conclude the following:

1. The operating current in this work is beneath the limiting current but despite of this there are portions, specifically the last portions, inside the working electrode are operating under mass transfer control, which can be shown by plotting the ratio of local reaction rate to local limiting current versus distance.
2. Equation (4.4) derived in chapter four for the total limiting current density has successfully described the true limiting current density when comparison with the work of Bennion and Newman [15] is made.
3. The model has been compared with the model of Olive and Lacoste [18] under limiting current conditions, where satisfied agreement is obtained.
4. In sub-limiting conditions, the present model has successfully described the effect of flow rate, bed length, and feed concentration on the concentration distribution as well as the effect of Re on the collection effectiveness at different bed lengths which has matched the expected from literature.
5. If the reaction rate is decreasing a long the bed this decease will not necessarily suppress the deposition because the reaction rate is increasing qualitatively.

6.2 Recommendations

Unfortunately there is no experimental work close enough to this simulation so that an experimental work with similar parameters to those studied is strongly recommended for comparison purposes. The method of comparison may be through the concentration distribution or through the collection effectiveness measurements (chapter five).

1. In present work the effect of temperature is not studied. It is recommended to study the reactor performance at different temperatures.
2. Another reactions may be studied especially electro-organic reactions.
3. The variables studied in this work are flow rate, feed concentration, and bed length. There are other important variables as the diameter of packing particles (spheres) and also the geometry of particles may be studied, e.g. cylindrical particles, as well as different types of metal particles.
4. The effectiveness of working electrode may be studied.
5. The side reaction mainly which is hydrogen evolution, may studied.

References

1. Gritzner, G. and Kreysa G., " Nomenclature, symbols and definitions in Electrochemical Engineering ", Pure & Appl. Chem., Vol. 65, No. 5. pp. 1009-1020, 1993.
2. Tobias, W.C.," The coming of age of electrochemical engineering ", AIChE Symp. Ser., Vol. 77, No.204, 1981, pp2-9.
3. Kirk–Othmer, "Encyclopedia of chemical technology", 3rd edition, John Wiley and sons, 1981.
4. Walsh, F.C., "Electrochemical technology for environmental treatment and clean energy conversion", Pure Appl. Chem., Vol.73, No.12, pp 1819-1837, 2001.
5. Alkire, R., "Modeling electrochemical reactors", AICHE, Vol.77, No.204. 1981.
6. Ross, S. M, " Simulation", 2nd edition, Academic Press, Orlando, 1996.
7. Fitzjohn, J. E., "Electro-organic synthesis" Chem. Eng. Prog. , Vol.71, No.2, 1972, pp. 85-87.
8. Caldwell, D. L., "Overview of the industrial inorganic electrolytic process ", AIChE symp. Ser. ,vol 79, No.229, 1983.
9. Al-Shammari, A. A., Rahman, S.U., and Chin, D.T., "An oblique rotating barrel electrochemical reactor for removal of copper ions from wastewater "J. Applied electrochem.,Vol.34, 2004
10. Perry, R .H., Green, D. W., and Maloney, J. O. " Perrey's Chemical Engineers Handbook ", 6th edition McGraw-Hill, 1984.
11. Bard, A. J. and Faulkner, L. R., "Electrochemical Methods fundamentals and application ", John Wiley & Sons, 1980.

12. Picket, David J., " Electrochemical Reactor Design", 2nd edition, Elsevier scientific publishing company, 1972.
13. Wang, J. " Analytical electrochemistry", 2nd edition, John Wiley & Sons, 2001.
14. Uhlig, H.H. and Revie, R. W., " Corrosion and Corrosion Control", John Wiley & Sons, 1985.
15. KarabacakoĞlu, A. B., Kocar, Ö. M., and Pekel, A. T., "The synthesis of Manganese (III) Acetate in bipolar Packed-Bed and Trickle-Bed electrode cells", J. Chem. Vol.24, 2000.
16. Masily, A.I. and Poddubny, N.P., "Influence of solid phase conductivity on spatial localization of electrochemical processes in flow through porous electrodes. Part II: Nonuniform porous matrix with variable conductivity profile", J. Applied electrochem, Vol.27. 1997.
17. Risch, T. and Newman, J., "A theoretical comparison of flow-through and flow-by porous electrode at the limiting current", J. Electrochem. Soci. Vol.131. No.11, 1984.
18. Olive, H. and Lacoste, G." Application of Volumetric Electrodes To The Recuperation of Metals in Industrial Effluents - II Design of An Axial Field Flow-Through Porous Electrode", Electrochemi. Acta. Vol. 25, 1980, pp. 1303-1308.
19. Geankoplis, C. J., " Transport processes and unit operations" 3rd edition prentice hall, 1993.
20. Newman, J. and Tiedemann, W., "Porous electrode theory with battery applications", AIChE J., Vol. 21, No.1, 1975.

21. Kuhn, A. T. and Houghton, R.W., "A comparison of the performance of electrochemical reactor design in the treatment of dilute solutions", Electrochimica Acta, Vol. 19, 1974.

22. Newman, J. and Tobias, C. W., "Theoretical Analysis of current distribution in porous electrodes", J. Electrochem. Soci, Vol.109, No.12, 1962.

23. Sioda, R. E., "distribution of potential in a porous electrode under conditions of flow electrolysis". Electrochim. Acta, vol.16, pp.1569-1576, 1971.

24. Alkire, R., and Gracon, B., "Flow through porous electrodes", J. Electrochem. Soci., Vol.122, No.12, 1975.

25. Coeuret, F., Hutin, D. and Gaundad, A. "Study of the effectiveness of fixed flow-through electrodes", J. Appl. Electrochem.,Vol.6, 1976, pp.417-423.

26. Trainham J. A. and Newman, J., "A flow through porous electrode model: application to ion-removal from dilute streams ". J. Electrochem. Soci, Vol.124, No.10, 1977.

27. Gaundad, A., Hutin, D., and Coeuret, F.,"Potential distribution in flow-through porous electrode under limiting current conditions", Electrochemical Acta, Vol. 23, 1978.

28. Lahurd, D. A., "Simplified models for use in electrochemical reactor Scale-up and system studies ", J. Electrochem. Soci, Vol.132, No.12, 1985.

29. Bertazzoli, R., Winder R. C., Marcos R. V. Lanza, Rozana A. Di Iglia, and Maria H.B. Sousa," Electrolytic removal of metals using a flow-

through cell with a reticulated vitreous carbon cathode ", J. Braz. Chem. Soc. Vol. 8, No. 5, 1997.

30. Masily, A.J. and Poddubny, N.P., "Influence of solid phase conductivity on spatial localization of electrochemical processes in flow through porous electrodes. Part I: Electrodes with uniform conducting matrix ", J. Applied electrochem. Vol.27, 1997.
31. Hunson, M., Hungues Vergnes, Patrick Duverneuil Kejvalee Pruksathorn, Somsak Damrongleed," Recovering of copper from synthetic solution in BPE reactor ", Science Asia No. 28, 2002.
32. Ayres, J. L. and Fedkiw, P. S. " Abatement of heavy metals in industrial effluents by catalyzed, electrochemical removal scheme ". The water resources research institute, Report No. 207, August 1983.
33. Bear, J., " Dynamics of Fluids In Porous Media", Dover Publications, New York, 1972.
34. Ruotolo, L.M., and Gubulin, J. C., " Electrodeposition of copper ions on fixed bed electrodes: kinetic and hydrodynamic study", Brazilian journal of chemical engineering, Vol. 19, No. 1, 2002.
35. Al-Azmi, B. S.," Analysis of Transport Models and Computation Algorithms for Flow Through Porous Media ". Ph.D. thesis Ohio State University, 2003.
36. Jolls, K.R. and Hanratty, T.J., A.I.Ch.E. Journal, Vol.15, 1969.
37. Yip, H.H-K, "Mass transfer coefficient in packed beds at low Reynolds numbers", M.Sc. Thesis, University of California, 1973.
38. Wilson, E.J., and Geankoplis C.J., Ind. Eng. Chem. Fund., Vol.5,1966.

39. Oloman, C. and Reilly, P., "Modeling and parameter estimation for a fixed bed electrochemical reactor", J. Electrochem. Soc., Vol. 134, No. 4, 1987.

40. Furnas, C.C., Ind. Eng. Chem., Vol. 23, 1993, p. 1052.

41. Horvath, A.L., " Handbook Aqueous of Electrolyte Solutions ", Ellis Horwood Limited, 1985.

42. Novak, J. " A technical handbook for industry", Hach company, 2003.

43. Neale, G. H. and Nader, W.K., A.I.Ch.E. Journal, Vol. 19, 1973.

44. Scott, K., "The influence of mass transfer on effectiveness of particulate bed electrode ", Electrochim. Acta, Vol. 28 No.9, 1983.

45. Bernion, D. N. and Newman, J. Journal of applied electrochemistry, Vol. 2, 1972, p. 115.

46. Olive, D. and Lacoste, G., Electrochemi. Acta, Vol. 21, 1979, p. 1109.

Appendix A

Simulation Results

Table A.1 Results of Run 7(0.001 M Cu^{2+} ion solution concentration, 5 mL / L flow rate, and 4 cm bed length)

Distance (m)	Overpotential (V)	Reaction Rate (A/m^2)	Concentration (gmol / L)
0	-0.013735	0.33641	0.001
0.0040	-0.013849	0.30862	0.0009
0.0080	-0.014092	0.28283	0.0008
0.012	-0.014477	0.2584	0.00071
0.016	-0.015011	0.23478	0.00062
0.020	-0.015707	0.2116	0.00053
0.024	-0.016573	0.18871	0.00046
0.028	-0.017621	0.1662	0.00039
0.032	-0.018864	0.14436	0.00032
0.036	-0.020315	0.12361	0.00026
0.040	-0.02199	0.10437	0.00021

Table A.2 Results of Run 8 (0.001 M Cu^{2+} ion solution concentration, 10 mL / L flow rate, and 4 cm bed length)

Distance (m)	Overpotential (V)	Reaction Rate (A/m^2)	Concentration (gmol / L)
0	-0.017211	0.4689386	0.001
0.0040	-0.0174579	0.4442267	0.0009265
0.0080	-0.0179615	0.4221537	0.00085464
0.012	-0.0187274	0.4012713	0.0007835
0.016	-0.0197595	0.3803011	0.00071281
0.020	-0.0210616	0.3583056	0.00064291
0.024	-0.0226394	0.334806	0.00057469
0.028	-0.0245017	0.3098099	0.00050928
0.032	-0.0266605	0.2837403	0.00044785
0.036	-0.029132	0.2572863	0.00039136
0.040	-0.0319353	0.2312264	0.00034045

Table A.3 Results of Run 9 (0.001 M Cu^{2+} ion solution concentration, 50 mL / L flow rate, and 4 cm bed length)

Distance (m)	Overpotential (V)	Reaction Rate (A/m^2)	Concentration (gmol / L)
0	-0.022937	0.850617	0.001
0.0040	-0.023706	0.848052	0.0009726
0.0080	-0.025236	0.856309	0.0009439
0.012	-0.027511	0.870226	0.000913
0.016	-0.030506	0.884503	0.0008799
0.020	-0.034196	0.894741	0.000845
0.024	-0.038558	0.898122	0.000809
0.028	-0.043578	0.893573	0.000773
0.032	-0.049249	0.881456	0.0007376
0.036	-0.055575	0.863022	0.0007036
0.040	-0.06257	0.839873	0.0006712

Table A.4 Results of Run 10 (0.01 M Cu^{2+} ion solution concentration, 5 mL / L flow rate, and 2 cm bed length)

Distance (m)	Overpotential (V)	Reaction Rate (A/m^2)	Concentration (gmol / L)
0	-0.041016	3.7727	0.01
0.002	-0.041242	3.6395	0.009402
0.004	-0.041775	3.5155	0.008807
0.006	-0.042713	3.3986	0.008209
0.008	-0.044165	3.2841	0.007601
0.010	-0.046235	3.1644	0.006982
0.012	-0.049021	3.0308	0.006356
0.014	-0.052608	2.8766	0.005735
0.016	-0.057065	2.7003	0.005137
0.018	-0.062443	2.5066	0.00458
0.020	-0.068779	2.3047	0.004077

Table A.5 Results of Run 11 (0.01 M Cu^{2+} ion solution concentration, 10 mL / L flow rate, and 2 cm bed length)

Distance (m)	Overpotential (V)	Reaction Rate (A/m^2)	Concentration (gmol / L)
0	-0.04761	4.87821	0.01
0.002	-0.04816	4.79479	0.00961
0.004	-0.04935	4.74352	0.00921
0.006	-0.05127	4.71681	0.0088
0.008	-0.05404	4.70244	0.00836
0.010	-0.05776	4.6837	0.0079
0.012	-0.06251	4.64224	0.00743
0.014	-0.06836	4.56325	0.00694
0.016	-0.07538	4.44053	0.00646
0.018	-0.0836	4.27798	0.00601
0.020	-0.09307	4.08657	0.00559

Table A.6 Results of Run 12 (0.01 M Cu^{2+} ion solution concentration, 50 mL / L flow rate, and 2 cm bed length)

Distance (m)	Overpotential (V)	Reaction Rate (A/m^2)	Concentration (gmol / L)
0	-0.0581729	8.084741	0.01
0.002	-0.0595788	8.193097	0.009869
0.004	-0.0625583	8.468513	0.009726
0.006	-0.0672989	8.889058	0.009566
0.008	-0.0739752	9.401376	0.009382
0.010	-0.082724	9.919454	0.009176
0.012	-0.0936368	10.34732	0.008956
0.014	-0.1067682	10.61853	0.008733
0.016	-0.1221497	10.72075	0.008518
0.018	-0.139798	10.68565	0.008317
0.020	-0.1597164	10.56046	0.008129

Table A.7 Results of Run 13 (0.01 M Cu^{2+} ion solution concentration, 5 mL / L flow rate, and 3 cm bed length)

Distance (m)	Overpotential (V)	Reaction Rate (A/m^2)	Concentration (gmol / L)
0	-0.037424	3.53317	0.01
0.003	-0.037308	3.34392	0.009166
0.006	-0.037121	3.14562	0.00836
0.009	-0.036897	2.94232	0.007585
0.012	-0.036846	2.74493	0.006837
0.015	-0.037425	2.56457	0.006094
0.018	-0.039271	2.39626	0.005321
0.021	-0.043012	2.21086	0.004513
0.024	-0.049129	1.97988	0.003725
0.027	-0.057913	1.71769	0.003041
0.003	-0.069468	1.467	0.002503

Table A.8 Results of Run 14 (0.01 M Cu^{2+} ion solution concentration, 10 mL / L flow rate, and 3 cm bed length)

Distance (m)	Overpotential (V)	Reaction Rate (A/m^2)	Concentration (gmol / L)
0	-0.04791	4.90142	0.01
0.003	-0.048	4.72325	0.00942
0.006	-0.04845	4.56249	0.00884
0.009	-0.04967	4.43128	0.00826
0.012	-0.05213	4.32876	0.00765
0.015	-0.05635	4.23234	0.007
0.018	-0.0628	4.10174	0.00632
0.021	-0.07187	3.90497	0.00565
0.024	-0.08386	3.64579	0.00503
0.027	-0.09901	3.35658	0.0045
0.003	-0.11742	3.06895	0.00405

Table A.9 Results of Run 15 (0.01 M Cu^{2+} ion solution concentration, 50 mL / L flow rate, and 3 cm bed length)

Distance (m)	Overpotential (V)	Reaction Rate (A/m^2)	Concentration (gmol / L)
0	-0.064863	8.887756	0.01
0.003	-0.0660908	8.899755	0.009785
0.006	-0.0692202	9.085558	0.009557
0.009	-0.075111	9.452673	0.0093
0.012	-0.0846351	9.918624	0.009005
0.015	-0.0985305	10.30826	0.008683
0.018	-0.1173754	10.46937	0.00836
0.021	-0.1416489	10.39091	0.008062
0.024	-0.1717519	10.16394	0.007792
0.027	-0.2079638	9.877538	0.007544
0.003	-0.2504013	9.578735	0.007309

Table A.10 Results of Run 16 (0.01 M Cu^{2+} ion solution concentration, 5 mL / L flow rate, and 4 cm bed length)

Distance (m)	Overpotential (V)	Reaction Rate (A/m^2)	Concentration (gmol / L)
0	-0.036193	3.44744	0.01
0.004	-0.035968	3.20993	0.008921
0.008	-0.035665	2.96054	0.007892
0.012	-0.035296	2.70123	0.006919
0.016	-0.03497	2.44112	0.006007
0.020	-0.034722	2.18205	0.005157
0.024	-0.034529	1.92559	0.004379
0.028	-0.03652	1.72608	0.003577
0.032	-0.042713	1.49463	0.002722
0.036	-0.054198	1.18339	0.002001
0.040	-0.071177	0.91685	0.001521

Table A.11 Results of Run 17 (0.01 M Cu^{2+} ion solution concentration, 10 mL / L flow rate, and 4 cm bed length)

Distance (m)	Overpotential (V)	Reaction Rate (A/m^2)	Concentration (gmol / L)
0	-0.04635	4.78247	0.01
0.004	-0.04611	4.54158	0.00925
0.008	-0.04575	4.29127	0.00853
0.012	-0.04534	4.03935	0.00784
0.016	-0.04538	3.81298	0.00717
0.020	-0.04703	3.6432	0.00646
0.024	-0.05188	3.50541	0.00566
0.028	-0.06141	3.29178	0.0048
0.032	-0.07669	2.95236	0.00402
0.036	-0.09847	2.58752	0.00342
0.040	-0.127	2.26961	0.00297

Table A.12 Results of Run 18 (0.01 M Cu^{2+} ion solution concentration, 50 mL / L flow rate, and 4 cm bed length)

Distance (m)	Overpotential (V)	Reaction Rate (A/m^2)	Concentration (gmol / L)
0	-0.0652162	8.928024	0.01
0.004	-0.0651931	8.765042	0.009717
0.008	-0.0655343	8.639256	0.009435
0.012	-0.0674114	8.656427	0.009141
0.016	-0.0730916	8.951239	0.008798
0.020	-0.0854424	9.467042	0.008376
0.024	-0.1069109	9.800161	0.007915
0.028	-0.1392474	9.703628	0.007504
0.032	-0.1838833	9.373145	0.007165
0.036	-0.2417918	8.997143	0.006865
0.040	-0.3132513	8.629189	0.006583

Table A.13 Solution current density distribution for 0.01 M Cu^{2+} ion solution concentration, 5, 10, and 50 mL / min flow rate, and 2 cm bed length

x	5 mL / min flow rate	10 mL / min flow rate	50 mL / min flow rate
0	0	0	0
0.002	7.5635	9.8706	16.61037
0.004	14.865	19.604	33.61236
0.006	21.92	29.257	51.32452
0.008	28.739	38.869	69.9886
0.010	35.319	48.447	89.70413
0.012	41.641	57.963	110.3849
0.014	47.669	67.357	131.7791
0.016	53.36	76.545	153.5543
0.018	58.673	85.441	175.398
0.02	63.582	93.97	197.0643

Table A.14 Solution current density distribution for 0.01 M Cu^{2+} ion solution concentration, 5, 10, and 50 mL / min flow rate, and 3 cm bed length

x	5 mL / min flow rate	10 mL / min flow rate	50 mL / min flow rate
0	0	0	0
0.003	10.526	14.732	27.22633
0.006	20.46	28.945	54.75542
0.009	29.778	42.711	83.13083
0.012	38.483	56.12	112.7814
0.015	46.61	69.224	143.7415
0.018	54.203	81.98	175.5446
0.021	61.255	94.236	207.4743
0.024	67.67	105.79	238.9364
0.027	73.329	116.51	269.6127
0.03	78.219	126.35	299.3924

Table A.15 Solution current density distribution for 0.001 M Cu^{2+} ion solution concentration, 5, 10, and 50 mL / min flow rate, and 4 cm bed length

x	5 mL / min flow rate	10 mL / min flow rate	50 mL / min flow rate
0	0	0	0
0.004	13.587	19.029	36.10902
0.008	26.18	37.056	71.62872
0.012	37.735	54.057	106.9267
0.016	48.229	70.083	142.8615
0.020	57.665	85.3	180.4505
0.024	66.048	99.889	219.7722
0.028	73.5	113.76	259.5766
0.032	80.073	126.5	298.5096
0.036	85.539	137.81	336.0007
0.040	89.862	147.74	371.9735

Table A.16 Pressure drop distribution for 0.01 M Cu^{2+} ion solution concentration, 5, 10, and 50 mL / min flow rate, and 2 cm bed length

x	5 mL / min flow rate	10 mL / min flow rate	50 mL / min flow rate
0	0	0	0
0.002	5.58096E-05	0.000117841	0.000838074
0.004	0.000111619	0.000235682	0.001676153
0.006	0.000167429	0.000353524	0.002514237
0.008	0.000223239	0.000471367	0.003352327
0.01	0.00027905	0.000589209	0.004190423
0.012	0.00033486	0.000707052	0.005028525
0.014	0.000390671	0.000824896	0.005866635
0.016	0.000446481	0.00094274	0.006704751
0.018	0.000502292	0.001060585	0.007542874
0.02	0.000558103	0.001178429	0.008381004

Table A.17 Pressure drop distribution for 0.01 M Cu^{2+} ion solution concentration, 5, 10, and 50 mL / min flow rate, and 3 cm bed length

x	5 mL / min flow rate	10 mL / min flow rate	50 mL / min flow rate
0	0	0	0
0.003	8.37145E-05	0.000176762	0.001257112
0.006	0.000167429	0.000353524	0.0025142310
0.009	0.000251144	0.000530286	0.003771358
0.012	0.000334859	0.00070705	0.005028495
0.015	0.000418574	0.000883814	0.006285642
0.018	0.00050229	0.001060578	0.007542798
0.021	0.000586005	0.001237343	0.008799965
0.024	0.000669721	0.001414109	0.010057141
0.027	0.000753437	0.001590876	0.011314326
0.03	0.000837153	0.001767643	0.01257152

Table A.18 Pressure drop distribution for 0.01 M Cu^{2+} ion solution concentration, 5, 10, and 50 mL / min flow rate, and 4 cm bed length

x	5 mL / min flow rate	10 mL / min flow rate	50 mL / min flow rate
0	0	0	0
0.004	0.000111619	0.000235682	0.001676149
0.008	0.000223239	0.000471365	0.003352307
0.012	0.000334859	0.000707048	0.005028476
0.016	0.000446479	0.000942733	0.006704655
0.02	0.000558099	0.001178418	0.008380847
0.024	0.000669719	0.001414103	0.010057052
0.028	0.00078134	0.00164979	0.011733271
0.032	0.000892961	0.001885477	0.013409501
0.036	0.001004582	0.002121165	0.015085743
0.04	0.001116203	0.002356853	0.016761996

Appendix B

Physical Properties of Electrolyte

B.1 Calculation of Density and Viscosity by ChemCAD

ChemCAD is computer package used for the design of chemical processes, ChemCAD have a database for physical properties of thousands of components and mixtures, so this database will be used in this work for the evaluation of electrolyte density and viscosity because of the lack of these data in the available literature. The method is done by introducing weight fractions of copperic sulfate, sulfuric acid, and water to the (ChemCAD) in, setting the temperature to 25C° and calculate density and viscosity for these weight fractions. Weight fractions input to the ChemCAD and results (density and viscosity) are given in Table B.1 below

Table B.1 Input weight fractions and results

H_2SO_4 weight fraction	$CuSO_4$ Weight fraction	Density (kg/m^3)	Viscosity ($N.s/m^2$) $*10^3$
0.100	0.1000	1170.41	1.1634500
0.075	0.2000	1268.93	1.1121000
0.010	0.3000	1335.52	0.9404630
0.005	0.4000	1492.69	0.9263100
0.005	0.5000	1702.05	0.9239030
0.100	0.0100	1077.37	1.1420200
0.100	0.0075	1075.00	1.1414800

The data of Table B.1 need to be converted into molar concentrations of copperic sulfate and sulfuric acid. The Molar concentration of species I is defined as

$$M_i = \frac{gmol\ of\ i}{Volume(liter)} = \frac{kgmol\ of\ i}{Volume(m^3)} \qquad \ldots(B.1)$$

the total volume in terms of electrolyte density

$$Volume(m^3) = \frac{m_T}{\rho} \qquad \ldots(B.2)$$

substitution of equation (B.2) into equation (B.1) and putting in terms of weight fraction

$$M_i = \frac{(kg\ of\ i / Mwt.\ of\ i)}{m_T}\rho$$

$$M_i = \frac{wt.fraction\ of\ i}{Mwt.\ of\ i}\rho \qquad \ldots(B.3)$$

Where m_T is the total mass of electrolyte, Mwt is the molecular weight, and ρ is the density of electrolyte.

Application of equation (B.3) on both Copperic sulfate and Sulfuric acid to get the following results as in Table B.2 below

Table B.2 Molar concentrations with density and viscosity at given weight fractions

H_2SO_4 weight fraction	$CuSO_4$ weight fraction	H_2SO_4 Molar Concentration (gmol/L)	$CuSO_4$ Molar Concentration (gmol/L)	Density (kg/m^3)	Viscosity ($N.s/m^2$) *10^3
0.100	0.1000	1.193322	0.7332937	1170.41	1.1634500
0.075	0.2000	0.970328	1.5900382	1268.93	1.1121000
0.010	0.3000	0.136166	2.5102187	1335.52	0.9404630

Table B.2 Continued

0.005	0.4000	0.076096	3.7408433	1492.69	0.9263100
0.005	0.5000	0.086768	5.3319028	1702.05	0.9239030
0.100	0.0100	1.098460	0.0675002	1077.37	1.1420200
0.100	0.0075	1.096044	0.0505138	1075.00	1.1414800

B.2 Electrical conductivity of Electrolyte at Various Molar Concentrations

The electrical conductivity for given concentrations of copperic sulfate and sulfuric acid are given in Table B.3 below.

Table B.3 Electrical conductivity of electrolyte at various molar concentrations of copperic sulfate and sulfuric acids

H_2SO_4 Concentration (gmol/l)	$CuSO_4$ Concentration (gmol/l)	Experimental Value ($\Omega^{-1}.m^{-1}$)
0.01	0	80
0.7086	1.25	25
0.002	1.5	55

B.3 Exchange current density at Various Molar Concentrations

The data for exchange current density vs. molar concentration are available at 30 °C [25] these data need be to converted for the temperature of 25 °C this is done using the equation

$$i_{oT} = i_{o298\,K}\, exp\left\{\frac{E_{activation}}{R}\left(\frac{1}{298.15} - \frac{1}{T}\right)\right\} \quad \ldots(B.4)$$

the value of $E_{activation}$ must be evaluated from knowing the exchange current density at 25 °C and 30 °C which are 1.94 A / m^2 and 0.774 A / m^2 respectively, therefore $E_{activation}$ / R = -16610.2858 J / mole.

Introducing this value into equation (B.4) so that the exchange current density values can be transformed from 30°C (column 2) to 25°C (column 3) as given in Table B.4 below

Table B.4 Exchange current density at given electrolyte concentration [25]

$CuSO_4$ Concentration	i_{oT} (A / m^2)	$i_{o298\,K}$ (A / m^2)
0.002	0.774	1.94
0.01	0.9	2.2558
0.1	2.2	5.15142
1	3.9	9.77

Data above for density, viscosity, electrical conductivity, and exchange current density versus molar concentrations are fitted using STATISTICA program to give the results shown in **Table B.5** below

Table B.5 Fitted physical properties values

Property	Equation
Density (kg / m^3)	$\rho = 1103.262 + 61.46 M_{H_2SO_4} + 131 M_{CuSO_4} + 77.63 \left(M_{H_2SO_4} \cdot M_{CuSO_4}\right)^{0.0232} - 180 M_{CuSO_4}^{0.0086 M_{H_2SO_4}}$
Viscosity (kg /m. s)	$\mu = -3 \times 10^{-3} + 2.23 \times 10^{-4} M_{H_2SO_4} + 8.3 \times 10^{-7} M_{CuSO_4} - 8.3 \times 10^{-7} \left(M_{H_2SO_4} \cdot M_{CuSO_4}\right)^{0.14} + 0.00406 M_{CuSO_4}^{2.287 \times 10^{-3} M_{H_2SO_4}}$
Electrical Conductivity (Ω^{-1}. m^{-1})	$\kappa_o = 74.92 - 6.1459 M_{CuSO_4} - 25.7 M_{H_2SO_4} - 3.92 M_{CuSO_4} M_{H_2SO_4}^{8.6} + 5.144 M_{CuSO_4}^{\left(-0.139 M_{H_2SO_4}\right)}$
hange current density (A / m^2)	$i_o = 1.861266 + 39.71 M_{CuSO_4} - 31.8 M_{CuSO_4}^2$

The error between curve fitting results & ChemCAD's for density and viscosity values are presented in **Table B.6**

Table B.6 Predicted values & ChemCAD's results density and viscosity

H_2SO_4 Molar Concentration (gmol/l)	$CuSO_4$ Molar Concentration	ChemCAD		Predicted values from curve fitting		% Error	
		Density (kg/m^3)	Viscosity (N.s/m^2) *10^3	Density (kg/m^3)	Viscosity (N.s/m^2) *10^3	Density (kg/m^3)	Viscosity (N.s/m^2) *10^3
1.193322	0.7332937 (gmol/l)	1170.41	1.1634500	1170.62	0.001161642	0.0178	1.553932
0.970328	1.5900382	1268.93	1.1121000	1268.72	0.001111910	0.01654	0.170643
0.136166	2.5102187	1335.52	0.9404630	1335.61	0.000939341	0.006844	1.193426
0.076096	3.7408433	1492.69	0.9263100	1492.56	0.000926546	0.007005	0.254622
0.086768	5.3319028	1702.05	0.9239030	1702.11	0.000922993	0.00371	0.984507
1.098460	0.0675002	1077.37	1.1420200	1077.36	0.001141493	0.00132	0.461648
1.096044	0.0505138	1075.00	1.1414800	1074.96	0.001140467	0.003663	0.887277

The density and viscosity of 0.002 M Cu^{2+} and 1.5 H_2SO_4 in literature [24] were 1065 and 1.18*10^{-3} respectively while the fitted equations give 1097.555 and 1.1941*10^{-3} with % error of 3.05633 for density and 1.1949 for viscosity

الخلاصة

تم في هذه الأطروحة إنجاز برنامج حاسوب لغرض أجراء محاكة لمفاعل كهروكيميائي ثابت الحشوة لدراسة كل من حركية التفاعل وهيدروديناميكية المفاعل. تمت المحاكاة تحت الظروف الآتية: انتظام مع الزمن ،جريان احادي البعد ، جريان المحلول خلال الحشوة ،استقطب مزدوج السيطرة. المحلول الالكتروليتي يمر بالحشوة موازي و معاكس للتيار. التفاعل الذي تمت دراسته هو ترسيب النحاس من محلول الكتروليتي يحتوي على كبريتات النحاس و حامض الكبريتيك كمحلول مساند و تم أفتراض عدم وجود تفاعل جانبي. تمت دراسة منطقة الاستقطب المزدوج و ذلك بتطبيق تيار ذو نسبة ٨٠% من التيار المحدد للتطليب. حبيبات الحشوة التي استعملت كروية الشكل و مصنوعة من النحاس.

تمت دراسة تأثير تغير سرعة جريان المحلول الالكتروليتي، سمك الحشوة، و تركيز محلول كبريتات النحاس الداخل على تصرف المفاعل كما يلي: سرع الجريان ٥٠،١٠٠ ٥٠،١٠٠ سليتر / دقيقة، تراكيز محلول كبريتات النحاس ٠،٠٠٠١ ، ٠،٠٠١ مولاري و سمك الحشوات ٣،٢ و ٤ سم.

الهدف الأساسي من هذه الدراسة هو إيجاد المتغيرين الأساسيين تغير التركيز و تغير الجهد اللذين من خلالهما يمكن إيجاد بقية المتغيرات. تغير التركيز و تغير الجهد تم حسابهما من الحل الآني لمعادلة Butler-Volmer و معادلة موازنة الكتلة بناءا على طريقة أقترحت في هذه الدراسة تجمع بين طريقتي الأختلافات المحدودة (finite difference) لحل المعادلة التفاضلية ذات الدرجة الثانية اللاخطية لجهد الكاثود و الحل التحليلي لمعادلة التفاضلية ذات الدرجة الثانية لموازنة الكتلة.

النتائج المستحصلة قسمت الى مجموعتين الأولى هي مجموعة النتائج الرئيسية و التي تضم تغير كل من التركيز ، الجهد المزاد، و سرعة التفاعل. لقد وجد أن تغير التركيز يقل بزيادة سرعة الجريان ويزداد بزيادة سمك الحشوة و تركيز أيون النحاس. الجهد المزاد يتأثر بتغير سمك الحشوة و تركيز أيون النحاس بصورة مشابهة لتأثر تغير التركيز ويتأثر بصورة معاكسة بالنسبة لسرعة الجريان. و وجد أن سرعة التفاعل تتأثر بصورة مشابهة لتأثر الجهد المزاد. المجموعة الثانية هي مجموعة النتائج الثانوية و التي تضم تغير كل من التيار و فرق الضغط. أن تصرف التيار هو نفس تصرف سرعة التفاعل من حيث الزيادة و النقصان أما تغير فرق الضغط فيزداد بزيادة سرعة الجريان و سمك الحشوة.

النموذج الحالي تمت مقارنة نتائجه مع الأدبيات العلمية: أولا مقارنة نتائج المعادلة التحليلية لأيجاد التيار المحدد الكلي المطبق على المفاعل مع النتائج العملية لـ Bennion and Newman (١٩٧٢)

حيث وجد أن التطابق الناتج كان جيداً جدا. ثانياً مقارنة النموذج الحالي مع نموذج Olive و Lacoste(١٩٨٠) تحت ظروف التيار المحدد حيث وجد تطابق جيد.

النموذج الحالي نجح بوصف تأثير سرعة الجريان, سمك الحشوة, و تركيز المحلول الداخل على تغير التركيز وكذلك تأثير رقم رينولدز على نسبة التحويل لعدة اطوال للحشوة الذي طابق التأثير المتوقع من الأدبيات العلمية.

شكر و تقدير

الحمد لله أولا على فضله و كرمه في إنجاز هذا البحث و جزيل الشكر و الأمتنان لأستاذي الدكتور قاسم جبار سليمان رئيس قسم الندسة الكيمياوية على متابعته المستمرة و توجيهاته القيمة وتشجيعي أثناء فترة البحث.

و أود التقدم بالشكر الى السيد عميد كلية الهندسة و كافة منتسبي القسم ممن كان له فضل في أتمام هذا البحث.

و أشكر عائلتي على ما قدمت لي من دعم و تشجيع غير محدود خلال البحث.

وأخيراً أشكر زملائي و أصحابي على دعمهم و تشجيعهم و كذلك كل من كان له فضل علي.

سيف طلال

موديل مبسط لمفاعل كهروكيمياوي
لغرض المحاكات والدراسة

رسالة
مقدمة إلى كلية الهندسة في جامعة النهرين
وهي جزء من متطلبات نيل درجة ماجستير علوم
في الهندسة الكيمياوية

من قبل

سيف ظلال منجي
بكالوريوس علوم في الهندسة الكيمياوية

رمضان ١٤٢٧
تشرين لأول ٢٠٠٦